Temperature-Dependent Dynamics in Disordered Metals

Ariel Eisenbachs
Department of Physics

Ph.D. Thesis

Submitted to the Senate of Bar-Ilan University
Ramat-Gan, Israel July 2017

This work was carried out under the supervision of

Prof. Richard Berkovits

and

Prof. Aviad Frydman

Department of Physics,

Bar-Ilan University

Acknowledgements

"I would rather have questions that can't be answered than answers that can't be questioned." (Richard Feynman)

The exciting world outside, as well as our very daily experiences, face us with innumerable puzzles which are too wonderful not to be learned. As a young kid, I found myself frequently astonished by nature profound mysteries, and Physics studies seemed like the best place to look for answers. But, as I learned the hard way, knowledge usually does not give answers, but only show the general direction in which they may be present. Fortunately enough, walking down this path taught me how to live in peace with the riddles of nature, and be thankful for our little great steps toward understanding.

The academic world, and in particular physics, is a great place for a believing person. Connecting the very basic of matter with great ideas such as mathematics, symmetries, uncertainty principle or entropy, let us sense the very reason and objective of this tremendous show. I believe that this connection between faith and mind is a truthful step toward the unity of existence.

I would like to deeply thank my supervisors, Richard Berkovits and Aviad Frydman, and to the many other people who supported throughout the years -

Richard, thank you for showing me what is the difference between knowing something and understand it, and for guiding me through the maze of the scientific way of thinking.

Aviad, thank you for taking care from the very first moment, helping to reveal my own path in research and not letting me give up in the hard times. Your deep insights and wide experimental knowledge were a great inspiration for me.

Many thanks to my great teachers at Bar Ilan University, and to all the Physics department staff. You have made these years much more fun and interesting than I could imagine. In particular, I would like to thank Prof. Valentin Freilikher, Dr. Denis Golosov and Prof. Ariel Amir for the fruitful collaborations and discussions.

I am grateful to all my colleagues and friends at Bar-Ilan, who supported and guided me, and especially to Ora, Noa, Tal, Shachaf, Pasha, Shaul, Naor and Tony.

Lastly, many thanks to my loving family, and to my supporting wife and best friend, Dvora, for walking together through this journey.

Contents

List of Abbreviations

DOS - density of states

EG - electron glass

HM - hidden mode

LB - Landauer Buttiker

LDOS - local density of states

MOSFET - metal-oxide-semiconductor field effect transistor

NEGF - non equilibrium Green's function

QC - quench condensation

QNM - quasi normal mode

QNS - quasi normal state

TB - tight binding

TDE - two dip experiment

UHV - ultra-high vacuum

VRH - variable range hopping

Abstract

“In all chaos there is a cosmos, in all disorder a secret order.” (Carl Jung)

The nature of disordered metals and their temperature dependence is the main subject addressed in this work, using theoretical, numerical and experimental methods. Like many other systems in condensed matter physics, the problem of electrons in disordered lattices is not yet completely understood. Due to the complex nature of such systems, exact theoretical solutions cannot be applied and statistical methods require extreme caution when used to describe all aspects of the physics. Moreover, a growing number of experimental studies on different disordered systems and materials show non-trivial and novel phenomena, such as the super-conductor to insulator transition [1,2], super-insulator [3,4], superradiance [5], and electron-glass [6,7].

Electron dynamics in disordered metals are very different from those of a perfect metal. In these disordered systems, the electrons are localized in space, and their dynamics is described by hopping between these localized states. Sensing the electronic dynamics by transport (i.e. conductance measurements) is a common method to examine the response of different systems to various external conditions, and under the right conditions, it provides comprehensive information on the very nature of the electron states in the system, and of the significance of the strength of disorder, Coulomb interactions, temperature, etc.

In this dissertation, I study the temperature dependence of a variety of dis-

ordered systems using different techniques: numerically, by the Non-Equilibrium Green's Function method (NEGF); and experimentally, by measuring the conductance of thin metal films.

Unlike the common statement asserting that temperature affects the electronic transport mainly by coupling to the lattice phonons, in the numerical section we show that the electric conductance strongly depends on temperature, even in the absence of phonons. This effect is attributed to the highly skewed distribution of the transmission function in disordered systems. Moreover, the conductance in disordered quantum systems turns out to be substantially different from the conductance of normal (non-disordered) metals, where a significant part of the electronic quantum states do not contribute to the conductance measurement.

In the experimental section we use the quench-condensation method to fabricate and measure thin films of highly disordered metals at low temperatures. These films turned out to be electron-glasses (EG), i.e. the interacting electrons within the metal share features of glass, including a very slow relaxation of the conductance after a thermal or electronic excitation, and a memory of the previous environmental conditions. EG systems are believed to be independent of temperature T, and therefore, are suggested as quantum-glass; i.e., the dynamics of the localized electrons are ruled by quantum-tunneling, rather than thermal activation by phonons. Nonetheless, we show that this phenomenon is true only for a limited range of low temperatures. Above a certain point in temperature the relaxation rates of the glass obey again the classical activation dependence. By analyzing the experimental results, we show that the energy scale of the thermal activated glass dynamics is characterized by a surprising parameter – the maximal temperature the system was previously heated to.

The observations in both paths, theoretical and experimental, face similar physical puzzle, namely: how do temperature affect transport in non-equilibrium disordered metals? They do, however, examine different systems and employ different methods, and thus answer this question from diverse aspects. In the first part of this work, I provide an introduction to disordered systems in condensed matter physics, as well as electronic transport and conduction of quantum electronic systems. The second part focuses on the calculation of transport in non-equilibrium systems, including a detailed description of the NEGF method, its implementation, and its results on a variety of systems and conditions. In the third part, I focus on the experimental work, including an introduction to the glass state of matter, the electron glass systems and a review of the previous results in the field. I then describe the experimental systems and techniques, and discuss this research's results and its contribution to the field.

Part I

Introduction to Transport in Disordered Systems

Chapter 1

Theoretical Background

1.1 Anderson localization

In the absence of disorder, the quantum mechanical nature of electrons in periodic lattices is described by the Bloch wave function

$$\psi(\vec{r}) = e^{i\vec{k}\vec{r}}u(\vec{r}), \tag{1.1}$$

where $\vec{r}$ is the position vector in the metal, $\vec{k}$ is the wave vector, and $u(\vec{r})$ is a function with periodicity of the lattice vectors $\vec{R}$, i.e. $u(\vec{r}+\vec{R}) = u(\vec{r})$ (Fig. 1.1**a**). This periodic solution of the Schrödinger equation means that the electrons are extended, and their charge density, $|\psi(\vec{r})|^2$, is uniformly distributed in space.

However, if disorder is present in the metal, the solution of the quantum mechanical problem becomes very different from the Bloch function, and the wave vector $\vec{k}$ is no longer a good quantum number. Anderson [8] showed that within the limits of a strong disorder, all electronic states are bounded to certain locations in the metal and decay exponentials around localization centers -

$$|\psi_i(\vec{r})| \propto \exp\left(-\frac{|\vec{r}-\vec{r_i}|}{\xi}\right), \tag{1.2}$$

where $\vec{r_i}$ is the localization center of i_{th} eigenstate $\psi_i(\vec{r})$, and ξ is the scaling factor of the exponential decay, named the 'localization length' (Fig. 1.1 **b**). A short derivation of this behavior using the transfer matrix method may be found in Ref. [9].

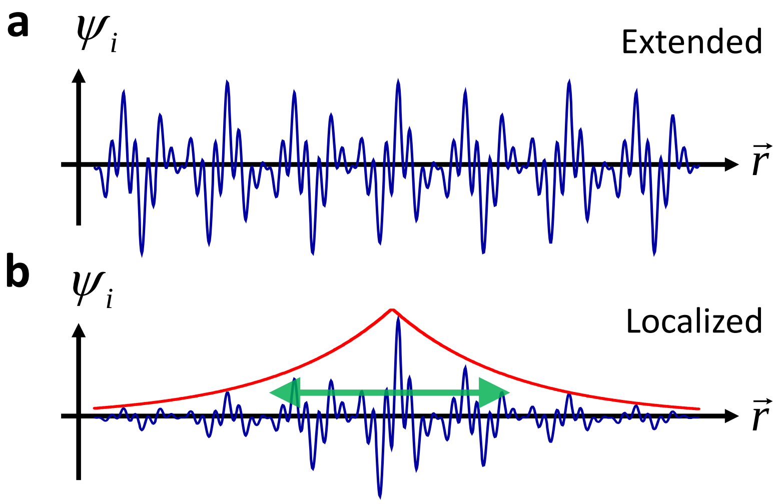

Figure 1.1: Illustration of extended (**a**) and localized (**b**) wave functions, ψ_i, as a function of location in a disordered system, $\vec{r}$ (blue lines). In the localized regime, the amplitude of ψ_i decays exponentially around the localization center (red line); the strength of this decay is the localization length (green arrow) (see Eq. 1.2).

The transport of electrons through a homogeneous metal (i.e. with no disorder) is a direct result of the Bloch function (Eq. 1.1), and the quantum current operator reduces to

$$j = \frac{\hbar}{2mi}\left(\psi^*\nabla\psi - \psi\nabla^*\psi\right) = \frac{\hbar k}{m}, \tag{1.3}$$

where i is the imaginary unit and m is electron mass.

In disordered quantum systems, however, this treatment leads to an exponentially small current. This has led Mott [10, 11] to suggest a different mechanism of transport in disordered systems, called Variable Range Hopping (VRH).

1.2 Variable range hopping

Transport of electrons in localized systems generally involves incoherent processes, particularly interactions between electrons and phonons. In the ground state, all electrons are bound and do not contribute to transport, hence, one might expect that conductivity would be enhanced at higher temperatures due to the influence of phonons on the electrons, similar to intrinsic insulators and semiconductors. This temperature-driven conductance is the basis of VRH theory.

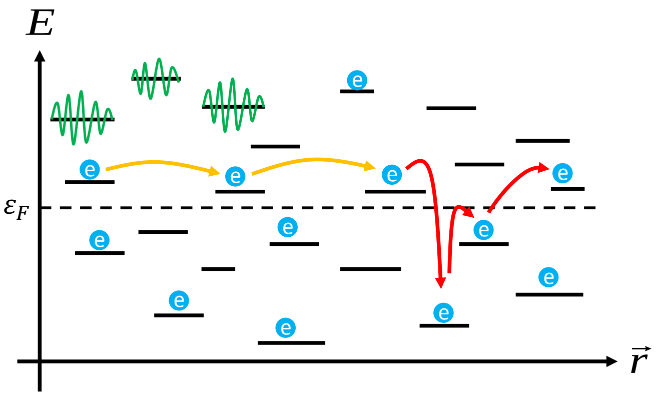

Figure 1.2: Illustration of the variable range hopping process. The wave functions (green lines) are localized in space ($\vec{r}$). The lateral positions of the electronic states are represented by short black lines with association to their eigen-energies. The hopping process of electrons (cyan circles) may occur at low temperatures via long range processes to states with similar energy (orange arrows), and at high temperatures by short range processes to adjacent states with diverse energies (red arrows).

Within the limits of a highly disordered system, where the localization length is much shorter than system length, each electronic state is bound to a small region in space and has a different energy level. In the 1D case, we can describe this electronic system by the $E(\vec{r})$ sketch in Fig. 1.2. In order to contribute to conduction, an electron must hop between the localized states. The rate of this hopping process, Γ, depends exponentially both on the spatial distance and on the difference between the energies of the states, using the following relation [12]:

$$\Gamma_{ij} = \gamma_0 \exp\left(-\frac{2\left|r_i - r_j\right|}{\xi}\right) \cdot \exp\left(\frac{\left|E_i - E_j\right|}{k_B T}\right), \tag{1.4}$$

where $r_{i/j}$ and $E_{i/j}$ are the localization center and the energy of state i/j, respectively. γ_0 is a proportional constant that is governed by the material properties. The spatial part of Eq. 1.4 is a consequence of the overlap integral between the two states

$$\int_{-\infty}^{\infty} \psi_i(\vec{r})\psi_j(\vec{r})d\vec{r}, \tag{1.5}$$

while the energy part is the activation probability of an electron by a phonon with corresponding energy at a given temperature. This relation sets an effective distance between adjacent localized sites in the $d+1$ dimensions of space and energy (d being the dimensionality of the system). This effective distance varies with temperature: At relatively high temperatures, the phononic distribution is wider, therefore the hopping rate to spatially closer sites is high even if the energy mismatch is great; on the other hand, at low temperatures, the electrons prefer farther sites, but with closer energy values.

The relation of the average spatial distance between two neighboring sites, Δr, and their mean energy difference, ΔE, is given by the density of states. Assuming constant density of states, $\mathcal{N}(E) = \mathcal{N}_0$, the energy difference between adjacent states can be presented by

$$\Delta E = \frac{1}{\mathcal{N}_0(\Delta r)^d}, \tag{1.6}$$

which leads to the following hopping rate

$$\Gamma = \gamma_0 \exp\left(-\frac{2\Delta r}{\xi} - \frac{1}{k_B T}\frac{1}{\mathcal{N}\cdot(\Delta r)^d}\right). \tag{1.7}$$

As a result of the exponential nature of Eq. 1.7, it can also be assumed that most of the electronic transport will occur between nearest neighboring sites in the $d+1$ dimensions. One can thus discover the mean spatial distance to this site $\overline{\Delta r}$ by demanding a maximum in Γ

$$\frac{\partial \Gamma}{\partial \Delta r} = \Gamma \cdot \left(-\frac{2}{\xi} + \frac{1}{k_B T} \frac{d}{\mathcal{N} \cdot (\overline{\Delta r})^{d+1}} \right) = 0, \tag{1.8}$$

and find that

$$\overline{\Delta r} = \left(\frac{\xi d}{2 \mathcal{N} k_B T} \right)^{\frac{1}{d+1}}. \tag{1.9}$$

By placing $\overline{\Delta r}$ back into Γ, we derive the temperature dependence of the hopping rate

$$\Gamma = \gamma_0 \exp \left[- \left(\frac{T_0}{T} \right)^{\frac{1}{d+1}} \right], \tag{1.10}$$

where

$$T_0 = \frac{2^d}{\xi^d \mathcal{N}_0 k_B}. \tag{1.11}$$

The conductance between adjacent states, G_{ij}, is proportional to the rate at which electrons hop between the sites, Γ_{ij}. Therefore, Eqs. 1.10-1.11 define a fractional power temperature dependence in the exponential for transport in the disordered system. This exponential dependence differs from the intrinsic band gap insulator temperature dependence, in which conductance is related directly to the probability of an electron to absorb phonon and to be excited into the conductance band, i.e. $G \propto \exp(-\Delta/k_B T)$, where Δ is the band gap amplitude. Hence, if T_0 is large enough, one may easily distinguish between the two mechanisms experimentally.

1.3 Percolation network

While the VRH method considers only a single hopping process to obtain conductance behavior, a model of transport in larger systems was developed by Miller and Abrahams [12] and further expanded by Ambegauker, Halperin and Langer [13]. In this framework, the disordered system is described as a network of resistors between localized states. The resistance values of these resistors are determined by the spacial and energetic differences between the states, similar to the premise of the VRH method, and therefore have an exponential distribution. This method allows the definition of a critical resistance value, R_c, by connecting the resistors one by one from the lowest resistance to the higher resistance ones. According to this process, R_c is the minimal resistance value which allows a direct percolative flow of electrons between sample edges. Due to the exponential distribution of the resistors, all higher resistors $R \gg R_c$ are considered as an effectively infinite resistance, and all lower resistors $R \ll R_c$ as an electric shortcut with zero resistance; hence, the overall conductivity of the whole network is defined as R_c. The behavior of R_c with temperature is directly related to the VRH analysis. In other words, the conductivity of the entire disordered system would resemble Eq. 1.10:

$$G = G_0 e^{-\left(\frac{T_0}{T}\right)^{\frac{1}{d+1}}}, \tag{1.12}$$

where G_0 is the saturated conductance at high T.

This percolation network analysis provides a more qualitative understanding of electronic transport in disordered media, as most of the electronic current is concentrated in a diluted percolation network, and all other areas are detached and do not contribute to electronic transport (Fig. 1.3). The characteristic length scale of the percolation network, the percolation length, is the average distance between critical resistors, and defines the minimal size of the percolation system.

In samples with high levels of disorder, the percolation length can be as large as a few tens of microns, whereas all other length scales in the metallic system are within the range of a few nanometers. This effect ascribes such systems as **mesoscopic** physics (meso = intermediate), i.e. it is neither microscopic nor macroscopic, but has the characteristics of both scales.

Due to the exponential nature of the critical resistors, the percolation network is highly sensitive to changes in external parameters. This gives rise to large fluctuations of conductance with changes in temperature, bias voltage, gate voltage, etc. In the case of highly disordered systems, the percolation length is large enough and the mesoscopic fluctuations are observable even in millimetric-in-size samples.

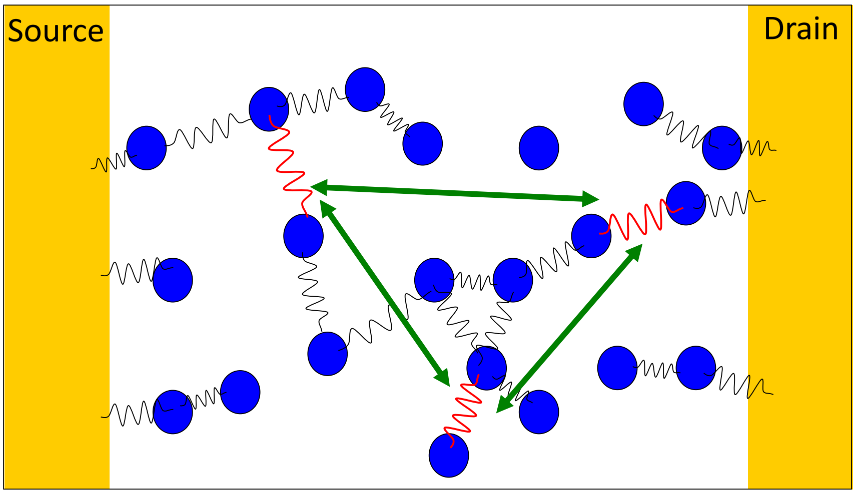

Figure 1.3: Illustration of the percolation network in a 2D system. The blue circles are the localization centers, connected by ”resistors” with various conductivities (black curved lines). The critical resistivity, R_c, can be found by hypothetically appending resistors between the localization sites from most conductive to most resistive; in this method, R_c (red curved lines) is on the scale of the resistors that connect the percolation network from between the contacts (yellow rectangles). The percolation length is the mean distance between two such resistors (green arrows).

1.4 The Coulomb gap

The energy value of each localized site is mainly determined by the disorder potential of the atoms in the metal. Nevertheless, Efros and Shklovskii [14] showed that the energies of states around Fermi energy (ϵ_F) gain an additional term due to Coulomb interactions between electrons. This phenomenon can be clarified by the following argument: while a system is in its ground state, all sites with energy below ϵ_F are occupied, and all sites with energy greater than ϵ_F are empty. Adding an additional electron to the system will result in an increase of E_j, the lowest energy state above ϵ_F. However, if instead of adding a particle to the system, an electron from site i below ϵ_F is excited into site j, the overall change in energy would be:

$$\Delta E_{ij} = E_i - E_j - \frac{e^2}{\Delta r_{ij}}, \tag{1.13}$$

where the additional subtracted term originates from the change in the Coulomb interaction due to moving of electron from site j to site i.

According to the definition of the Fermi energy, ΔE_{ij} should remain positive to maintain the system in its ground state, we can conclude that the states must be far enough from each other to prevent such a process, which results in an energy gap around ϵ_F.

Quantitatively, the DOS relates the mean spatial distance Δr to the mean energy differences ΔE, as mentioned in Eq. 1.6. Therefore, the level spacing between states i and j should be as follows

$$\Delta E_{ij} = E_i - E_j - e^2(\mathcal{N}_0 \Delta E)^{1/d}. \tag{1.14}$$

If the energy difference $E_i - E_j$ is small enough, the right-hand side of Eq. 1.14 is negative, but ΔE_{ij} is defined as the absolute value. The solution to this contradiction is the depletion of states from Fermi energy, which changes the DOS to the following form

$$\mathcal{N}(E) = \frac{\tilde{\mathcal{N}}}{e^{2d}} \left(E - \epsilon_F\right)^{d-1}, \tag{1.15}$$

where $\tilde{\mathcal{N}}$ is a scaling factor. This means that at $E = \epsilon_F$, the DOS is equal zero, forming a 'soft' gap around the Fermi energy, which has been termed as the Coulomb gap.

By combining the DOS of the Coulomb gap (Eq. 1.15) with VRH theory (Eq. 1.4), Efros and Shklovskii [14] show that the temperature dependence power α becomes independent of the dimensionality d

$$G(T) = G_0 \exp\left(-\frac{T_0}{T}\right)^{\frac{1}{2}}, \tag{1.16}$$

where

$$\tilde{T}_0 = \frac{8e^2}{\tilde{\mathcal{N}} k_B \xi}. \tag{1.17}$$

The above two temperature dependencies have become the hallmark of hopping systems, as demonstrated in Fig. 1.4 [15]. At low enough temperatures, the Coulomb interactions form a Coulomb gap, and conductance is as presented in Eq. 1.16, whereas at higher temperatures, the thermal energy washes out the Coulomb gap, and conductance follows Eq. 1.12.

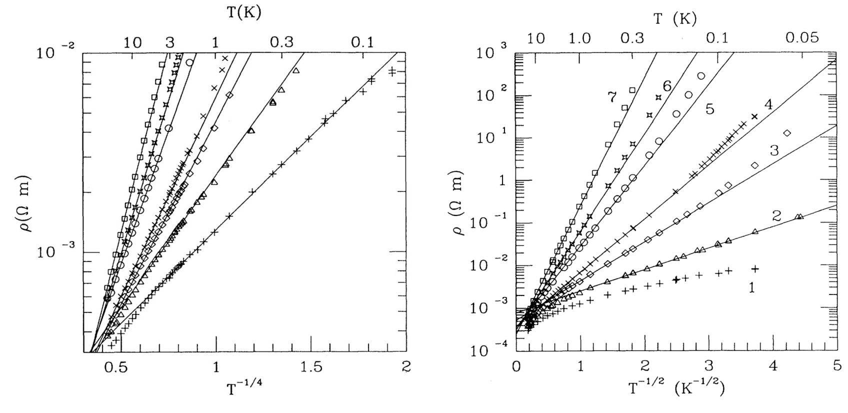

Figure 1.4: Resistivity as function of temperature for three dimensional ion-implanted Si:P,B samples. At relatively high temperatures **(left frame)** the resistivity is successfully scaled with $T^{-\alpha}$ where $\alpha = 1/(d+1)$, while at lower temperatures **(right frame)** the results are better fitted with $\alpha = 1/2$. (Zhang, 1993 [15])

1.5 Scaling theory of localization

As was described above, in the presence of strong disorder, the wave functions of electrons are localized in space and conductance decreases exponentially with the system size, L. This behavior is true in one-dimensional (1D), two-dimensional (2D) and three-dimensional (3D) systems. However, if the level of disorder is not large enough, a fundamental difference is found between the various dimensions. A highly accredited paper by a group of researchers, known as the "Gang of Four" (Abrahams, Anderson, Licciardello, and Ramakrishnan) [16], had shown that a scaling relation between conductance G and system length L can be described by a single parameter β, defined as -

$$\beta \equiv \frac{\log(G)}{\log(L)}. \tag{1.18}$$

In the case of a strong enough disorder, conduction decreases exponentially when enlarging the system, $G \propto e^{-L/\xi}$; hence, β is negative in this range and depends linearly on ξ for every dimension.

On the other hand, for weak disorder, the system is Ohmic and has constant conductivity. In the 1D case, enlarging the system length L will result in linearly lower conductance ($\beta < 0$); in 2D, enlarging L on both axes by the same amount will not change G ($\beta = 0$), and in the cubic 3D case, G would even *increase* with L ($\beta > 0$). The overall dependence is depicted in Fig. 1.5.

This demonstraits a substantially different behavior of the disorder in different dimensions. While a 1D system is localized at any value of disorder, in 3D this is true only for a strong enough disorder. A transition from a localized to extended case occurs when changing the disorder level of the system, known as the "Metal-insulator transition". The 2D case is marginal, and may therefore be affected by secondary effects, such as temperature, interactions, long range periodicity or

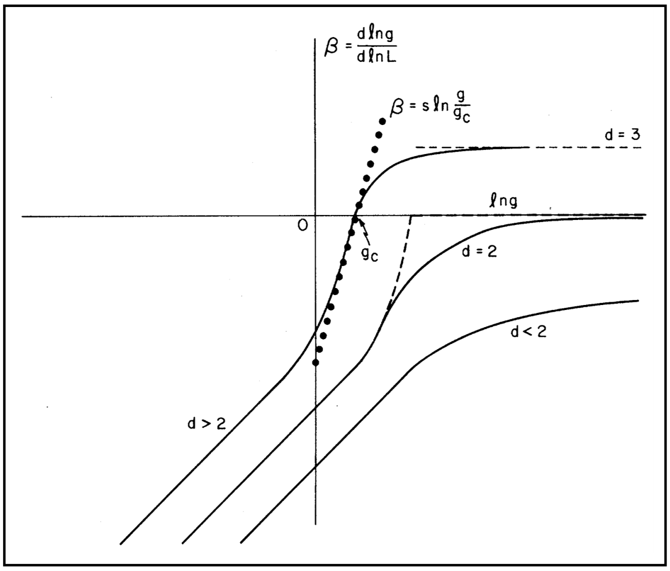

Figure 1.5: The scaling parameter of localization β, as a function of the logarithm of differential conductance, $\ln(g)$. $\beta < 0$ means exponentially lower conductance when enlarging the system size L in every dimension, indicating a localized regime. (Abrahams et al., 1979 [16])

external fields [17].

The theory of transport through disordered systems presented in this chapter is based on a set of premises on the microscopical behavior of electrons in matter, such as equilibrium conditions, effective single particle picture, a well-defined localization length, and the importance of electron-phonon interactions.

Furthermore, solving the full quantum mechanical equations of electronic levels and conductance is usually impossible due to the complexity of the macroscopical problem. However, in some cases, more detailed quantum considerations are important to comprehend the very nature of electronic transport, and must be taken into account.

In the following parts, I present two such systems, namely: the elastic transport of non-interacting electrons (Part II), and electron glass (Part III). The two subjects are different in many aspects, yet both show a non-trivial behavior of electronic transport in the presence of temperature, due to quantum mechanical nature of the system.

Part II

Conductance in Quantum Systems: Theoretical and Numerical Study

Chapter 2

Theoretical Study: Introduction

2.1 The Anderson Hamiltonian

A common way to present electron behavior in disordered electronic systems is via the tight-binding (TB) model, based on a matrix representation of the Hamiltonian and assuming a discrete form of the Schrödinger equation. This method assumes that the electronic wave functions of the atom are the convenient basis from which to approximate the wave functions of the whole system. Therefore, the basis for the electrons in the system can be treated as discrete in space, located at the exact locations of the lattice points of the periodic lattice.

Starting with the quantum Hamiltonian operator (in the 1D case) -

$$\hat{H} = -\frac{\hbar^2}{2m}\frac{d^2}{dx^2} + U(x), \tag{2.1}$$

we can rewrite the second derivative in a discrete formulation

$$\frac{d\psi_j}{dx} \to \frac{1}{a}\left(\psi_{j+1} - \psi_j\right), \tag{2.2}$$

$$\frac{d^2\psi_j}{dx^2} \to \frac{1}{a^2}\left(\psi_{j+1} - 2\psi_j + \psi_{j-1}\right), \tag{2.3}$$

where ψ_j is the electronic wave function in the j_{th} atom, and a is the lattice constant.

Hence, operating the Hamiltonian on ψ_j will result in -

$$\hat{H}\psi_j = (\epsilon_j + 2t)\psi_j - t\psi_{j+1} - t\psi_{j-1}, \tag{2.4}$$

where ϵ_j are the on-site energies of the atoms and t is the energy scale of the hopping element between adjacent atoms,

$$t \equiv \frac{\hbar^2}{2ma^2}. \tag{2.5}$$

In this discrete representation, $\hat{H}$ may be presented by the following matrix -

$$\hat{H} = \begin{bmatrix} \epsilon_1 + 2t & -t & 0 & 0 \\ -t & \epsilon_2 + 2t & -t & 0 \\ 0 & -t & \ddots & \vdots \\ 0 & 0 & \dots & \epsilon_L + 2t \end{bmatrix}, \tag{2.6}$$

which its eigenvectors and eigenvalues are the electronic eigen-states and eigen-energies, respectively.

One may represent disorder in the system by assuming a random distribution of the on-site energies ϵ_i. The eigen-states vectors of $\hat{H}$ will not follow the Bloch form, but will exhibit localized behavior (Eq. 1.2). This representation of the Hamiltonian, termed the Anderson Hamiltonian [8], assumes that all atoms are in their crystalline locations in space and therefore all hopping terms t are identical, while each atom has a random on-site energy [1].

Under the assumptions of the TB model, Eq. 2.4-2.6 may also be formulated

---

[1] A similar approach could be to assume the opposite, i.e. that the atomic levels are identical, $\epsilon_j = \epsilon_0$, and the hopping terms, t_{ij}, are randomized. Nevertheless, the resulting behavior of the eigen-states was shown to be similar [18].

in the second quantization form -

$$\hat{H} = \sum_j (\epsilon_j + 2t)\, \hat{c}_j^\dagger \hat{c}_j - t\hat{c}_j^\dagger \hat{c}_{j+1} - t\hat{c}_{j+1}^\dagger \hat{c}_j, \tag{2.7}$$

where $\hat{c}_j^\dagger$ and $\hat{c}_j$ are the creation and annihilation operators of electrons in site j, respectively.

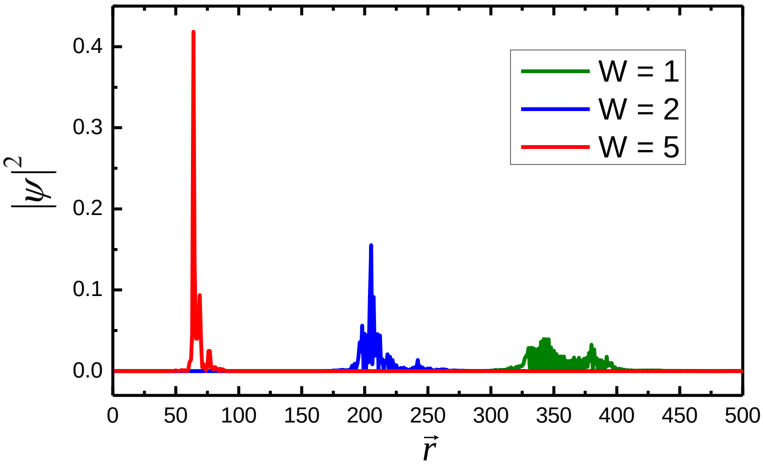

Figure 2.1: Representative electron density as a function of location in a 1D array with a length of $L = 500$, calculated by the 250th eigen-vector of the Anderson Hamiltonian. In agreement with Eq. 2.8, different disorder levels W result in different localization lengths: $W = 1$ leads to $\xi \approx 105$, $W = 2$ to $\xi \approx 26$, and $W = 5$ to $\xi \approx 4$ (see text).

As mentioned earlier, the electronic localized wave-functions are defined by localization length, ξ, which is equal to the length at which they decay to e^{-1} of their maximal value. As demonstrated in Fig. 2.1, in a case where ϵ_j are uniformly distributed between $-W/2$ and $W/2$, ξ was shown to be approximated by the following relation [19]:

$$\xi \approx \frac{105t^2}{W^2}. \tag{2.8}$$

Hence, W represents the disorder strength in the system.

2.2 Perfect conductance

A common way to evaluate conductance through a quantum system is by the transmission function, which is basically the probability of an electron with energy E to cross the system from end to end. This method assumes single-electron (i.e. non-interacting) picture, as well as electronic equilibrium.

In a perfect 1D metallic wire, the transmission probability equals one for all energy values. The amount of current generated by a single electron with energy E is therefore $-e\nu(E)$, where e is the electron charge and $\nu(E)$ is the electron velocity. However, in order to have a current flow through a system, one should apply a voltage, which results in a difference in the chemical potential at the source and drain ends, μ_S and μ_D. At zero temperature, only energy levels associated to an occupied electronic state in the source lead, and to an empty state in the drain lead, will contribute to the total current. The number of such levels is equal to $\mathcal{N} \cdot (\mu_S - \mu_D)$, where $\mathcal{N}$ is the density of states in the system. Thus, the total current equals -

$$I_{perfect} = -e\nu\mathcal{N} \cdot (\mu_S - \mu_D) = -e\nu\mathcal{N} \cdot eV_{SD}. \tag{2.9}$$

Both the electron velocity and the density of states are derivatives of the electronic dispersion relation (written here for the 1D case) -

$$\nu = \hbar\frac{\partial E}{\partial k}, \tag{2.10}$$

$$\mathcal{N}_{1D} = \frac{1}{\pi\hbar^2}\left(\frac{\partial E}{\partial k}\right)^{-1}, \tag{2.11}$$

which sets a simple relation between them:

$$\mathcal{N} = \frac{2}{hv}, \tag{2.12}$$

and therefore a universal quantized conductance value

$$G_{perfect} = \frac{I}{V_{SD}} = \frac{2e^2}{h}. \tag{2.13}$$

This conductance value, which equals $7.75 \cdot 10^{-5}$ Ohm^{-1}, is the conductance of a single channel in the metal, or equivalently, of a quantum point contact [20, 21].

In the case of finite temperature, however, the current calculation (Eq. 2.9) requires an additional integration over all energies, as the step distribution of the level occupations in the leads are replaced with Fermi distributions

$$f_(S/D) = \frac{1}{exp\left(\frac{E-\mu_{S/D}}{k_B T}\right) + 1}. \tag{2.14}$$

i.e. the probabilities to find an electron with energy E in the source (S) and drain (D) lead, respectively. Nevertheless, it is easy to show that even at finite temperature the overall integration on the $f_S - f_D$ remains equal to the biased voltage:

$$I_{perfect} = \frac{2e^2}{h} \int_{-\infty}^{\infty} (f_S - f_D)\, dE = \frac{2e^2}{h} \cdot V_{SD}. \tag{2.15}$$

2.3 Landauer-Buttiker formalism

In general, the transmission function is an $N \times N$ matrix, where $\mathcal{T}_{ij}(E)$ represents the probability of an electron with energy E to be transferred from site i to site j. Hence, the value $\mathcal{T}_{SD}(E)$ represents the transmission probability from the source lead (S) to the drain lead (D) through the entire wire.

In the case of a non-perfect metal, conductance electrons can be either transmitted through the 1D system or reflected backwards, and therefore $\mathcal{T}_{SD}(E) \leq 1$. As a result, the conductance in the disordered wire is also lower than the perfect conductance (Eq. 2.13) -

$$G = \frac{I}{V_{SD}} = \frac{2e^2}{V_{SD} \cdot h} \int_{-\infty}^{\infty} \mathcal{T}_{SD}(E) \left(f_S - f_D\right) dE, \tag{2.16}$$

where f_S and f_D comprise the dependence on the source-drain voltage V_{SD}, temperature T, and chemical potential μ.

This equation, known as the Landauer-Buttiker formalism, provides a simple yet useful method of calculating conductivity in quantum systems. An illustration of the current flow in a localized system is presented in Fig. 2.2, showing Mott's picture of localization and the role of the leads' populations (see also Fig. 5.1 further on).

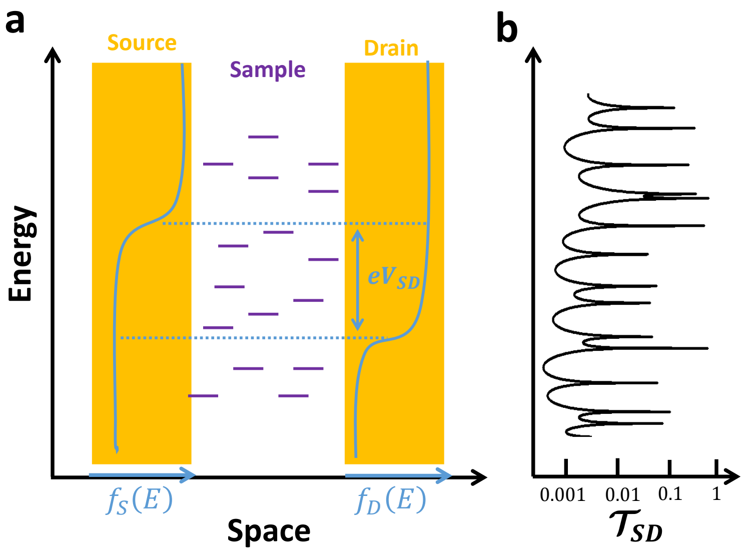

Figure 2.2: Illustration of the Landauer-Buttiker method of current calculation. **a:** The sample eigen-states (purple) are presented in Mott's picture at their localized positions and with their eigen-energies. When biased voltage is applied between the source and drain leads (yellow), their electrochemical potentials change, and electrons can flow from the occupied states in the source to the empty states in the drain. **b:** The system transmission, that is, the probability of available electrons to flow through the 1D sample. In the localized regime, $\mathcal{T}_{SD}$ has sharp resonances on the spectral lines, which are associated with the presence of an electronic state in the sample, and exponentially lower values between them.

However, this method assumes that the transmission function is not affected by the connection to the leads, and does not take into account interactions between electrons or between electrons to phonons. Furthermore, the transmission function also does not consider non-equilibrium situations, such as strong bias voltages and non-uniform temperatures. In order to consider the above phenomena one should employ a more precise method for the calculation of the conductance. Here, we resort to the Non-Equilibrium Green's Function method (NEGF).

2.4 Non-Equilibrium Green's Function

The NEGF method[2], known also as the Kubo formalism [22], uses a generalized method to calculate conductivity in quantum systems based on Green's function method within the limit of linear response (i.e. small V_{SD}). As we shall see shortly, this method inherently enables the inclusion of interactions and non-equilibrium effects.

The Green's function is the response of a field, described by a differential equation, to an excitation from a delta-function source.

Considering the time independent Schrödinger equation -

$$\left[\hat{H} - E\hat{I}\right]\psi = 0, \tag{2.17}$$

where $\hat{H}$ is the Anderson Hamiltonian matrix, $\hat{I}$ is the identity matrix and ψ is the wave function. The associated Green's function $\hat{G}^0$ should solve -

$$\left[\hat{H} - E\hat{I}\right]\hat{G}^0(E) = \delta_i, \tag{2.18}$$

---

[2] Here we adopt the notation presented in a book by Supriyo Datta *"Electronic Transport in Mesoscopic Systems"* [23].

or equivalently, in the TB representation -

$$\hat{G}^0 = \left[E\hat{I} - \hat{H}\right]^{-1}. \tag{2.19}$$

In this framework, the Green's function element G^0_{ij} is the wave function amplitude at site j due to the existence of an electron in site i. Therefore, Green's function is also named 'propagator', since it represents the probability amplitude of the electron's to propagate in space (and time).

Taking into account the time-dependent Schrödinger equation leads to a different formulation of the advanced Green's function, G^A, and the retarded Green's function, G^R:

$$\hat{G}^A_{ij} = \left[E\hat{I} - \hat{H} - i\eta\hat{I}\right]^{-1}, \tag{2.20}$$

$$\hat{G}^R_{ij} = \left[E\hat{I} - \hat{H} + i\eta\hat{I}\right]^{-1}, \tag{2.21}$$

where η is an infinitesimal small positive number. G^A_{ij} and $G^R ij$ correspond to electron propagation from i to j or vice versa, respectively. The two matrices are the Hermitian conjugate of each other.

In order to calculate the conductance of a wire using Green's function, one should apply more explicit boundary conditions of the source and drain leads. This can be done by writing the full Green's function of the wire-leads system.

The Hamiltonian of the wire, $\hat{H}_w$, is the Anderson Hamiltonian (Eq.2.7)

$$\hat{H}_w = \sum_{j=1}^{L} \varepsilon_j \hat{c}_j^\dagger \hat{c}_j - \left(t \sum_{j=1}^{L-1} \hat{c}_j^\dagger \hat{c}_{j+1} + h.c.,\right), \tag{2.22}$$

while the two leads are represented by semi-infinite homogeneous chains

$$\hat{H}_{S/D} = -t\sum_{j'=1}^{\infty} \hat{c}_{j'}^{(S/D)\dagger}\hat{c}_{j'+1}^{(S/D)} + h.c., \tag{2.23}$$

where $H_{S/D}$ is the source/drain Hamiltonian, $\hat{c}_{j'}^{(S/D)\dagger}$ and $\hat{c}_{j'}^{(S/D)}$ are the single-particle creation and annihilation operators of the source/drain lead, respectively, and j' is the site index in the leads.

The leads are coupled to the wire by -

$$\hat{H}_{w,S/D} = -t_{S/D}\hat{c}_{1/L}^{(S/D)\dagger}\hat{c}_{1/L} + h.c., \tag{2.24}$$

where $t_{S/D}$ is the coupling amplitudes between the source/drain lead and the wire. Thus, the complete Hamiltonian of the system composed of the wire and leads is:

$$\hat{H} = \hat{H}_w + \hat{H}_S + \hat{H}_D + \hat{H}_{w,S} + \hat{H}_{w,D}. \tag{2.25}$$

2.5 Leads' self-energy

To proceed, we express Green's function $\hat{G}$ by its components - the wire ($\hat{G}_w$) and the left ($\hat{G}_S$) and right ($\hat{G}_D$) leads. The overall Green's functions can be written in the following form:

$$\hat{G} = \begin{pmatrix} \hat{G}_{S/D} & \hat{G}_{S/D,w} \\ \hat{G}_{w,S/D} & \hat{G}_w \end{pmatrix} = \begin{pmatrix} \left[(E \pm i\eta)\,\hat{I} - \hat{H}_{S/D}\right] & \hat{\tau}_{S/D} \\ \hat{\tau}_{S/D}^{\dagger} & \left[E\hat{I} - \hat{H}_w\right] \end{pmatrix}^{-1}, \tag{2.26}$$

where the matrices $\hat{\tau}_{S/D}$ represent the connection between the site inside the wire to the source/drain leads. Multiplying both sides by the inverse right-hand matrix results in two independent equations for $\hat{G}_w$:

$$\hat{\tau}^{\dagger}_{S/D}\hat{G}_{S/D,w} + \left[E\hat{I} - \hat{H}_w\right]\hat{G}_w = \hat{I}, \tag{2.27}$$

$$\left[(E \pm i\eta)\,\hat{I} - \hat{H}_{S/D}\right]\hat{G}_{S/D,w} + \hat{\tau}_{S/D}\hat{G}_w = 0. \tag{2.28}$$

Combining the two equations and taking into account both leads, one gets

$$\hat{G}_w = \left[E\hat{I} - \hat{H}_w - \hat{\Sigma}\right]^{-1}, \tag{2.29}$$

where the total self-energy is equal to $\hat{\Sigma} = \hat{\Sigma}_S + \hat{\Sigma}_D$ and $\hat{\Sigma}_{S/D}$ is given by -

$$\hat{\Sigma}_{S/D} = \hat{\tau}^{\dagger}_{S/D}\left[(E \pm i\eta)\,\hat{I} - \hat{H}_{S/D}\right]^{-1}\hat{\tau}_{S/D}, \tag{2.30}$$

where $+i\eta$ and $-i\eta$ refer to $\hat{\Sigma}^R_{D/F}$ and $\hat{\Sigma}^A_{S/D}$, respectively.

In the case of a 1D wire, $\hat{\tau}_S$ has only one non-zero term, as the wire-lead contact is only through the first element. As a result, the only relevant element in the left lead Green's function $\hat{G}_S$ is the $(1,1)$ element. For a semi-infinite homogeneous lead, it can be calculated analytically[3],

$$\hat{G}_{S,(1,1)} = \left[(E \pm i\eta)\,\hat{I} - \hat{H}_S\right]^{-1}_{(1,1)} = -\frac{1}{t}e^{\pm ika}, \tag{2.31}$$

where a is the lattice constant and k is the wave number of the electron, which follows the tight-binding dispersion relation

$$E = -2t\cos(ka). \tag{2.32}$$

---

[3] See Exercise 3.3 in Ref. [23].

Consequently, the self-energy of the source lead also has a single non-zero term, which is equal to

$$\hat{\Sigma}_S(1,1) = t_S^2 \left(-\frac{1}{t} e^{\pm ika} \right). \tag{2.33}$$

In a similar way, the single non-zero term of the drain lead's self-energy, $\Sigma_D(L,L)$, is equal to

$$\hat{\Sigma}_D(L,L) = t_D^2 \left(-\frac{1}{t} e^{\pm ika} \right).$$

2.6 Transmission from Green's function

Following Ref. [23], it is shown that transmission through the wire is related to $\hat{G}_w^{R/A}$ and to the self-energy $\hat{\Sigma}_{S/D}^{R/A}$ by -

$$\mathcal{T}_{SD} = \mathrm{Tr}\left[\hat{\Gamma}_S \hat{G}_w^R \hat{\Gamma}_D \hat{G}_w^A \right], \tag{2.34}$$

where $\hat{\Gamma}_{S/D}$ is the scattering rate from and into the wire -

$$\hat{\Gamma}_{S/D} = i\left[\hat{\Sigma}_{S/D}^R - \hat{\Sigma}_{S/D}^A \right] = -2 \cdot \mathrm{Im}\left(\hat{\Sigma}_{S/D}^R \right). \tag{2.35}$$

Writing Eqs. 2.34-2.35 in a more explicit form, and considering the single non-zero elements of $\hat{\Sigma}_S^R$ and $\hat{\Sigma}_D^R$, becomes -

$$\mathcal{T}_{SD} = \mathrm{Tr}\left[4 \cdot \mathrm{Im}\left(\hat{\Sigma}_S^R \right) \cdot \hat{G}_w^R \cdot \mathrm{Im}\left(\hat{\Sigma}_D^R \right) \cdot \hat{G}_w^A \right] = 4 \cdot \frac{t_S^2 t_D^2}{t} \cdot \mathrm{Im}\left(e^{ika} \right) \cdot \hat{G}_w^R(1,L) \hat{G}_w^A(1,L). \tag{2.36}$$

This results in a simple relation between the transmission function and the $(1, L)$ element of Green's function of the wire:

$$\mathcal{T}_{SD} = \left(\frac{t_S t_D}{t}\right)^2 \cdot (\hbar\nu)^2 \cdot \left|\hat{G}_w^R(1, L)\right|^2, \tag{2.37}$$

where ν is the electrons' velocity in the leads -

$$\hbar\nu = \frac{\partial E}{\partial k} = 2at \cdot \sin(ka). \tag{2.38}$$

2.7 Conductance from Green's function

Similar to the Landauer-Buttiker method, for the calculation of the total current through the system, one should take into account the electronic population in the leads and applied voltage. Assuming that the leads are in thermal equilibrium at temperature T, the probability of finding an electron with energy E in the source/drain lead is given by the Fermi distribution $f_{S/D}$. Hence, the current also depends on the electro-chemical potential in the leads μ_S/D, with a voltage drop V_{SD} between them -

$$\mu_D = \mu_S - eV_{SD}. \tag{2.39}$$

In order to calculate the current through the system using the NEGF method, we have to define the in-scattering and out-scattering functions, which represent the rate at which electrons enter and escape the wire at energy E:

$$\hat{\Sigma}^{in}_{S/D}(E) = f_{S/D}\hat{\Gamma}_{S/D}, \tag{2.40}$$

$$\hat{\Sigma}^{out}_{S/D}(E) = (1 - f_{S/D})\hat{\Gamma}_{S/D}, \tag{2.41}$$

In addition, we must define the correlation functions that describe the occupation of electrons (n) and holes (p) within the wire, $\hat{G}^n$ and $\hat{G}^p$. To find the correlation functions, we utilize one of the main results of the NEGF method, the kinetic equation[4]:

$$\hat{G}^{n/p} = G^R \hat{\Sigma}^{in/out} G^A, \tag{2.42}$$

where

$$\hat{\Sigma}^{in/out} = \hat{\Sigma}_S^{in/out} + \hat{\Sigma}_D^{in/out}. \tag{2.43}$$

Using these definitions, one can derive that current density in the wire is equal to -

$$i_{S/D}(E) = \frac{e}{h} \mathrm{Tr} \left(\hat{\Sigma}_{S/D}^{in} G^p - \hat{\Sigma}_{S/D}^{out} G^n \right). \tag{2.44}$$

where the current is proportional to the rate at which the incident electron succeeds in finding an empty state in the wire, $\Sigma_{S/D}^{in} G^p$, minus the rate at which electrons succeed in leaving the wire, $\hat{\Sigma}_{S/D}^{out} G^n$.

In a case where the temperature in both leads is equal and there are no incoherent effects (such as electron-electron or electron-phonon interactions) the current density in Eq. 2.44 can be represented by a transmission function, $\mathcal{T}_{SD}$, multiplied by Fermi distributions, similar to the Landauer-Buttiker formalism -

$$I = \int i_{S/D}(E) dE = \int \frac{2e^2}{h} \mathcal{T}_{SD}(E) \left[f_S \left(E, \mu_S, T \right) \right) - f_D \left(E, \mu_D, T \right) \right] dE. \tag{2.45}$$

This coherent current and associate conductance $G = I/V_{SD}$, as derived above, are an exact result that arises from the quantum mechanical considerations in the wire, by assuming only the tight-binding model the semi-infinite leads. However, in the non-equilibrium case, such as when the temperature is unequal in the leads or when large source-drain voltage exist, or alternativel, in the presence of interactions - both $\Sigma^{in/out}$ and $\Sigma^{R/A}$ become dependent on other parameters, and one cannot

---

[4] See Sections 8.3-8.6 in [23].

reduce Eq. 2.44 to the above simple form. Hence, Eqs. 2.40-2.44 must be solved explicitly.

Even though the above method's result was a relatively simple calculation for the 1D non-interacting case, in Chapters 4 and 5, we demonstrate that in the disordered case, the coherent conductance, calculated numerically by the NEGF method, shows both an unexpected temperature dependence even without considering phonons, and a surprising anomaly of modes that could considerably affect the experimental conductance measurements in such systems.

2.8 Density of states calculation

The NEGF method allows the calculation of the electronic density in space as well as the DOS in energy, using the local density of states function (LDOS). As one may expect, for an isolated wire whose Hamiltonian H_w is given by Eq. 2.7, LDOS is equal to a set of Dirac delta functions -

$$\rho\,(j,E) = \sum_i |\psi_i(j)|^2\,\delta(E-E_i). \tag{2.46}$$

However, as soon as the wire is connected to leads, the delta functions are broadened, the system becomes non-Hermitian and the wave vectors $\psi_i(j)$ cannot be extracted directly from $\hat{H}_w$. In this case, LDOS is expressed via the spectral function, defined as[5]:

$$\hat{A} = i\left[\hat{G}^R - \hat{G}^A\right] = -2\cdot\mathrm{Im}(\hat{G}^R). \tag{2.47}$$

The diagonal elements of $\hat{A}$ represent the LDOS, $\rho\,(j,E)$, while its trace is the

---

[5] See pages 149-155 in [23].

DOS -

$$\mathcal{N}(E) = \frac{1}{2\pi}\mathrm{Tr}\hat{A} \tag{2.48}$$

As noted above, $\hat{G}^R$ represents the the probability of an electron to be transferred from one state to another. In a like manner, the imaginary part of $\hat{G}^R$ is associated with the probability of an electron to be measured at a specific point, a factor directly related to the electronic density.

2.9 Characteristic results of transmission and DOS in 1D systems

In a perfect wire (i.e. in the absence of disorder) and with perfect connections to leads ($t_{S/D}$=1), one may expect a perfect transmission for every energy E. This is indeed the case within the range of the tight binding dispersion bandwidth $[0, 4t]$ (see Eq. 2.32), as depicted in Fig. 2.3 (red line).

Naturally, for a disconnected wire there is no transmission. A weakly connected wire ($t_{S/D} \ll 1$), however, results in large peaks in the transmission function (blue line in Fig. 2.3), similar to an optical cavity. The locations of these peaks in E are associated with the presence of electronic eigen-states with similar eigen energies, as can be seen by comparing these to the density of states $\mathcal{N}(E)$ plot. Additionally, as is also seen from the plot, the DOS is higher at the edges of the energy band. This result is in agreement with the theoretical derivation of DOS in 1D systems -

$$\mathcal{N}(E) = \frac{1}{2\pi}\frac{1}{\sqrt{t \cdot E}}, \tag{2.49}$$

where as was derived earlier, $t = \hbar^2/2ma^2$.

Equivalently, adding even a small degree of disorder to a perfect-coupled system

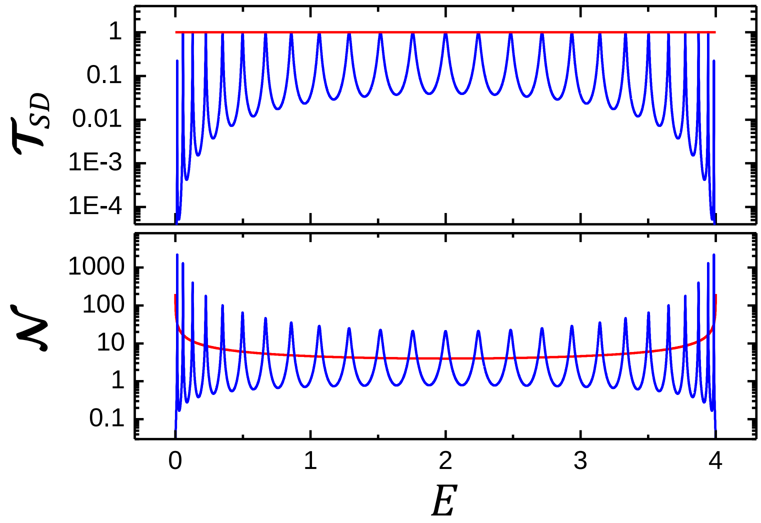

Figure 2.3: Transmission function (upper panel) and DOS (lower panel) of non-disordered wire ($W = 0$), with $L = 25$ and perfect connections to the leads $t_S = t_D = 1$ (blue lines), as well as with small connection $t_S = t_D = 0.1$ (see text).

results in fluctuations in transmission (Fig. 2.4). The inhomogeneity of the atomic potential is separating regions in the wire, and the result is multiple semi-isolated 'cavities' which generate these random maxima. As W increases, the localization length ξ eventually becomes shorter than the system length L, and the system is localized. In this case, the average value of the transmission has an exponential dependence on the ratio ξ/L -

$$\langle \mathcal{T}_{SD} \rangle \propto \exp\left(-\frac{L}{2\xi}\right). \tag{2.50}$$

Moreover, as we shall see in the next chapters, in the presence of disorder, the system shows several non-trivial phenomena, such as the breaking of the one-to-one correlation between energy levels and transmission resonances, and a surprising temperature dependence.

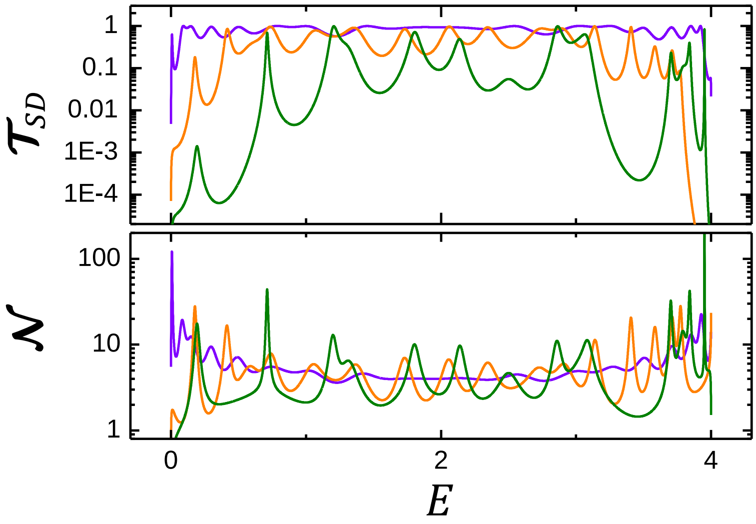

Figure 2.4: Transmission function (upper panel) and DOS (lower panel) of disordered wire with $W = 0.5$ (purple), $W = 1$ (orange) and $W = 0.5$ (green), with $L = 25$ and perfect connections to the leads $t_S = t_D = 1$ (see text).

Chapter 3

Numerical Methods

As result of the NEGF method presented in Chapter 2, the calculation of quantum system conductance involves the inversion of $L \times L$ complex matrices (Eq. 2.29), and overall integration of relevant energies (Eq. 2.45). In this chapter, these issues are discussed from a numerical point of view. A sample of MATLAB code for the calculation of conductance in a typical disordered system is presented in the appendix.

3.1 Inversion of Green's function matrices

The Green's function calculation of a wire of length L requires the inversion of the matrix $\left[E\hat{I} - \hat{H} - \hat{\Sigma}\right]$, where E is the electron energy, $\hat{I}$ is the identity matrix, $\hat{H}$ is the Anderson Hamiltonian, and $\hat{\Sigma}$ is self-energy. Using the LU decomposition method, the inversion of an $L \times L$ matrix requires up to $2L^3/3$ operations. In addition, each inversion gives a single energy value of the transmission function $\mathcal{T}(E)$, as the conductance is a result of transport of electrons with all possible energies (or at least within the TB energy band). These two requirements limit the wire length to about 1000 sites for considerable computational time (hours or a few days).

However, in following with Eq. 2.25, the Hamiltonian that represents the 1D wire is a tridiagonal matrix, as the only allowed hopping process occurs between neighboring sites. The latter part in $\hat{G}$, the self-energy term, has only two non-zero elements that are also on the diagonal, as derived in Sec. 2.5. Thus, the inversion is applied on sparse matrices that have a tridiagonal form, i.e. all elements are zero except for the matrix diagonal and the two adjacent off-diagonal rows.

Inversion and diagonalization of sparse matrices are less complex, but a different method must be derived for each type of matrix. Here, we use a method that was developed by Usmani [24, 25].

For a given $L \times L$ tridiagonal matrix of the form -

$$\hat{M} = \begin{bmatrix} a_1 & b_1 & & & \\ c_1 & a_2 & b_2 & & \\ & c_2 & \ddots & \ddots & \\ & & \ddots & \ddots & b_{L-1} \\ & & & c_{L-1} & a_L \end{bmatrix}, \tag{3.1}$$

the $(\hat{M}^{-1})_{ij}$ element is given by -

$$\left(\hat{M}^{-1}\right)_{ij} = \begin{cases} (-1)^{i+j} b_i \cdots b_{j-1} \theta_{i-1} \varphi_{j+1} / \theta_L & \text{if } i \leq j \\ (-1)^{i+j} c_i \cdots c_{i-1} \theta_{j-1} \varphi_{i+1} / \theta_L & \text{if } i > j \end{cases} \tag{3.2}$$

where θ_i and φ_i follow recurrence relations as follows:

$$\theta_i = a_i \theta_{i-1} - b_{i-1} c_{i-1} \theta_{i-2} \tag{3.3}$$

for $2 \leq i \leq L$, with the initial condition $\theta_1 = a_1$ and $\theta_0 = 1$, and -

$$\varphi_i = a_i \varphi_{i+1} - b_i c_i \phi_{i+2} \tag{3.4}$$

for $L-1 \leq i \leq 1$ and initial condition $\varphi_{L+1} = 1$ and $\varphi_L = a_L$.

In our case, $b_i = c_i = -t$ for every i. Since we normalize the energy scale to $t = 1$, the relation is even simpler:

$$\left(\hat{M}^{-1}\right)_{ij} = \begin{cases} (-1)^{i+j}\theta_{i-1}\varphi_{j+1}/\theta_L & \text{if } i \leq j \\ (-1)^{i+j}\theta_{j-1}\varphi_{i+1}/\theta_L & \text{if } i > j \end{cases} \tag{3.5}$$

where -

$$\theta_i = a_i\theta_{i-1} - \theta_{i-2}, \tag{3.6}$$

$$\varphi_i = a_i\varphi_{i+1} - \phi_{i+2}. \tag{3.7}$$

This procedure involves the extraction of θ and φ (complexity of order L) only once, and the multiplication of the result for every i and j (Eq. 3.5); namely, the total complexity is $\mathcal{O}(L^2)$.

Furthermore, as was mentioned, the transmission function of a 1D wire can be calculated from a single element in Green's function, $\hat{G}^R_w(1, L)$. We thereby only need to calculate θ_L and place it in the following equation:

$$\hat{G}^R_w(1, L) = \frac{(-1)^{1+L}}{\theta_L} \tag{3.8}$$

while the transmission function is (Eq. 2.37) -

$$\mathcal{T}_{SD} = \left(\frac{t_S t_D}{t}\right)^2 \cdot (\hbar\nu)^2 \cdot \left|\hat{G}^R_w(1, L)\right|^2. \tag{3.9}$$

This simple $\mathcal{O}(L)$ method allow us to easily calculate the conductance of larger systems of up to $L = 10000$ at much shorter times. In larger systems, the dynamic memory serves as problem, as it consumes above 1 gigabyte. To overcome this memory issue, we must keep in mind that our tridiagonal Hamiltonian and self energy terms are not trivial (i.e. they do not equal zero or one) only on the diagonal. Using the above method to find $\hat{G}^R_w(1, L)$, we do not need the $L \times L$ matrix, and can keep only the diagonal in the computer's memory. By utilizing this method, we were able to calculate even $L = 10^6$ systems.

Still, other than accuracy issues, the only important length scale of localized systems is the ratio ξ/L. Hence, enlarging the system is equivalent to increasing disorder, and there is no reason to spend computer time on overly large wires. Additionally, in contrast with the transmission function, the density of states $\mathcal{N}(E)$ has to be calculated by the trace of the Green's function (Eq. 2.48). Therefore, in cases where $\mathcal{N}(E)$ is needed, one should calculate the whole diagonal of $\hat{G}$, which leaves us with $\mathcal{O}(L^2)$ complexity.

3.2 Integration with the transmission function

According to the Landauer-Buttiker method, in the presence of temperature, the total current (and therefore the conductance) receives contribution from all available energies in the system (Eq. 2.45), due to the broadening of Fermi distributions. Furthermore, in a localized regime($\xi < L$), $\mathcal{T}_{SD}$ exhibits sharp peaks at certain energy values, with exponentially lower valleys between them. Numerical integration with such a function is a challenging task, as even at extremely high resolution in E, the integration could miss these exponentially higher transmission peaks.

As will be discussed in Chapters 4 and 5, interesting phenomena occur also in moderate disorders, and the disorder can be limited by $\xi = L/20$ or less. In this range, exponential decay around the highest peaks is relatively slow, which means that the area enclosing the resonance in $\mathcal{T}_{SD}$ is finite, so that the overall integration is barely affected after a certain resolution (R). For instance, in the above case of $\xi = L/20$, 1 million samples within the $[0, 4t]$ tight-binding bandwidth results in a reasonable accuracy, as demonstrated in Fig. 3.1 for $L = 500$ and $\xi \approx 25$. By using the $\mathcal{O}(L)$ inversion method, we were able to calculate enough iterations to evaluate the conductance in a variety of disorders, temperatures, bias voltages, etc.

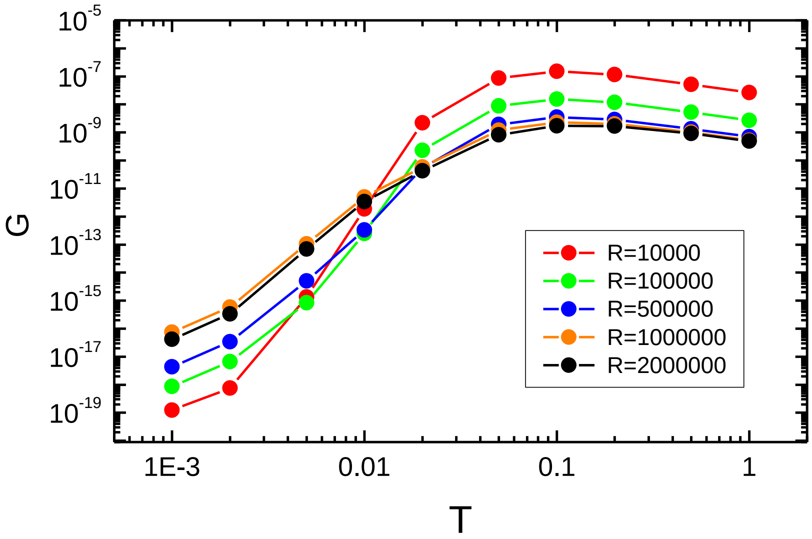

Figure 3.1: The impact of the integration resolution R, demonstrated by calculation of conductance as a function of temperature for a system with $L = 500$ and $W = 2$, i.e. $\xi \approx L/20$. As can be seen, the integration converges at a resolution of about 1 million samples from the [0,4t] bandwidth.

3.3 Appendix: Characteristic MATLAB code for calculating conductivity

```
% Control Parameters
    L = 500; W = 2; V_SD = 0.00001;
    t = 1; t_S = 1; t_D = 1; mu = 0;
    minE = -2; maxE = 2; resE = 1000000; deltaE = (maxE-minE)/(resE);
    Tvec = [0,0.001,0.005,0.01,0.05,0.1,0.5,1];

% Initialization
    H = zeros(L);    B = zeros(L);
    Trans = zeros(resE-1,2);    G = zeros(length(Tvec),2);

% Setting Hamiltonian
    for i=1:L-1
        H(i,i+1) =-1;   H(i+1,i) =-1;   H(i,i) = W*(rand()-0.5);
    end
H(L,L) = W*(rand()-0.5);

% Calculating transmission by Green's function
    for Ei=1:(resE-1)
     E = minE+deltaE*Ei;
     k = acos(-E/(2*t));
     invG = E*eye(L)-H;
     invG(1,1) = invG(1,1)+t_S*exp(1i*k);
     invG(L,L) = invG(L,L)+t_D*exp(1i*k);
     Gr1L = TriDiagInv1L(invG);
     Trans(Ei,1) = E;
     Trans(Ei,2) = 4*t_S*t_D*(((sin(k))).^2)*(abs(Gr1L))^2;
    end

% Calculating conductance from transmission
for T_i=1:length(Tvec)
      T = Tvec(T_i);
      G(T_i,1) = T;
    for Ei=1:(resE-1)
            fSminusfD = (1/(exp((E-mu-V_SD)/T)+1))-(1/(exp((E-mu)/T)+1));
            E = minE+deltaE*(Ei);
            G(T_i,2) =G (T_i,2)+Trans(Ei,2)*deltaE*fSminusfD/V_SD;
    end
end

% Plotting
figure(1)
loglog(G(:,1),G(:,2))
```

And the calculation of $\hat{G}_{1L}$:

```
function [InvMat1L] = TriDiagInv1L(Mat)
    L=length(Mat);
    theta=zeros(1,L);
    theta(1)=Mat(1,1);
    theta(2)=Mat(2,2)*theta(1)-1;
    for i=3:L
        theta(i)=Mat(i,i)*theta(i-1)-theta(i-2);
    end
    InvMat1L=(-1)^(L+1)/theta(L);
end
```

Chapter 4

Transmission resonance anomaly in 1D disordered quantum systems

This chapter presents a study that investigates the relations between electronic eigenstates and conductance in one-dimensional disordered systems[1]. This study was carried out with the guidance of Prof. Richard Berkovits, in fruitful cooperation with Prof. Valentin Freilikher and Prof. Moshe Kaveh, both from Bar-Ilan University, as well as with Dr. Yuri. P. Bliokh from the Technion - Israel's Institute of Technology.

We show that, in contrast with homogeneous (i.e. non-disordered) systems, in systems with open boundary conditions and weak or moderate disorder, only a part of the states exhibits resonant transmission and contributes to conductivity. The rest of the eigenvalues are not associated with peaks in the transmission, and the amplitudes of their wave functions do not exhibit a significant maxima within the sample. In a wide range of disorder strengths, the average ratio of the number of transmission peaks to the total number of eigenstates is close to the value $\sqrt{2/5}$. We derive this universal number analytically in the weak-scattering

---

[1] This study was recently published in Physical Review B as an identically entitled paper [26].

approximation. Moreover, unlike ordinary states, the lifetime of these 'hidden' modes remains constant or even decreases as disorder becomes more pronounced, depending on coupling with the leads.

These results are a perfect analogy of the spectral and transport properties of light in one-dimensional, randomly inhomogeneous media [27], which provides strong grounds to believe that the existence of hidden, non-conducting modes is a general phenomenon inherent to 1D open random systems, and their fraction of the total number of states is the same for quantum particles and classical waves.

4.1 Open systems and quasinormal modes

Electromagnetic transmission through optical cavities (etalons) is a well known phenomenon, demonstrating peaks in transmission at frequencies that are exactly a multiplication of the optical path. The standing waves in the cavity are directly related to the eigen-modes of the system. However, these two statements are only true for isolated systems with perfect reflection at the cavity's ends (or very close to unity). If the mirrors are only partially reflective, the modes are not well-defined and the transmission resonances change.

In a recent paper by Bliokh et al. [27], an interesting finding regarding transmission through disordered optical cavities was presented. It was analytically, numerically and experimentally shown that in weakly disordered one-dimensional dielectric media, a substantial fraction of optical quasinormal modes (QNMs) is hidden, that is, it could not be detected by transmission measurements (see Fig. 4.1).

In the following sections, we show that such behavior should also be expected

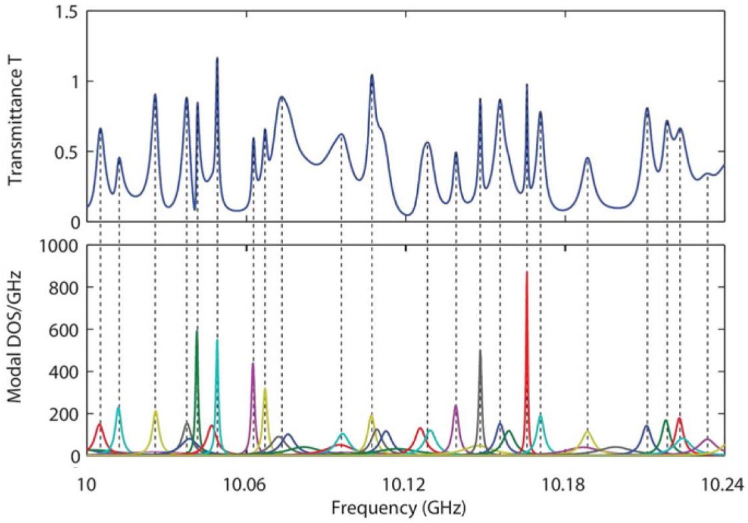

Figure 4.1: Upper panel: Experimental result of the optical transmittance (i.e. the power transmission) of microwaves through a disordered quasi-1D copper waveguide tube (7.3cm diameter, 40cm length), filled with alumina spheres (refraction index=3.14) at random positions, for frequencies with a range of 10 to 10.24GHz (wavelengths from 2.998cm to 2.928cm). **Lower panel:** Fit of the experimental data to the sum of Lorentzian broadened modes shows 39 modes in the frequency range, while only 22 maxima are presented in the transmission. All other 17 modes are hidden (**Bliokh et al., 2015 [27]**).

in the transmission of other physical systems, particularly electron transport in disordered conductors.

Connecting an optical system to the outer environment and allowing a flow of energy and particles through it, usually causes the system to become non-Hermitian, hence, the eigen-modes do not represent any well-defined physical quantity. However, it was suggested to analyze open optical systems using the approximated method of quasinormal modes (QNMs) [28–32], described below. Similarly, states of an open electronic system can also be interpreted in terms of quasinormal states (QNSs) [28, 33].

Quasinormal state analysis is a powerful tool for investigating different open systems. Since energy can escape, open systems do not conserve energy, therefore, the associated mathematical operators are not Hermitian [28]. From a mathematical point of view, QNSs are a generalization of the notion of eigenstates of closed (Hermitian) systems, and can be found as a solution for satisfying outgoing-wave boundary conditions. In the limit of zero leakage, these QNSs reduce to the normal states of the corresponding closed system. QNSs form a complete set, and are orthogonal under a modified definition of the inner product, providing an eigenfunction expansion of Green's function and the time-evolution operator [29, 30]. The imaginary parts of eigenvalues of a non-Hermitian Hamiltonian depict the lifetimes of QNMs [31, 32], which are finite due to the flow of electrons between leads.

4.2 Motivation - conductance resonances

Recasting the classical problem considered in Bliokh et al.'s paper [27] for electronic systems is of interest, since one can ask additional questions regarding QNSs, which are difficult or non-relevant in optics.

Specifically, one can delve deeper into the hidden modes' (HM) response to non-equilibrium conditions, such as large applied source-drain voltage and biased temperature, or examine other effects, e.g. electron-electron or electron-phonon interactions, etc. Moreover, many experimental procedures use conductance to probe and count the electronic states of mesoscopic and microscopic systems, such as narrow channels of semiconductors [34–38],carbon nanotubes [39, 40], and quantum point ontacts [41]. As we show here, adding even a small degree of disorder will result in the disappearance of modes. Hence, a better understanding of this nontrivial relation between eigen-modes of isolated systems and transmission peaks in open systems is essential.

Although there is common belief that after more than fifty years of intensive study, the transport properties of 1D disordered systems are clearly understood - surprisingly, the existence of hidden modes in such systems has been completely overlooked. This is perhaps due to the attention being mostly focused on the localization in strong disorders, while the limit of weak impurities (ballistic regime) was deemed trivial.

4.3 Observation overview

Here, we study the electronic spectra of one-dimensional disordered systems in the non-equilibrium Green's function (NEGF) formulation, presented in Sections 2.4-2.8, which enables us to address the problems unique to electronic transmission.

We investigate the evolution of the transmission (Eq. 2.37), the conductance (Eq. 2.45) and density of states (Eq. 2.48) of quantum-mechanical particles in a random 1D potential (tight-binding wire), for a wide range of disorder strengths, from ballistic to strong localization regimes.

In partially open homogeneous structures, like clean quantum wires, open resonators and so forth, each QNS has a corresponding transmission resonance (TR) (peak in the frequency spectrum of the transmission coefficient) with resonant energy equal to the real part of the eigenvalue [42]. This is not necessarily the case in open *disordered* samples. In the presence of disorder, the position and height of the TR fluctuate, a phenomenon associated with mesoscopic conductance fluctuations [43, 44].

Furthermore, the calculations show that one-to-one correspondence between a number of QNSs and TRs can be broken as well. Due to complex interference between multiple scattered random fields in weakly disordered systems, some QNSs become invisible in transmission (hidden), and the number of transmission peaks falls to $\sqrt{2/5} \cdot N_{QNM}$ (where N_{QNM} is the total number of QNSs).

In the following sections, we show that the coexistence of two types of QNSs (ordinary and hidden) is a rather general phenomenon intrinsic to randomly inhomogeneous one-dimensional quantum-mechanical systems as well. Not only do the hidden electron states exist and manifest analogues properties as the corresponding solutions of Maxwell equations, the relative number of hidden states for weak and moderate disorders is also the same. Its mean value in a given energy interval remains close to the constant $1 - \sqrt{2/5}$ over wide range of disorder strengths and lengths of the system. The value $1 - \sqrt{2/5}$ follows from general statistical properties of random trigonometric polynomials.

In contrast to the well-known behavior of localized states, the lifetime of a hidden state does not increase with increasing fluctuations of the potential, but rather remains unchanged or even decreases, depending on the strength of the coupling to the leads. The eigenvectors (solutions of the Schrödinger equation satisfying the outgoing boundary conditions) of such modes are also very unusual. The spatial profiles of their amplitudes are neither concentrated near both edges of the system with a minimum in the center as in symmetric clean systems, nor are they localized as in a potential with strong fluctuations. On the contrary, the wave functions of the hidden states nestle near one of the wire edges and exponentially decrease toward the other.

An important feature of HMs that is particular to electronic systems is that though they appear in the DOS in the same way the ordinary modes do, they are non-conducting, i.e. they do not contribute to conductance, even in the ballistic regime. The quantum mechanical treatment of these hidden QNSs by the NEGF method enables a simple analysis of their spatial behavior. We show that the TR anomaly is directly related to hybridization with the leads, and therefore, it becomes more subtle at higher disorders and vanishes when the localization length is shorter than the system length.

To complete the chapter, in the last section, we repeat the derivation of the ratio $\sqrt{2/5}$ based on the single scattering approximation in 1D, and on the nature of trigonometric polynomial functions.

4.4 Results and discussion

Transmission resonances

In an isolated wire composed of L sites with random potentials, the eigenstates vary with the on-site disorder strength, yet each state has a real energy eigen-value, and the DOS, $\mathcal{N}(E)$, is in following with Eq.(2.46).

However, once the wire is coupled to the leads, the eigenvalues become complex, but the DOS can nevertheless still be defined (see Eq. 2.48). In this case, $\mathcal{N}(E)$ shows peaks at energies close to the eigenvalues of the isolated system E_i, with a broadening that becomes wider as $t_{S/D}$ approaches 1. The total number of quasinormal states is given by the integration $N_{QNS} = \int_{-\infty}^{\infty} \mathcal{N}(E')dE'$. Obviously, the conservation of degrees of freedom oblige $N_{QNS} = L$.

The transmission function $\mathcal{T}_{SD}$ in an open and disordered system, similar to the DOS, shows sharp resonances located close to the eigen-energies of the wire E_i, with exponentially lower valleys between them. Naturally, the mean value of the transmission is attenuated as the disorder increases and can be scaled by

$\mathcal{T}_{SD} \sim \exp(-L/\xi)$, as was shown in Fig. 2.4. However, in contrast to the DOS, the transmission significantly changes in an open wire, as some of the peaks that existed in the clean wire disappear.

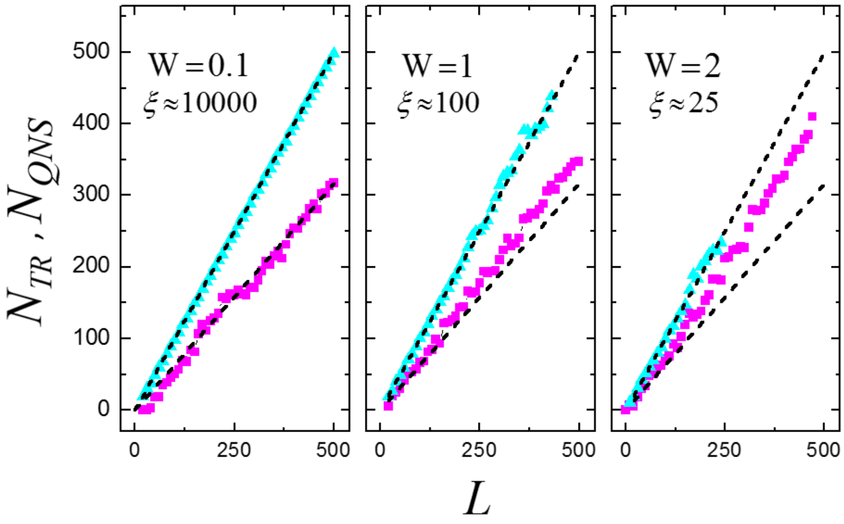

Figure 4.2: The number of the transmission maxima N_{TR} (magenta squares) and the number of quasi normal modes, N_{QNS}, calculated by integration with the density of states (cyan triangles) for a disordered 1D wire as a function of the length L. The cases of low disorder $\xi \approx 10000$ (left); medium disorder $\xi \approx 100$ (middle); and strong disorder $\xi \approx 25$ (right) - are presented. In the low disorder case, the number of transmission peaks fits $N_{TR} = \sqrt{2/5}L$ (lower black dashed lines), while the integrated density of states is in following with L (upper black dashed lines). In higher disorders, more transmission resonances are seen (i.e. $N_{TR} > \sqrt{2/5}L$) due to localization. The missing data of N_{QNS} at higher disorder levels is due to numerical inaccuracies in the integration with the exponentially high and narrow peaks of $\mathcal{N}(E)$.

In Fig. 4.2, we present the results for the number of quasi-normal states, N_{QNS}, and for the number of transmission resonances (maxima in $T_{SD}(E)$), N_{TR}, as functions of the wire size L for different strengths of disorder (hereinafter, all lengths are presented in units of the lattice constant a, which is set to unity).

As can be seen, the dependence of N_{TR} on L is quite different from that of N_{QNS}. For a weak disorder ($\xi \sim 10^4 \gg L$) , N_{TR} is smaller than N_{QNS} and equals $\sqrt{2/5}L$. The rest of the QNSs are hidden, exactly as they are in optical systems considered in Ref. [27]. As the disorder becomes stronger, the hidden (with no associated transmission resonances) modes gradually reappear as peaks in the transmission function. This can be seen in the increase of the slope of N_{TR} versus L with increasing W. In a stronger disorder, this ratio is closer to one.

Hidden modes' behavior in space

To understand the nature of the hidden states, let us juxtapose the transmission peaks with the eigen-vectors of the disconnected wire. In the upper panel in Fig. 4.3 we plot $\mathcal{N}(E)$ and $\mathcal{T}_{SD}(E)$ for a typical realization of disorder in a $L = 500$ wire with $W = 1$, $\xi \sim 10^2$. The corresponding modulus-squared eigen-vectors for the isolated system $|\psi_i(r)|^2$ are plotted in the middle panel. It is easy to see that each transmission peak (and the associated peak in DOS) corresponds to an eigenstate of the isolated wire, and the peaks in $\mathcal{N}(E)$ and $\mathcal{T}_{SD}(E)$ are close to the real eigenvalue ϵ_i (indicated by vertical dashed lines). However, the hidden state #216 does not show a peak in the transmission, and the DOS exhibits only a very broad maxima in this eigenvalue. The distinction between hidden and ordinary states also shows up in the local density of states, which for an i_{th} eigenstate we define as $\rho_i(r) = \int_{\epsilon_i-\Delta/4}^{\epsilon_i+\Delta/4} \rho\,(r, E)\, dE$,where ϵ_i is the level's-eigen energy and Δ is the level spacing. Indeed, while for the ordinary states the local DOS of the connected wire is similar to the density of the disconnected wire i.e., $\rho_i(r) \sim |\psi_i(r)|^2$, for the hidden mode (state 216), there is a huge difference between $\rho_{216}(r)$ and $|\psi_{216}(r)|^2$ (see lower frame of Fig. 4.3).

In Fig. 4.4, the LDOS map of the same system in the relevant energy range is presented. The hidden mode originally located at $E = 1.58$ (#216) is broadened much beyond the mean level spacing. The spatial distributions of the two types of states are also quite different. Namely, the hidden ones are always nestled against

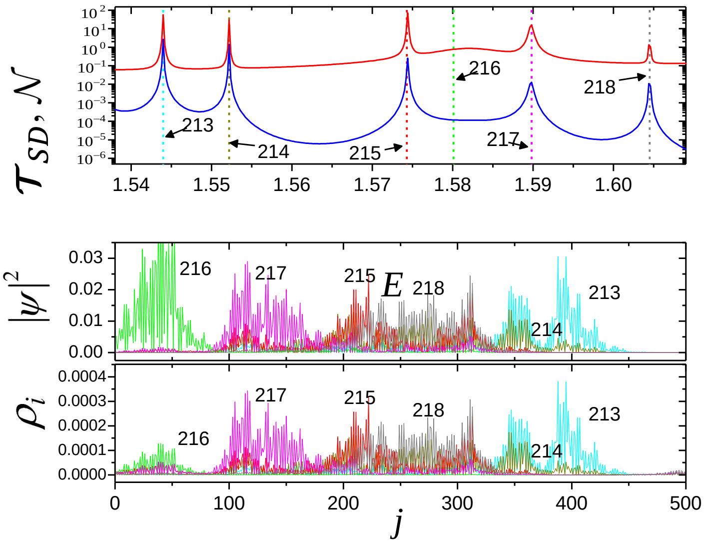

Figure 4.3: Upper frame: Typical density of states $\mathcal{N}(E)$ (top red line) and transmission $\mathcal{T}_{SD}(E)$ (bottom blue line) spectra of a particular realization of disorder ($L = 500$, $W = 1$, $t_{S/D} = 1$). The positions of the isolated Hamiltonian eigenvalues ϵ_i are indicated by the vertical dashed lines. **Middle frame:** The squared eigenvectors $|\psi_i(r)|^2$ of the isolated Hamiltonian as a function of the position along the wire, j. The 216th eigenstate is located close to the system edge, therefore, its transmission resonance is washed out (see upper frame) when the wire is coupled to the leads. **Lower frame:** The local density of states integrated in the vicinity of the i-th disconnected eigenvalue ϵ_i, $\rho_i(r) = \int_{\epsilon_i-\Delta/4}^{\epsilon_i+\Delta/4} \rho(r, E)\, dE$. For most states $\rho_i(r) \sim |\psi_i(r)|^2$, except for the hidden mode (the 216th eigenstate) for which the local density close to the leads is strongly suppressed.

an edge of the sample, so that when the wire is coupled to the leads, these modes become strongly hybridized with the states of the neighboring lead and do not reach the opposite edge of the sample.

Moderate disorder

Numerical calculations show that in a weak disorder, where ξ is larger than the system size, only $\sqrt{2/5N}$ transmission peaks exist, exactly as they do in the case of weakly scattered electromagnetic waves. However, for stronger disorders where $\xi < L$, only a small fraction (of order $2\xi/L$) of the states hybridize with the leads. States that do not hybridize with the leads might have a very small transmission,

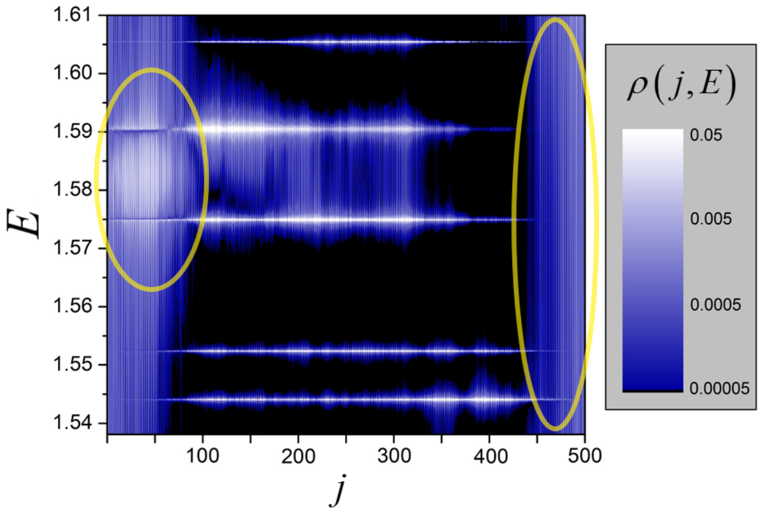

Figure 4.4: A color map of the local density of states $\rho(j,E)$ of the system described in Fig. 4.3. The 'ordinary' modes (in $E \sim 1.544, 1.552, 1.575, 1.59, 1.604$) show a relatively narrow energy distribution, while the hidden mode originally located in $E \sim 1.58$ (marked with a yellow circle on the left) is significantly broadened due to coupling to the left lead. A similar hidden mode's tail can be noted at the right end, relating to a state hidden at higher energy (long yellow circle).

but nevertheless, they do have a distinct transmission peak. Thus, we expect that N_{TR}/N_{QNS} will scale with ξ/L. Indeed, as can be seen in Fig. 4.5, this seems to hold for different values of L and disorder strength W.

One can present the above argument in a more quantitative form. The overlap of a localized state with the left lead should be proportional to $\exp(-bj_0/\xi)$, where j_0 is the center of the localized state and b is a numerical constant of order unity, depending on the details of the boundary condition. Averaging the region $0 < j_0 < L/2$ for the left lead and $L/2 < j_0 < L$ for the right lead results in:

$$f = \frac{2}{L} \cdot \sum_{j_0=1}^{L/2} e^{-bj_0/\xi} = \left(\frac{2}{L}\right) \frac{1 - e^{-bL/2\xi}}{e^{b/\xi} - 1} \sim \left(\frac{2\xi}{bL}\right) \left(1 - e^{-bL/2\xi}\right). \tag{4.1}$$

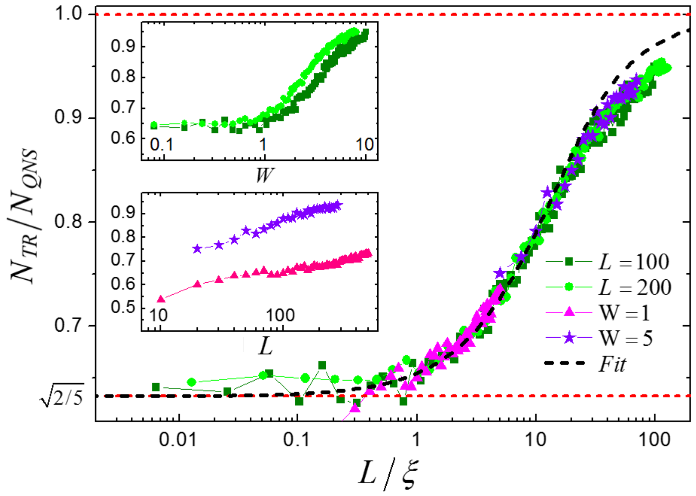

Figure 4.5: The ratio of the number of observed transmission peaks to the length of the wire N_{TR}/N_{QNS} for various disorder strengths, W, and wire lengths L. **Upper inset:** Systems with lengths $L = 100$ and $L = 200$ for various disorder values. **Lower inset:** Systems with disorder strengths $W = 1$ and $W = 5$ for various lengths. **Main panel:** The ratio N_{TR}/N_{QNS} as a function of the scaling parameter L/ξ for the results presented in the insets. All curves of N_{TR}/N_{QNS} fall on top each other. For $L/\xi < 1$, $N_{TR}/N_{QNS} \sim \sqrt{2/5}$ remains. Once $L/\xi > 1$, the ratio increases until $N_{TR}/N_{QNS} \to 1$ for large values of L/ξ, i.e. for strong localization, all modes have transmission resonances. The black dashed line represents the dependence of N_{TR}/N_{QNS} on L/ξ, according to Eq. 4.1-4.2 with $b = 1/4$.

Finally, the ratio of the number of transmission peaks to total number of states is obtained by subtracting the fraction of hidden modes times the probability they overlap with the leads -

$$N_{TR}/N_{QNS} = 1 - f \cdot \left(1 - \sqrt{2/5}\right), \tag{4.2}$$

which after fitting the parameter b, reasonably matches the numerical results (Fig. 4.5).

In Fig. 4.6, we demonstrate the evolution of the transmission spectrum with an increasing strength of disorder. As W grows, the hidden modes gradually disconnect from the boundaries of the wire and form transmission resonances, until all of them become ordinary, $N_{TR}/N_{QNS} \to 1$, for a large W.

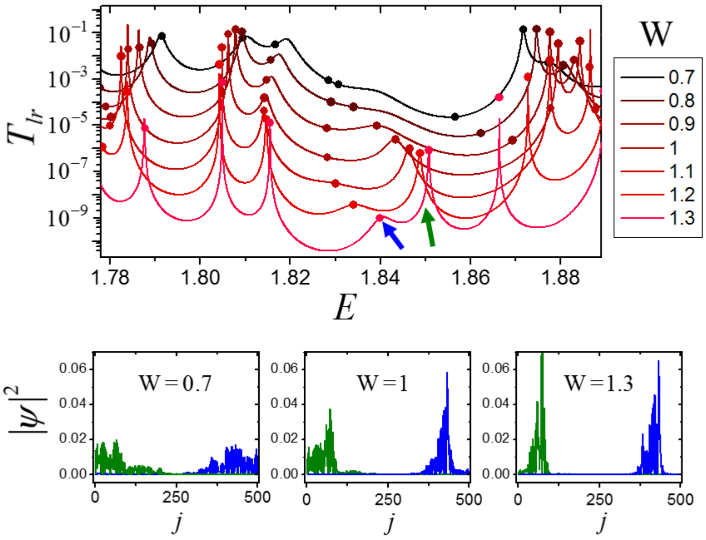

Figure 4.6: Upper frame: The transmission $T_{SD}(E)$ for a given realization of disorder at different strengths W from 0.7 (top black line) to 1.3 (bottom red line), for a $L = 500$ sample with $t_{S/D} = 1$. The eigen-energies of the corresponding isolated wires are marked by circles. Two modes are hidden at a low W, and become visible only at higher disorder levels (marked by arrows). **Lower frame:** The modulus-square of the isolated eigen-vectors relates the two above hidden states. As the disorder increases, the width of the modes becomes smaller, and eventually, they disassociate from the states of the wire.

It is also interesting to note that the height of the transmission peak is a non-monotonous function of W. While one may naively expect that peaks will reduce as disorder becomes stronger, this is correct only on average, and particular peaks may actually increase when disorder increases.

Hidden states' life-time

The spectral broadening of the wire eigenstates (or of the imaginary parts of the eigenvalues in Hamiltonian language) is inversely related to their lifetime. In disordered open systems, as the localization length becomes shorter (i.e. larger disorder), one can expect all modes' lifetimes to increase. This is indeed the case for regular modes, as seen in Fig. 4.7. However, the hidden states behave in an

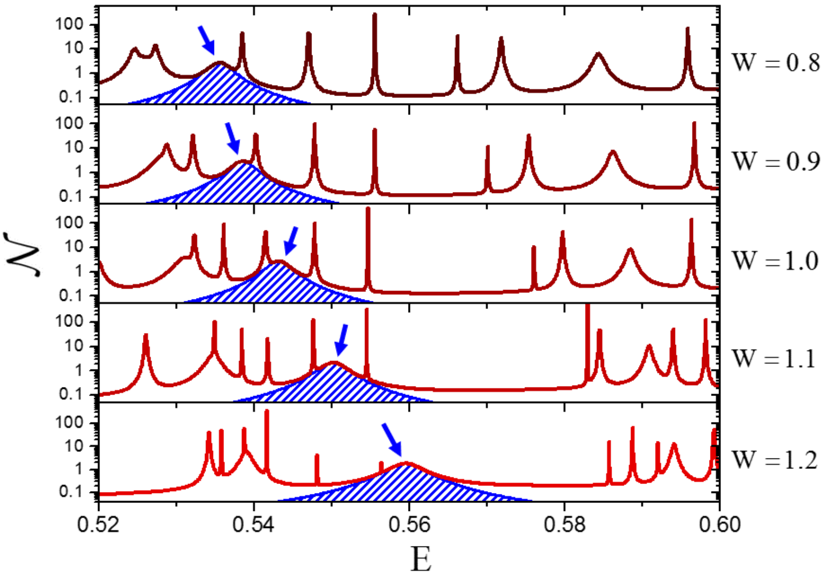

Figure 4.7: Density of states $\mathcal{N}(E)$ of the system depicted in Fig. 4.6 at different energy range. As disorder increases, the ordinary states become narrower and with larger fluctuations, while the hidden mode (marked with blue arrows) widens. Fit to Lorentzian broadening in accordance with Eq. 4.3 (blue patterned areas) results in $\gamma_i^{0.8} = 0.00165$, $\gamma_i^{0.9} = 0.00168$, $\gamma_i^{1.0} = 0.00172$, $\gamma_i^{1.1} = 0.00201$ and $\gamma_i^{1.2} = 0.00249$, namely, a shorter lifetime at higher disorder levels (see text).

unusual way, and remain wide. One can show [23] that if the self-energy term (Eq. 2.33) varies slowly with E, the DOS broadening has a Lorentzian shape:

$$\mathcal{N}(E) \propto \sum_i \frac{\gamma_i}{(E - \tilde{E}_i)^2 + (\gamma_i)^2}, \tag{4.3}$$

where γ_i is the imaginary part of the i_{th} eigenvalue, and $\tilde{E}_i$ is its real part, modified by the connection to the leads. This relation allows one to evaluate the lifetime of the i_{th} mode, $\hbar/4\gamma_i$, by fitting $\mathcal{N}(E)$ to Eq. 4.3. For the system depicted in Fig. 4.7, the life time of the hidden mode in the lower disorder ($W = 0.8$, $\gamma_i = 0.00165$) is longer than in the higher disorder ($W = 1.2$, $\gamma_i = 0.00249$).

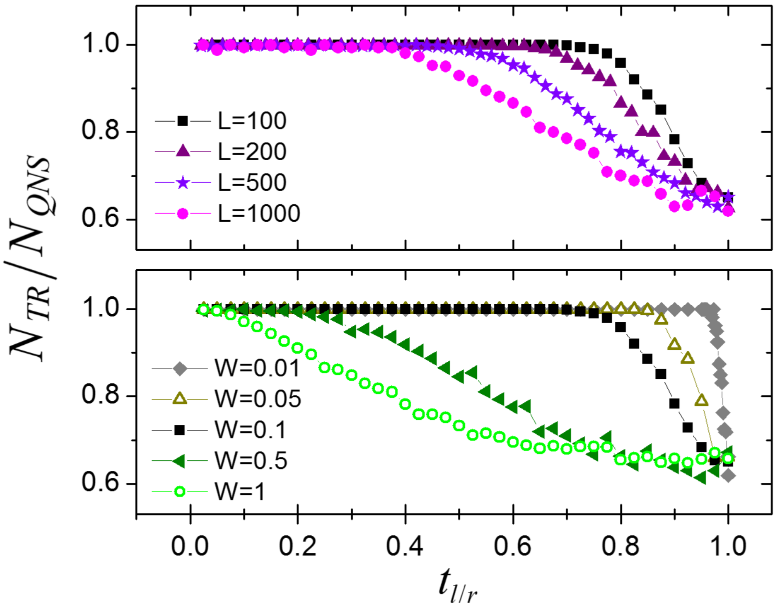

Figure 4.8: The ratio of the number of observed transmission peaks to the number of QNSs, N_{TR}/N_{QNS}, versus lead-system coupling strength, $t_{S/D}$. **Top panel:** $W = 0.1$ for different system lengths L. **Bottom panel:** $L = 100$ for different disorder strengths W. In both cases, as $t_{S/D} \to 0$, $N_{TR}/N_{QNS} \sim 1$, while in $t_{S/D} \to 1$ $N_{TR}/N_{QNS} \sim \sqrt{2/5}$.

Coupling strength and hidden states

Since the number of observed transmission resonances depends on both disorder and coupling to the environment, the ratio N_{TR}/N_{QNS} can be tuned by varying $t_{S/D}$. As this coupling parameter decreases, hidden modes decouple from the leads and develop peaks in the transmission spectrum. As can be seen in Fig. 4.8, in a weak disorder ($W = 0.01$), this transition is sharp: all hidden modes become visible due to a very small change at the vicinity of $t_{S/D} \sim 1$. As the disorder increases (or the system becomes longer), the coupling amplitude needed to resolve all transmission resonances becomes smaller, and the jump in the ratio N_{TR}/N_{QNS} broadens. This behavior is counterintuitive, as one may presume that the enhancement of disorder makes the sample more ‘closed’, and will thereby be more easily disconnected from the leads. In actual fact, the disorder anchors the electronic states firmly to their position in the sample (the edges, in the case of hidden modes); therefore, a lower $t_{S/D}$ is required in order to disconnect them.

Conductance peaks

While transmission is the natural quantity to measure for optical systems, in electronic systems, it is much more common to measure conductivity. Measuring conductivity is different than measuring transmission, due to several aspects: Unlike the ease of generating a single-mode laser beam, electrons are naturally widely distributed in the energy domain due to thermal broadening. Therefore, observing the modes by measuring conductance is possible only if the mean level spacing, Δ, is larger than $k_B\mathcal{T}$. Thus, the ratio of the number of observable conductance peaks, N_{cp}, to total number of states N_{cp}/N_{QNS}, falls to zero as $k_B\mathcal{T}/\Delta \gg 1$. Moreover, the applied source-drain voltage also affects the visibility of the modes. Even when no interactions are considered (thus allowing Eq. 2.45 to be used), an interesting difference between voltage and temperature emerges. As can be seen in Fig. 4.9, since temperature is very effective in smearing conductance peaks, once $k_B\mathcal{T} \sim \Delta$, it is impossible to observe the conductance peaks (the modes). However, for the source drain voltage, even when $V/\Delta \sim 10\Delta$, most modes are still observable in the conductance. This stems from the fact that source drain voltage is equivalent to a sharp cut-off in energy, thus being more sensitive to the discrete nature of the modes. It would be very interesting to study the interplay of these effects in the presence of electron-electron or electron-phonon interactions.

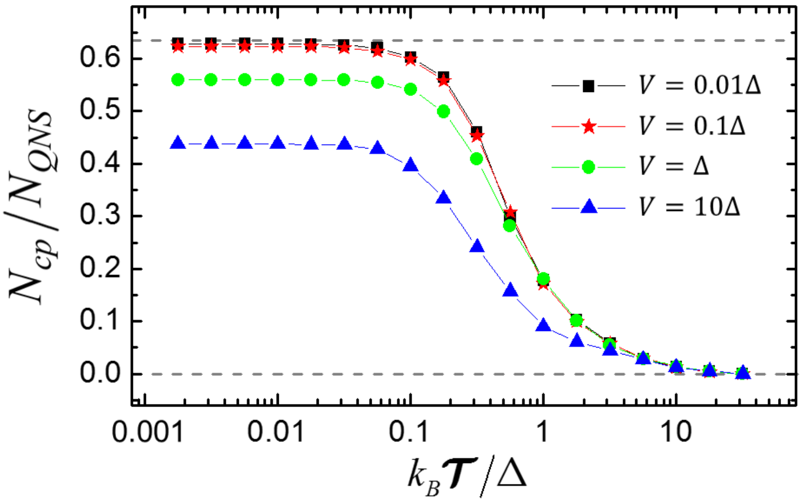

Figure 4.9: The ratio between the number of conductance peaks to the number of QNSs, N_{cp}/N_{QNS}, for different values of temperatures $k_B\mathcal{T}$ and voltages V, in a system with $L = 500$ and small disorder $W = 0.1$ (i.e. $\xi \gg L$). N_{cp} is calculated by counting the maxima in the current and changing the chemical potential in the leads μ. Both quantities are scaled by $\Delta = 4t/L$, the mean level spacing of the disconnected wire. The transition from zero temperature behavior and infinitesimal bias $N_{cp}/N_{QNS} \sim \sqrt{2/5}$ to high temperature/voltage behavior $N_{cp}/N_{QNS} \to 0$ occurs around $k_B\mathcal{T}/\Delta = 1$, while even for quite a large source-drain bias $V/\Delta = 10$, a finite number of modes is still observed in conductance at low temperatures.

4.5 Analytical calculation of the ratio N_{TR}/N_{QNS}

The ratio between the number of transmission resonance and the quasi normal states at weak disorder was shown repeatedly to equal $\sqrt{2/5}$. The origin of this irrational number is not a miracle, and was elegantly calculated for electromagnetic waves in [27]. In the following paragraphs, we repeat these calculations for completeness.

Assuming a single scattering process and free electron wave propagation between scatterers, the transmission probability of an electron with momentum k in a wire with on-site disorder can be written as:

$$T\left(k\right)=1-\left|r\left(k\right)\right|^{2}=1-\left|\sum_{n=1}^{L}r_{n}\cdot e^{i2kan}\right|^{2}, \tag{4.4}$$

where r_n is the random reflection amplitude at site n, and a is the lattice constant. For convenience, we introduce the unit-less length scale so that $a = 1$. Transmission resonances are defined as local maxima of the transmission coefficient $T\left(k\right)$, so that the resonant values of the momentum, k_n, are the roots of the equation $\frac{dT(k_n)}{dk}=\frac{d|r(k)|^2}{dk}=0$, which can be presented as -

$$\sum_{n=1}^{N}\sin(2kn)\cdot A_{n}=0, \tag{4.5}$$

where

$$A_n=\Sigma_{l=1}^{N-n}r_{n+l}r_ln+\Sigma_{l=n}^{N}r_{l-n}r_ln.$$

Generally speaking, Eq. 4.5 is a trigonometric polynomial with random coefficients. The statistics of zeroes of such polynomials have been studied in [45]. Using the results of [45], it can be shown that in a certain interval Δk, the ensemble-averaged number of the real roots N_{root} of the sum in Eq. 4.5 equals -

$$N_{root}=\frac{2\Delta k}{\pi}\sqrt{\frac{\sum_{l=1}^{N}l^{4}(N-l)}{\sum_{l=1}^{N}l^{2}(N-l)}}. \tag{4.6}$$

Calculating the sums in Eq. 4.6 within the limit $N \gg 1$, one gets [46] -

$$N_{root}\approx\frac{2a\Delta kN}{\pi}\sqrt{\frac{2}{5}}. \tag{4.7}$$

Since the total number of QNSs in the interval Δk is equal to $\Delta kLa/\pi$, and

$N_{TR} = N_{root}/2$, from Eq. 4.7 it follows that -

$$\frac{N_{TR}}{N_{QNS}} = \sqrt{\frac{2}{5}}. \tag{4.8}$$

In Fig. 4.2, it is clearly seen that within the limits of a weak disorder ($\xi \gg L$), this relation is perfectly followed by the numerical quantum calculations.

4.6 Conclusions

In this chapter, we discussed the effect of disorder on the transmission and conductivity resonances. We have shown that, like in disordered optical systems, in a 1D wire with on-site random potential a ballistic regime exists, in which a significant amount of eigen-states does not show clear peaks in transmission measurements. These 'hidden' modes have extremely broad spectral distributions which, contrary to ordinary Anderson modes, become even broader (i.e. have shorter life-times) as the disorder increases. The primary cause of this phenomenon is hybridization with the states of the attached open leads, which falls off as the localization length ξ becomes shorter than the system length L, or as the coupling to the leads is reduced. In a weak disorder, the average ratio of the number of hidden modes to the total number of electron states in a given energy interval deviates only slightly from the constant, $1 - \sqrt{2/5}$, as the fluctuations of the potential or length of the wire are increased. This constant coincides with the value analytically calculated in the single-scattering approximation. The existence of the hidden modes may substantially affect transport measurements in quantum dots, nanotubes, and topological insulators, in both weak and moderate disorders.

Chapter 5

Temperature-dependent conductance in the absence of phonons

In continuation with the transmission and conductance calculation presented in the previous chapter, in the following chapter, we focus on the relation of overall conductance with temperature. Based on the NEGF method, the numerical calculations show that conductance is significantly increased with the rise of temperature, despite the fact that electron-phonon interactions were not taken into account.

As we show below, this effect, which occurs only in a temperature range where the mean level spacing between electronic states is comparable to thermal energy, originates from the unique statistical behavior of transmission function resonances. Due to the broadening of Fermi distribution with T, at higher temperatures, the probability that a highly transmitting resonance will participate in the conductance increases. On average, this effect generates an increase of several orders of magnitude in conductance with temperature, over a wide range of temperatures.

We discuss this novel result and suggest that this effect may have a significant role at low enough temperatures, where effectively phonons do not contribute to hopping, or alternatively, in systems with a weak electron-phonon coupling. In these cases, where Mott's VRH theory predicts zero conductivity and no temperature dependence, the inherent effect we present here is still relevant.

5.1 Conductance calculation in the presence of temperature

As a general rule, the relation between conductance and temperature in highly disordered systems is usually discussed in the framework of the variable range hopping (VRH) picture, where phonons play a major role driving the electrons between localized states [10]. As was discussed in Section 1.2, according to the VRH picture, the probability of an electron hopping between localized states is proportional to the chance of absorbing or emitting a phonon with energy associated with the energy difference between the sites. The conductance temperature dependence in the VRH process has a softer than activated exponential form, $G \propto \exp[-(\frac{T_0}{T})^{\frac{1}{d+1}}]$ (Eq. 1.12). This prediction and its implications in various systems was demonstrated in many experiments, with different disorders, dimensions and materials [15, 47, 48], and it is commonly used as an indication for a hopping system, where T_0 provides information on the exact disorder level of the samples.

However, many of the experimental evidences of the VRH relation show deviations in the lower temperature range, which might originate from many other physical processes. Furthermore, the VRH model is based on several main assumptions, among them neglecting boundary conditions and the broadening effect of the leads, incoherence between adjacent localized states, and hopping between nearest neighbors only. It also assumes that all states have an exact localization length, which is much shorter than the system length. All of these presumptions could alter the exact relation in Eq. 1.12 in an actual quantum system.

In the following chapter, we face similar questions from a different angle. We numerically calculate the full transmission function $\mathcal{T}_{SD}$ of coherent (i.e. non interacting) electrons in systems which are connected to leads, and change the temperature in the leads. According to the Landauer-Buttiker formalism (Eq. 2.16), the current through the system, I, is equal to the integral over all transmission channels with a probability factor governed by the Fermi-Dirac distributions in the leads, i.e.

$$I = \frac{2e^2}{h} \int \mathcal{T}_{SD}(E) \left[f_S\left(E\right) - f_D\left(E\right) \right] dE, \tag{5.1}$$

where $f_{S/D}$ is the Fermi-Dirac distribution in the source/drain lead (Eq. 2.14).

In other words, the current is proportional to the probability to find an occupied state in the source lead and an empty state in the drain lead, multiplied by the transmission probability, as illustrated in Fig. 5.1.

5.2 Results and discussion

Conductance at $T = 0$

At zero temperature, and within the limit of infinitesimal bias voltage, Eq. 5.1 may be approximated by -

$$I(T = 0, V_{SD} \to 0) = \int \frac{2e^2}{h} \mathcal{T}_{SD}(E) \left[V\delta(E - \mu) \right] dE, \tag{5.2}$$

where δ is Dirac's delta function, and μ is the chemical potential.

The result of Eq. 5.2 is a linear relation of the conductance and transmission

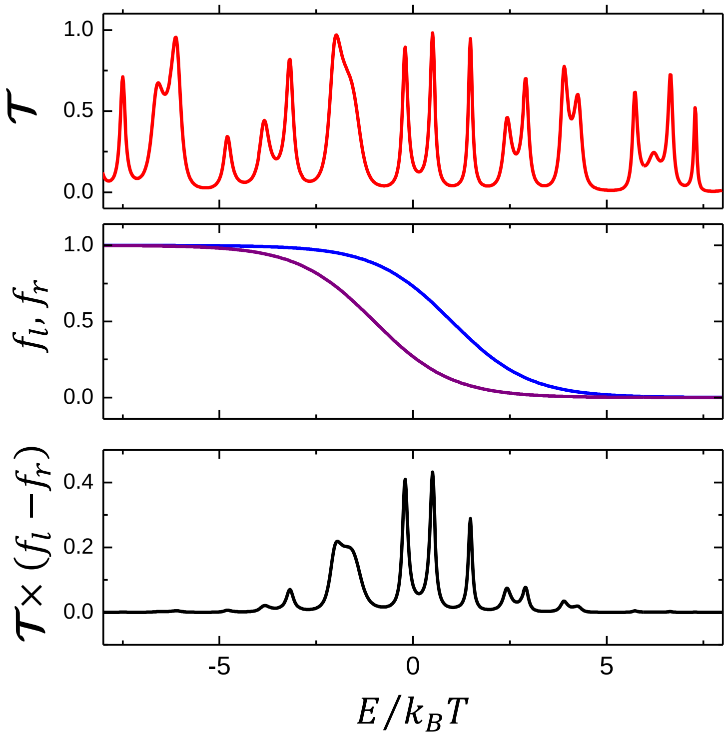

Figure 5.1: Demonstration of the Landauer-Buttiker calculation of conductance in finite temperatures. **Top panel:** Characteristic transmission function of disordered one-dimensional system. **Middle panel:** Fermi distributions of the leads for chemical potential $\mu = 0$ and biased voltage $V_{SD} = 2k_BT$. **Bottom panel:** The contribution of an electron with energy E to the current. The total conductance is proportional to the integral over the black curve (Eq. 5.1).

function -

$$G(T = 0, V_{SD} \to 0) = \frac{I}{V_{SD}} = \frac{2e^2}{h}\mathcal{T}_{SD}. \tag{5.3}$$

However, when applying higher voltages, this approximation is not valid and one should have a closer look at the relation in Eq. 5.1.

Disordered conductance distribution

In a case where the disorder level is high enough and the localization length of the wire, ξ, is shorter than the total length L, the system is 'localized' and the transmission presents sharp resonance peaks randomly distributed in the spectrum,

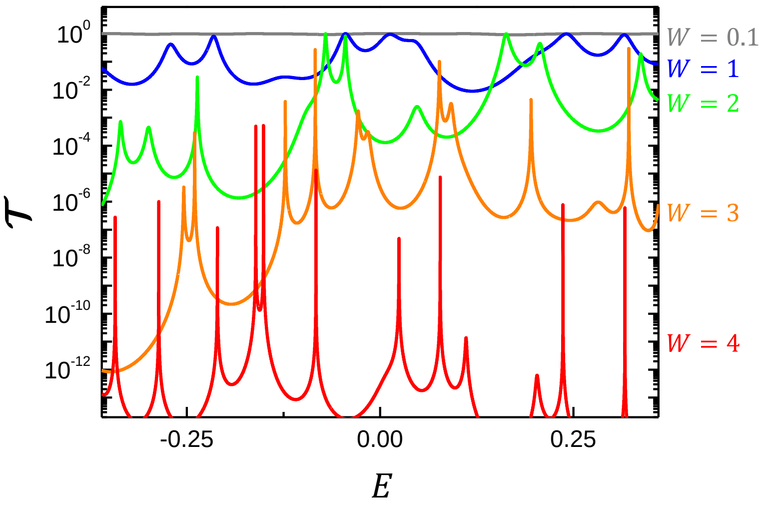

Figure 5.2: Transmission probability as a function of incident electron energy through a 1D wire in a length of $L = 100$, for the same array of on-site disordered energies, but with different amplitudes: $W = 0.1$ (gray, top), $W = 1$ (blue), $W = 2$ (green), $W = 3$ (orange), and $W = 4$ (red, bottom).

while between the peaks, the transmission value decays exponentially.

This random nature of conductance leads us to describe it from a statistical point of view. In the localized regime, the incident electrons are scattered many times before being transmitted through the wire; hence, the full distribution of the transmission function may be approximated by a production of the independent probability of being scattered by a single scatterer many times.

According to the central limit theorem the result is a log-normal distribution -

$$P(\mathcal{T}_{SD};\kappa,\sigma) = \frac{1}{\mathcal{T}_{SD}} \cdot \frac{1}{\sqrt{2\pi\sigma^2}} \cdot \exp\left(-\frac{(\ln \mathcal{T}_{SD} - \kappa)^2}{2\sigma^2}\right), \tag{5.4}$$

where e^{κ} and e^{σ^2} are the mean and variance of the single scatterer distribution, respectively. The mean value of the transmission is related to κ and σ by -

$$\langle \mathcal{T}_{SD} \rangle = e^{(\kappa+\sigma^2/2)}. \tag{5.5}$$

An explicit calculation of several transmission distributions for a different strengths of disorder of the 1D wire are presented in Fig. 5.3, showing that the log-normal distribution is extremely skewed.

Since the log-normal distribution is highly skewed, its mean value is substantially different from the **median** value, which is the maxima in the $\ln(\mathcal{T}_{SD})$ PDF plots, and equals $e^{-\kappa}$. This difference may be understood better from Fig. 5.2: While it is much more probable to find a transmission value in $\mathcal{T}_{SD}(E)$ with a low value, there are resonances with exponentially higher transmission. Therefore, averaging over energies (or equivalently, according to the ergodic assumption, avaraging over different realizations of disorder) will result in average values that are much closer to the maximal values at the peaks.

This effect, originating from the skewed behavior of the log-normal distribution, plays a major role in the calculation of the current in Eq. 5.1 when the temperature increases.

Conductance at $T > 0$

At finite temperature, the Fermi distribution is no longer a step function, and the linear relation between transmission and conductance (Eq. 5.3) is broken.

In the case of a low disorder strength ($\xi \gg L$), the transmission is close to unity, and conductance is on average constant with temperature. However, as the disorder increases, the distribution of $\mathcal{T}_{SD}$ generates large mesoscopic fluctuations with changing T, generated by the broadening of $f_{S/D}$, which opens current paths to farther areas of the spectrum.

We demonstrate this behavior in more detail in Figure 5.4. In the first panel (**a**) we present $G(T)$ plots of several wires with low disorder, i.e $\xi > L$ (blue solid lines), and their average value (red dotted line). Remembering the resonant nature

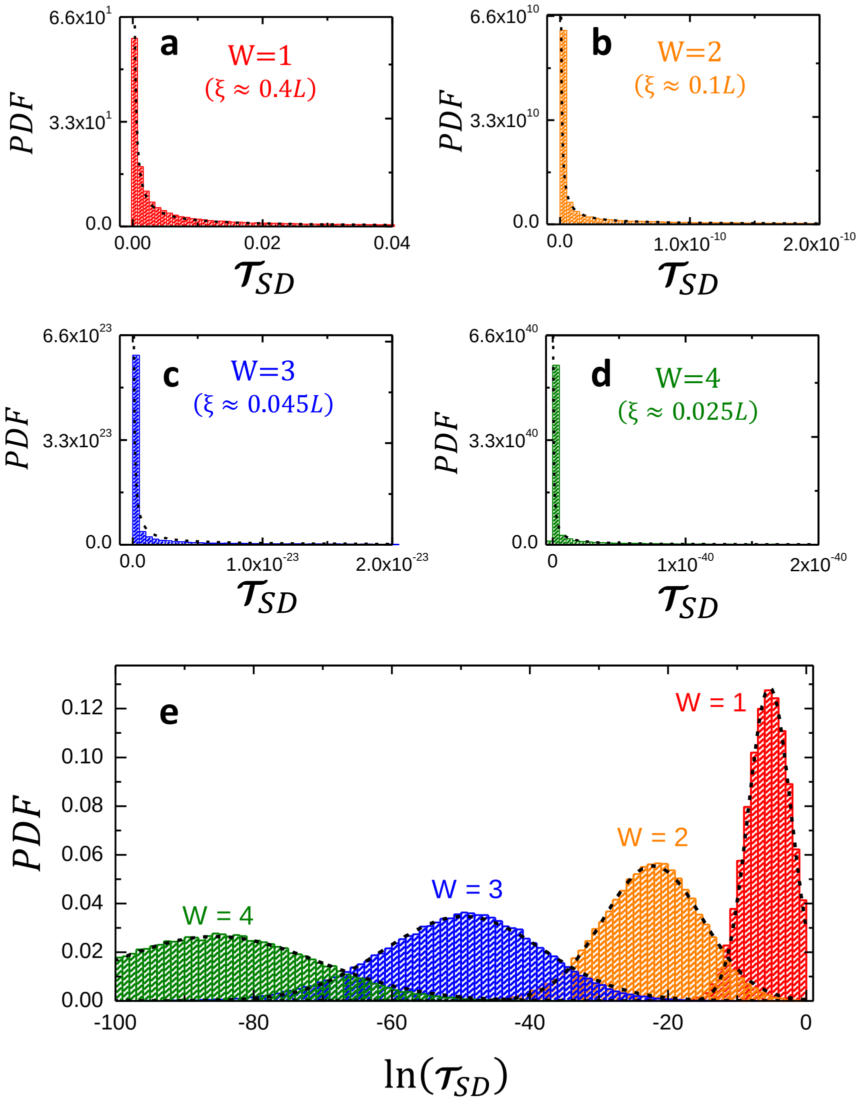

Figure 5.3: Panels a-d: Probability density functions of the transmission, calculated using 100,000 different realizations of disorder with a length of $L = 250$ and various strength of disorder in the localized regime ($\xi < L$), demonstrating the log-normal nature of the transmission distribution. **Panel e:** Distribution of the above transmission function's logarithm. Black dashed lines fit with Gaussian.

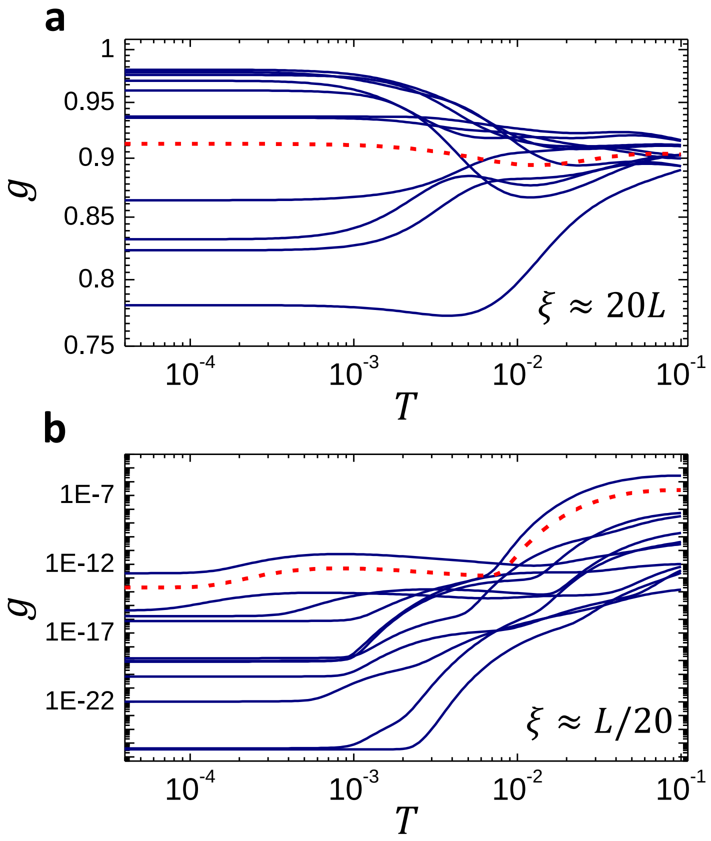

Figure 5.4: Conductance as a function of temperature of 11 wires with $L = 500$ and $\mu = 0$ - for **a:** $\xi \approx 10000$ ($W = 0.1$), and **b:** $\xi \approx 25$ ($W = 2$). While in low disorder the mean value (red dashed lines) is a good representative of the conductance, as ξ becomes larger than L the wide distribution of g deviates the mean value from the typical average value to be much closer to the occasional maximal curve.

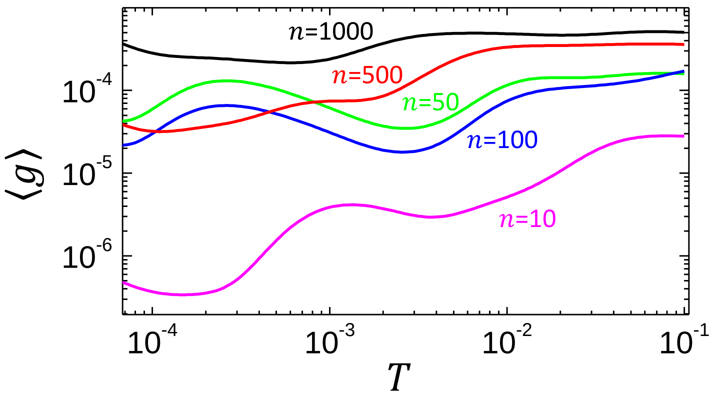

Figure 5.5: Linear average of conductance as a function of temperature for a wire with $L = 100$ and $\xi \approx 10$, with different sampling sizes n for $n = 10, 50, 100, 500$ and 1000. Due to the wide distribution of $\mathcal{T}_{SD}$, the averaged result does not converge for any reasonable n.

of the transmission function, we deduce that in some of the wires, the chemical potential μ is situated in a gap between transmission peaks, and therefore at $T \to 0$ the conductance is small. As the temperature increases, the Fermi distribution is spread over a wider region, and at some point, a transmission peak is included and conductance is increased. In other cases, μ is originally located close to a resonance, and increasing T results in a *decrease* of G. In the case of high disorder, where $\xi \ll L$ (panel **b**), the probability of having a resonance peak originated exactly at μ is practically zero, and all curves are positive.

Moreover, due to the broad form of the log-normal distribution of $\mathcal{T}_{SD}$, the variations in G with T are also exponentially larger. This variance does not allow using the simple average of the distribution (red dashed lines), which results in a meaningless curve and reflects only the coincidental highest value of the transmission. A few similar attempts to calculate mean conductance are presented in Fig. 5.5, with different sampling sizes n (number of averaged systems), showing that the result does not converge even at $n = 1000$.

Averaging conductance

The wide and skewed distribution of $\mathcal{T}_{SD}$ in the localized regime and the failure to calculate a meaningful average of the conductance, obliges the use of a different method to define its temperature dependence. The logarithmic nature of the lognormal distribution and the exponential behavior of conductance fluctuations, leads us to claim that the natural parameter that properly reflects the temperature dependence is the median m_g of the conductance.

From an experimental point of view, there is no way to evaluate the true mean value of the conductance of a 1D sample, as we demonstrate in Figures 5.4 and 5.5. Even measuring a large number of different systems does not reflect the distribution of conductance, as it is governed by the occasional highest peaks in the conductance, which, as we have seen, are exponentially higher than the average conductance.

Moreover, as was described earlier, the lognormal distribution in Eq. 5.4 is a result of multiplying the probability of being scattered by a single scatterer many times. Therefore, the characteristic conductance is the product of its random variables -

$$\left(\Pi_{i=1}^{n} G_i\right)^{1/n}, \tag{5.6}$$

or equivalently, the exponential of the summation over its logarithm -

$$\exp\left(\frac{1}{n}\sum_{i=1}^{n} log(g)\right). \tag{5.7}$$

According to the central limit theorem, at $n \gg 1$, these values will converge to the mean value -

$$\exp\left(\frac{1}{n}\sum_{i=1}^{n} log(g)\right) \to \exp\left(\frac{1}{n}\sum_{i=1}^{n} \kappa\right) = \exp\left(\kappa\right), \tag{5.8}$$

which is exactly equal to the median of Eq. 5.4.

The median values of conductance for the exact set of systems presented in Figures 5.4**b** and 5.5 are presented in Figures 5.6 and 5.7, respectively, demonstrating that the median is a true indication of conductance despite its large fluctuations, showing a clear convergence even with a low sampling size n.

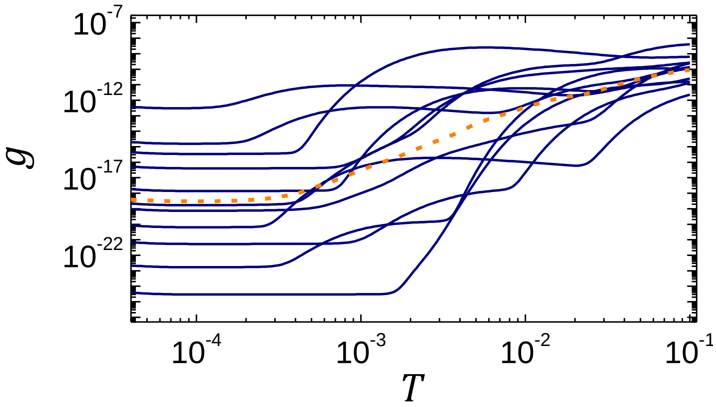

Figure 5.6: Conductance as a function of temperature in 11 wires with $L = 500$ and $\mu = 0$, similar to Fig. 5.4**b**. The median value (orange dashed line) calculated in Eq. 5.8 is a good representative of the conductance curves.

Temperature dependence

The resulting relation of conductance with temperature, as depicted in Fig. 5.8 for several strengths of disorder, shows a significant increase of conductance at higher T within a wide region of temperatures. As was aforementioned, the temperature range is bounded from above by the $4t$ width of the tight-binding band (Eq. 2.32), and from below by the mean level spacing in the finite wire, which is proportional

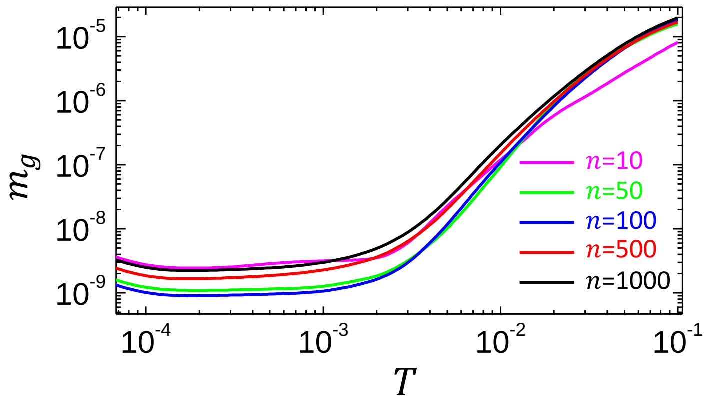

Figure 5.7: Logarithmic average of conductance as a function of temperature for the exact set of wires in Fig. 5.5. This averaging method is an indication of the median m_g, which is a better inherent parameter of the disordered system.

to $1/L$.

The origin of this positive relation of conductance with temperature is basically statistical. As the temperature increases, Fermi distributions are widened and more channels participate in the transmission. In ballistic systems, where $\mathcal{T}_{SD} \to 1$, the conductance does not change with T, since the area between f_S and f_D (middle panel of Fig. 5.1) remains constant. This area can be easily shown to be equal to the applied bias voltage, V_{SD}. However, a log-normal distribution of the transmission values in localized 1D systems means that most transmission channels are effectively zero, yet once in a while the system finds an exponentially higher resonance peak in $\mathcal{T}_{SD}(E)$. This phenomenon leads to an effective increase of the total conductance $G = I/V_{SD}$ with temperature, as the Fermi distribution is widened and the probability of finding such a channel is larger at a higher T. This effect, in addition to the highly skewed log-normal behavior of these peaks, overcomes the linear decay from the smearing of $(f_S - f_D)$.

Although the overall conductance is lower at higher disorder strength, the resonant nature of $\mathcal{T}_{SD}(E)$ leads to a stronger effect of many orders of magnitude at

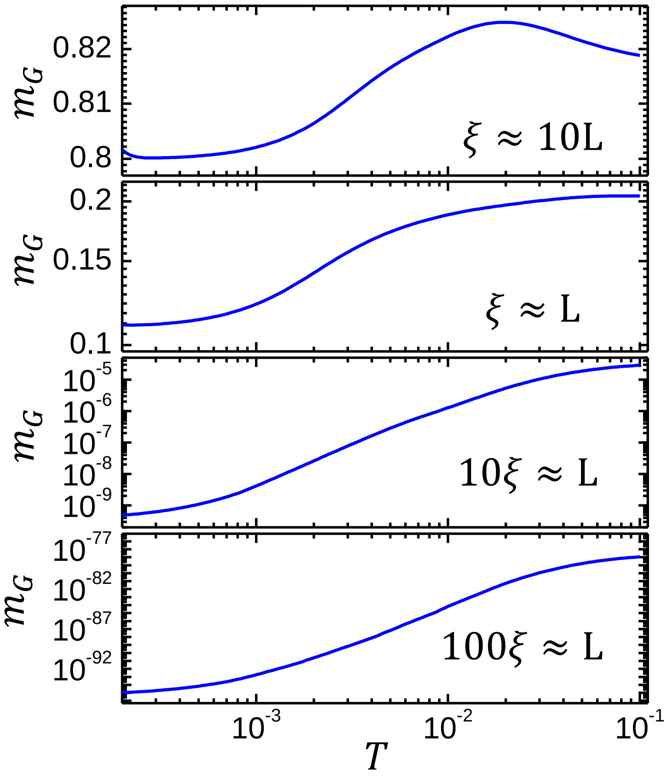

Figure 5.8: The median of conductance as a function of temperature in a wire of length $L = 500$ for different localization lengths. The conductance shows a clear positive temperature dependence in the accessible range (see text).

higher disorders, and for a wider range in T. The relevant temperature scale is within the range of the mean level spacing. In mesoscopical systems, this range is around the available measurement range (from a few tenths up to a few hundreds Kelvin). In macroscopical systems, however, this effect will be much smaller, as conductance is already relatively saturated. On the other hand, in small microscopical systems, mean level spacing is within the range of much higher energies. Therefore, the probability that the Fermi distribution will occasionally include a higher TR due to an increase in temperature is very low.

5.3 Conclusions

In contrast to common statement that the increase of conductance with T in disordered metals is attributed to the VRH theory and to the contribution of phonons to the transport process - in the above model we have demonstrated a different reason for such temperature dependence. We have shown that at sufficiently low temperatures, where electronic mobility is governed mainly by coherent transmission, a large region exists, in which conductance is increased with T even in the absence of phonons. The origin of this temperature dependence is mainly the unique statistics of the transmission function in highly disordered systems, the log-normal distribution, which originates from the fact that the electrons are scattered many times during the transport process.

In most macroscopic cases, the magnitude of this temperature dependence is not comparable to hopping conductivity, since it requires direct tunneling throughout the entire sample. Nevertheless, it may be significant in a temperature range in which the VRH is less effective, such as $T \ll T_0$, in systems with low coupling between electron and phonons, or in nanoscopical systems. Moreover, many conductance-versus-temperature experiments in disordered materials show clear VRH behavior but only in a limited region. Few models have been suggested to explain these deviations, such as more than a single energy scale in the system, many-body transport, and different dimentionalities at different temperatures. However, the inherent relation presented in the above study could shed some light on the origin of many of the experimental deviations from the VRH model.

Part III

Temperature Dependent Conductance Dynamics in Electron Glasses: An Experimental Study

In this part, I present novel experimental results of conductance in discontinuous two-dimensional metallic layers fabricated at low temperatures. In these samples, electronic conductance shows a slow relaxation after an excitation, as well as memory of the previous electronic condition. These effects are attributed to the electron glass phenomenon (EG), where electrons in the disordered metal strongly interact with the lattice and with other electrons, and therefore show glass-like dynamics.

In contrast to previous studied systems, EG conductance dynamics in our samples show a strong slowdown with decreasing temperature T. Furthermore, this slowdown was found as dependent not only on T, but also on T_{max}, the maximal temperature the sample was exposed to. In addition, at a finite temperature below T_{max}, this slowdown stops, and the dynamics become independent of T, an effect that is attributed to a crossover from thermally activated glass to quantum glass. These three observations are explained in the framework of the configuration space, indicating that this behavior is more general and may also be present in other types of glass, if prepared below glass temperature.

The first part of the results, namely: the slowdown of dynamics with T and the relation to T_{max}, was recently published in PRL [49]. The latter part, the crossover to quantum glass at low temperatures, is currently in preparation and will be submitted shortly.

This study was performed under the supervision of Prof. Aviad Frydman, following preliminary work by Dr. Tal Havdala (Bar-Ilan University) [50], and in collaboration with Thierry Grenet and Julien Delahaye (Insitut NEEL, Grenoble) for the experimental aspects of the work, and with Ariel Amir (Harvard University) for the theoretical aspects.

In the following introductory Chapter 6, I provide an introduction to the glass state of matter and to EG in particular, including a brief overview of experimental observations in previous studies, and a theoretical explanation employing the concept of configuration space.

In Chapter 7, an overview of the experimental setup is presented. I discuss the methods we utilize to fabricate and measure the metallic films, and present characteristic results of the glassy behavior of our samples.

In the last two chapters (8 and 9), I present and discuss the novel results of the glassy dynamics of conductance, and the associated theory.

Chapter 6

Introduction: Electron Glass Phenomenon

6.1 Glass state of matter

Common soda-lime glass, which we use for windows, mirrors and bottles, appears to be a solid substance at room temperature. However, in reality, this material can be described as a completely different phase of matter, since it is different in many aspects from both the solid and liquid phases.

The phase transition between solid and liquid is defined by the non-continuity of the order parameter (usually the density or the volume) as a function of temperature. As a result, the entropy is sharply changed at the melting temperature T_m, and the heat capacity diverges. In glasses, on the other hand, this phase transition does not exist. Cooling a SiO_2-based glass ('window glass') from a high T makes it become more and more viscous, until below a certain temperature, named "glass temperature" (T_G), the changes in time due to external force cannot be observed in any reasonable time scale[1], [2] and the matter seems to be a solid. This lack

---

[1] Several different definitions of T_G are in use in the different glass systems, most are an arbitrary choice of temperature at which the changes cannot be observed in any reasonable timescale. In other systems, T_G is defined as a point where the order parameter exhibits a relative saturation. In this dissertation, we adopted a more theoretically-oriented definition for EG glass temperature (see section 6.2 below).

[2] An example of this behavior is the pitch drop experiment [51], where a piece of pitch (asphalt) was inserted into a funnel, extruding a single drop circa every 10 years! operating since 1927,

of a well-defined phase transition implies that window glasses never form a solid structure, and in fact, can be interpreted as liquids with extremely high viscosities.

The origin of this unique behavior is attributed to the disordered nature of the glass phase, which generates strong internal frustrated interactions between the atoms. When a glass is cooled too fast, the atoms remain disordered, and frustrated inter-atomic interactions are preserved even at low temperatures. Accordingly, it has been shown [52, 53] that many other substances can exhibit glassy behavior if cooled fast enough, while, on the other hand, the glass temperature of glasses decreases at very low cooling rates (Fig. 6.1).

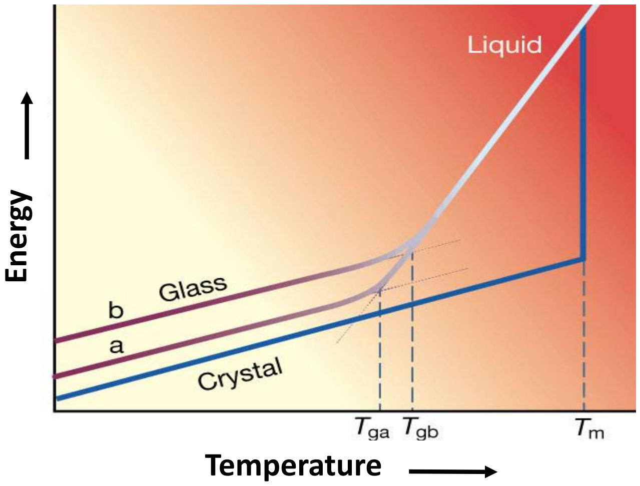

Figure 6.1: Internal energy of a glassy system as a function of temperature, for different cooling rates. At infinite slow rates, the system experiences a phase transition to a solid phase at T_m. At faster cooling ratess the liquid shows a smooth transition through a variable glass temperature (demonstrated by T_{ga} and T_{gb}.(Debenedetti et al., 2001 [52]).

Similar to window glass and other structural glasses, these two conditions, namely, strong frustraetd interactions and disorder, are common in other physical systems that present glass-like behavior. In this category, one could consider systems of interacting spins (spin-glass) [54, 55], bonded polymeric chains [56], flux

---

it is currently waiting for the 10th drop, and is considered the longest running experiment in history.

relaxation in superconductors [57], dipole moments (dipole glass") [58], porous silicon [59], and even crumpled nylon or paper foils [60].

To demonstrate this frustration behavior, one may consider a system that consists of four spins with ferromagnetic and antiferromagnetic interactions, as illustrated in Fig. 6.2.

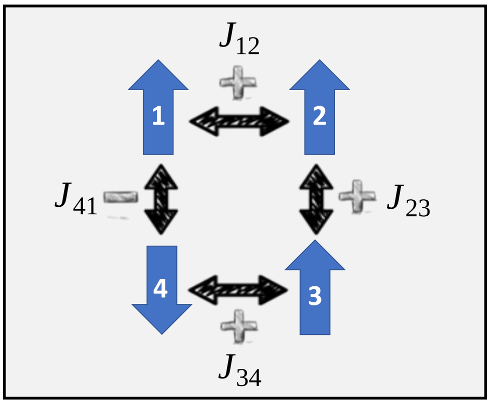

Figure 6.2: A system of 4 spins with ferro/antiferromagnetic interactions between them, where blue arrows represent the spins, and black arrows represent the interaction between them. Following the Ising Hamiltonian between nearest neighbors- $H = -\sum_{ij} J_{ij} S_i S_j$, with a gray '+' sign that represents $J_{ij} > 0$ and '−' $J_{ij} < 0$, one can easily see that the interaction between 3 and 4 is frustrated, and that there is no true equilibrium in this simple system.

Due to the disorder in the interaction term J_{ij}, two main results occur: A. There is no true equilibrium in the system, as at least one interaction is not satisfied. B. Switching only one spin at a time, the system has to pass through more frustrated configurations in order to switch between low energy (i.e. less frustrated) configurations.

Even in cases where there is no inherent frustration in the system (such as in structural glass), when cooling it rapidly below the melting point, some restrictions evolve in the internal structure, and the dynamics become glassy.

6.2 Configuration space

The demonstration of frustrated spins in Fig. 6.6 leads one to think of a simple way to describe the dynamics of disordered glassy systems via the configuration space (often referred to as the 'phase space'). In this representation, each configuration of microscopical elements in the system is a point in a multidimensional space, while changes in the locations/orientation of the microscopical elements (spin reversion, atom movement, etc.) are a vector in this space. The internal energy E of this particular configuration is plotted in an additional dimension, and the resulting surface is the potential landscape of the system.

Since each dimension is attributed to the movement of a single element, the configuration space number of dimensions is equal to the degrees of freedom in the system. Nevertheless, despite its huge dimensionality, the configuration space can provide useful insights into the dynamics of glass by examining it in a smaller dimension case. In Fig. 6.3, a characteristic potential landscape in a disordered system is plotted. The landscape consists of many local minima, with energy barriers between them.

Above the glass-transition temperature, T_G, which we define here as the energy of the highest barrier in the system [61], the system is free to 'move' to any configuration by statistical processes (Fig. 6.4). Cooling the system rapidly traps the system in one of these meta-stable states (marked with a black circle), meaning it is not a true equilibrium, and a lower energy configuration may be found if the system is cooled slower.

In the presence of finite temperature, the system has a chance to gain enough energy from phonons, overcome the barrier and eventually find a lower energetic

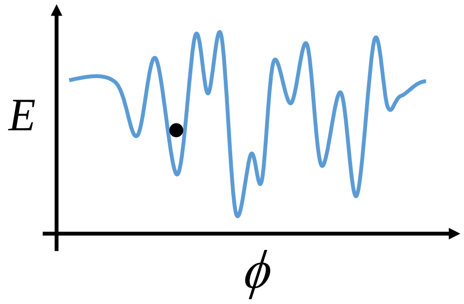

Figure 6.3: Illustration of the typical energy configuration space of a disordered system. After rapid cooling from a high temperature, the system configuration (marked with a black circle) is trapped in a metastable state.

configuration. This process is the essence of glassy dynamics[3].

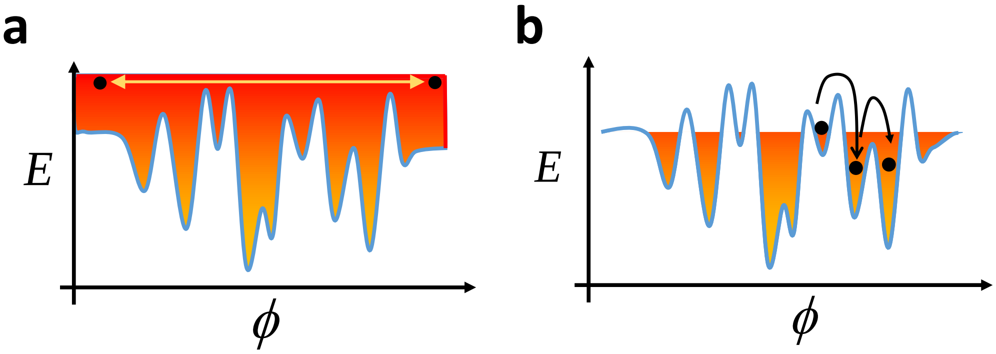

Figure 6.4: Illustration of glassy dynamics in the configuration space. At temperatures above the glass temperature T_G, the system is determined as liquid, i.e. free to move to any configuration (**a**). Below T_G, the dynamics are ruled by thermal activation over energy barriers to a lower-in-energy meta-stable state (**b**).

The rate of such a thermal activation process, λ, is exponential with T, following an Arrhenius law -

$$\lambda = \gamma_E \exp\left(-\frac{U}{k_B T}\right), \tag{6.1}$$

where γ_E is the minimal rate of a single process in the system, U is the height of the energy barrier, and k_B is the Boltzmann constant. In a highly disordered system,

---

[3] The assumption that the only process is thermal activation is entirely true only in a group of systems known as ‘strong’ glasses [52]. Many other glasses are ruled by additional processes (such as diffusion), and are termed ‘fragile’. Since our system, the electron glass, presents ‘strong’ glass behavior, we will not elaborate on other types of glasses.

the distribution of potential barriers is wide, hence, some processes might take an extremely long time. Therefore, as is commonly seen in glasses, the relaxation process continues even after decades [51] and millennia [62].

6.3 Logarithmic relaxation

The relaxation process of glass toward a better quasi-equilibrium occurs simultaneously by all degrees of freedom in the system (or equivalently, in all directions in the multi-dimensional configuration space); hence, the overall measured relaxation is a sum of many activation processes with all possible rates -

$$\Delta F_{tot} = \delta F_0 \cdot \sum_{\lambda} e^{-\lambda t}, \tag{6.2}$$

where t is the time after an excitation, δF_0 is the average contribution of each relaxation process to the change in the value of interest, and ΔF_{tot} is the total relaxation.

Assuming thermal activation as the relevant process driving the relaxations (Eq. 6.1), as well as an approximately uniform density of energy barriers $\mathcal{D}$ in a bounded spectrum interval between $U_{\min}$ and $U_{\max}$, the distribution of rates is given by [6]:

$$P(\lambda) = \mathcal{D} \cdot \frac{dU}{d\lambda} = \frac{\mathcal{D} \cdot T}{U_{\max} - U_{\min}} \cdot 1/\lambda \equiv C/\lambda. \tag{6.3}$$

Considering macroscopical systems and taking Eq. 6.2 to the continuum limit, the sum is approximated by a weight integral -

$$\sum_{\lambda} e^{-\lambda t} = \int_{\lambda_{\min}}^{\lambda_{\max}} e^{-\lambda t} P(\lambda) d\lambda \approx C\left[-\gamma_E - \log(\lambda_{\min} t)\right] \tag{6.4}$$

with γ_E as the Euler-Mascheroni constant, and $\lambda_{\min}$ and $\lambda_{\max}$ as the lower and upper cutoffs of the relaxation rate distribution, respectively [63].

This logarithmic relation is therefore a characteristic behavior of glassy systems with a uniform distribution of barriers. An example of this behavior may be found in the crumpled foils experiment presented in Fig. 6.5. In this experiment, a heavy weight is placed on top of a pile of crumpled Mylar sheets, tissue foils or cotton balls at $t = 0$, and the height of the pile is measured over time. As can be seen, the relaxation process is perfectly logarithmic in the nylon and tissue cases, over seven orders of magnitude in time (!). In the cotton balls case, however, the process is faster than logarithmic, which implies a larger distribution of slow processes over fast ones, leading to a different function for $P(\lambda)$.

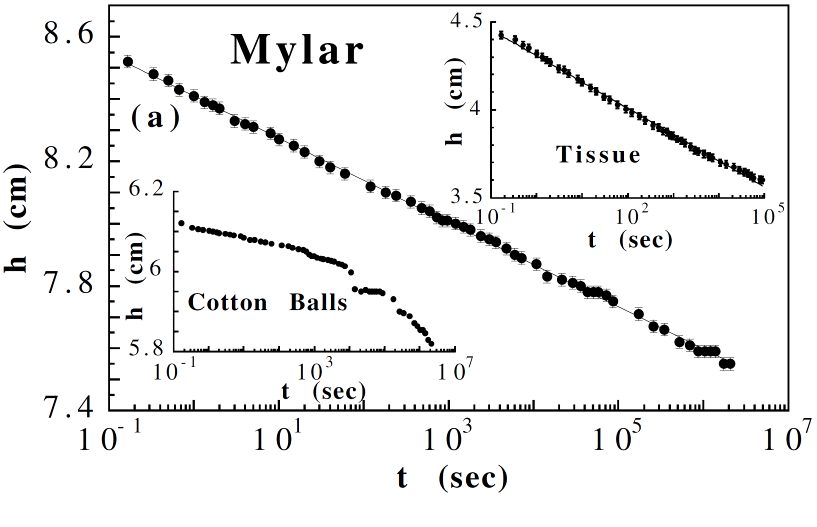

Figure 6.5: The height of a pile of Mylar sheets (main panel), tissue paper (upper right inset), and cotton balls (lower left inset) - after placing a 200 gram weight on top. The resulting height in all three cases shows slow relaxation even after $2 \cdot 10^6$ seconds (about a month). The two first experiments obey the logarithmic dependence of Eq. 6.4 (Matan et al., 2002 [60]).

6.4 Memory effect

Although slow relaxation is common to all glassy systems, other physical processes that show such long relaxations periods in time yet are not related to glass dynamics exist, such as nuclear decay, chemical reactions, etc. Therefore, a better fingerprint of glassy systems is the memory effect. In spite of other relaxing systems, in which a change in the physical conditions results in an independent, new relaxation process, in glassy systems, the previous conditions are still imprinted on the internal configurations of the system. Namely, even though the external parameters are very different, and the overall magnetization/conductance/pressure/etc. are very different from the original ones, there are regions in the configuration space that still hold information on the history of the glass.

The memory effect was first demonstrated in the spin-glass system [64, 65]: A set of disordered spins is induced by a slow ac magnetic field H, while the magnetization M is measured simultaneously. Starting above T_G, the system's response shows zero out-of-phase susceptibility between H and M, χ''. Then, the system is cooled below T_G and χ'' rises to a finite value - the spins become 'stuck' in a metastable state and cannot follow the ac magnetic field. Measuring χ'' over time (Fig. 6.6**a**) after cooling from a high T to below glass temperature shows logarithmic glassy relaxation to a lower energetic (and therefore less responsive) phase.

To observe the memory effect, one applies the following protocol: While cooling the system, cooling is arrested at several intermediate temperatures below glass temperature, $T_1, T_2 < T_G$, for a significant time (relative to the cooling rate), during which the glass continues to relax. Soon afterwards, the system is heated back through T_1 and T_2 to T_G. Throughout most of the heating process χ'' follows its cooling curve. However, around the temperatures at which the cooling was halted, χ'' presents clear lower values, as depicted in Fig. 6.6**b**.

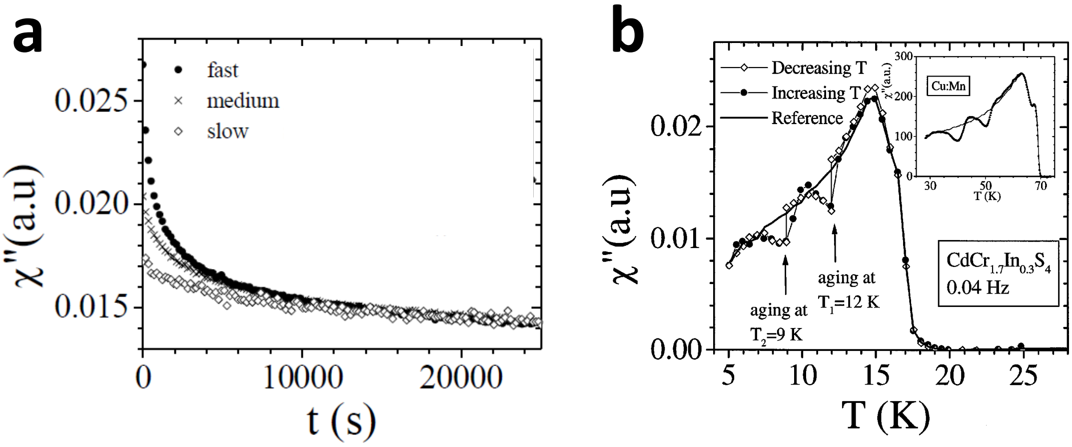

Figure 6.6: Relaxation of the out-of-phase susceptibility χ'' of $\mathrm{CdCr_{1.7}In_{0.3}S_4}$ sample, induced by an ac magnetic field (0.3Oe, 0.04Hz) below glass temperature $T_G = 16.7$K. **a**: χ'' as a function of time after cooling from above T_G to 12K at different rates (circles - 2.6K/min, crosses - 0.08K/min, diamonds - 0.015K/min) showing the logarithmic glassy relaxation. **b**: The memory dip protocol - cooling from 25K to 5K, allowing the system to 'age' for 7 hours at 12K and 40 hours at 9K (open diamonds), and heating it back up (solid circles) (K. Jonason et al., 1998 [64]).

This memory dip is well-explained by the configuration space picture: At each temperature, the energy scale is different, and therefore the relevant region of the potential landscape is also different. In other words, as long as the system was not exposed to $T > T_G$, it experiences a completely different landscape at every T. Thus, the system is found in lower energy wells at configuration regions that are related to T_1 and T_2. During re-heating of the sample, the spins are arranged more easily at these values of T, and the resulting χ'' is lower.

6.5 Electron glass

Electron glass (EG) is a relative newcomer to the family of glasses (for reviews, see Ref. [6, 7]). The electronic properties of strongly disordered interacting metallic systems (Anderson insulators) exhibit glassy behavior, such as slow relaxation of conductance and memory effects, like the glassy systems presented above. These phenomena were first predicted theoretically several decades ago [66–70] and were termed electron glass [66], as the glassy properties are attributed to conduction electrons. Experimentally, a growing number of systems have been reported to show such glassy behavior, including discontinuous Au [50, 71], amorphous and poly-crystalline indium oxide films [72–77], ultrathin Pb and B films [78, 79], granular Al [80, 81], thin Be films [82], NbSi [83], Tl_2O_{3-x} [84], GeSbTe [85], and discontinuous films of Ag, Al, and Ni [50, 86].

Conductance dynamics

Conductance in EG systems was shown to decay logarithmically in time after an abrupt cooldown or an electrical excitation out of equilibrium, in accordance with Eq. 6.4:

$$G(t) = G_0 - S \cdot \log(t), \tag{6.5}$$

where G_0 is the conductance at $t = 1$ second after the excitation and S is the slope of the logarithm. Two typical experimental observations of this conductance relaxation are shown in Fig. 6.7.

The most common way to excite an EG system is to introduce it to gate voltage, V_g, by field effect geometry (e.g. the MOSFET setup). A change of V_g instantly alters the underlying potential, introduces or depletes electrons, and thus pushes the system out of equilibrium (Fig. 6.8**a**). This causes conductance to abruptly

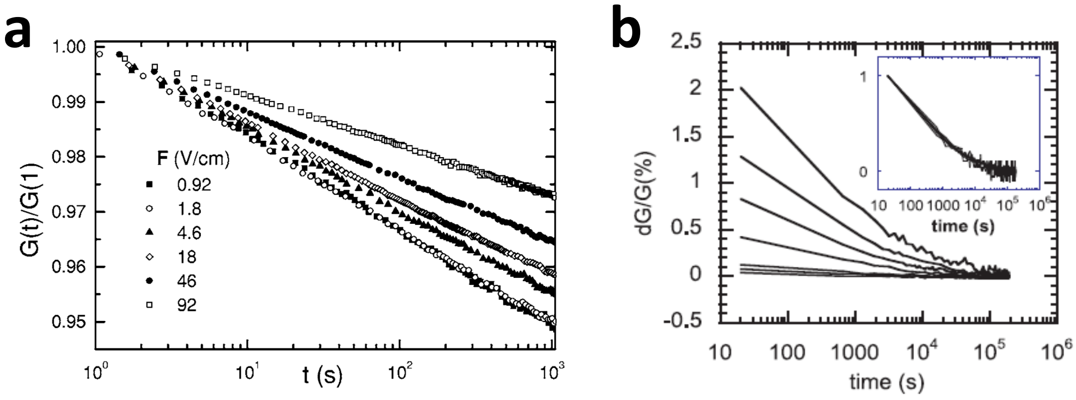

Figure 6.7: Panel a: Conductance as a function of time in an In_2O_{3-x} sample after an abrupt change of gate voltage, showing a perfect logarithmic slope. Different plots are related to different source-drain electric fields (Z. Ovadyahu, 2006 [77]). **Panel b:** Conductance as a function of time in a granular aluminum thin film sample, at different temperatures from 4.5K (top) to 20K, after an abrupt change of V_g (T. Grenet et al., 2007 [81]). **Inset:** All curves collapse when normalized by the initial conductance change ΔG_0.

increase by an amount denoted as ΔG_0, followed by a slow logarithmic relaxation toward equilibrium (Fig. 6.8**b**).

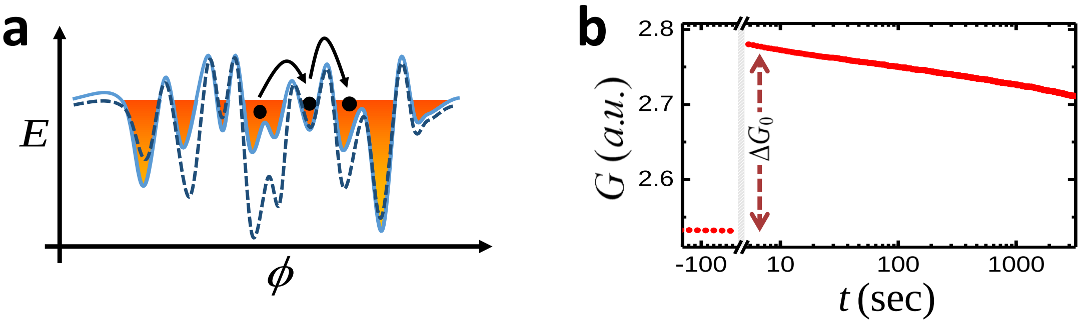

Figure 6.8: a: Illustration of the configuration space of an electron glass system before (dark dotted blue line) and after (bright blue solid line) a gate voltage change at $t = 0$. The system starts flowing to its new quasi-equilibrium immediately after the V_g abrupt change. **b:** The associated conductance change at $t = 0$ and logarithmic relaxation soon after.

This method enables good control of the glassy process, which serves as a significant advantage over other glasses, as one can change V_g at any rate, in any direction, and even apply sudden changes to it. Furthermore, it allows the observation of a 'memory dip' as a function of V_g at a fixed temperature [73, 76], as presented in Fig. 6.9. In contrast to spin-glass systems, in EG, one can scan a whole range of gate voltages almost instantaneously, and effectively sample the relaxation status in each case. These $G(V_g)$ scans show the memory effect at the specific gate voltage in which the glass was allowed to equilibrate and draw a dip shape around it. This memory dip has been suggested as the hallmark of 'intrinsic' EG [82, 87].

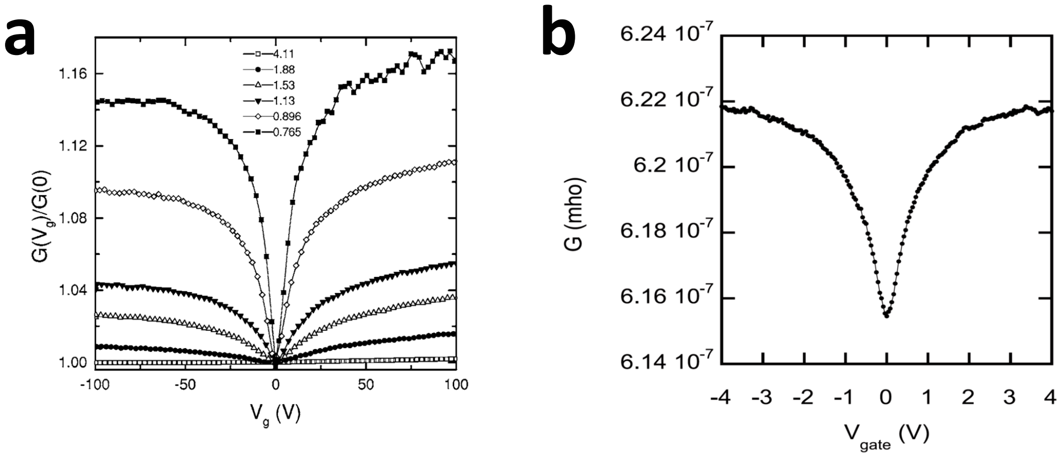

Figure 6.9: Panel a: Conductance as a function of gate voltage in an $\mathrm{In_2O_{3-x}}$ sample at varied temperatures from 4.11K (bottom) to 0.765K (top), showing the memory dip effect (Z. Ovadyahu, 2006 [77]). **Panel b:** Conductance as a function of gate voltage in a granular aluminum sample at 4K, showing a memory dip with an amplitude of approximately 1% (T. Grenet et al., 2007 [81]).

In addition, due to the ease of controlling the applied gate voltage (in comparison to variations in temperature) in EG systems, it is possible to explore the very start of glassy relaxation in Eq. 6.5 after an abrupt change of V_g.

The amplitude of the change in conductance with V_g is usually a few percent of the overall conductance, and may vary with the degree of disorder, carrier concentration and ambient temperature.

Indeed, one may claim that conductance in glassy disordered metals is not a good macroscopical measurement, since the current flows only in a sparse percolation network and does not sense the whole sample[4]. Furthermore, the measured current through the system is carried by a macroscopical amount of electrons, which flows at a relatively high rate in the percolation paths. Hence, extremely slow relaxation is not directly related to the current electrons, but rather, is ruled by a secondary process.

As is the case with many other open questions, the exact mechanism of conductance relaxation and the glassy processes in the percolation network are still under debate. Here, we suggest one common hypothesis: The current does indeed flow in a dilute percolation backbone, but it is surrounded by many localized electronic sites separated from the current path. The electrons in these sites do not contribute to the overall current, yet influence it by long-range Coulomb interactions. When the gate voltage is changed, several electrons enter or escape these sites, effectively changing the potential landscape in the main paths[5].

Another basic question regarding EG dynamics is why does conductance **increase** after an excitation? Based on Mott's picture of variable range hopping (Ch. 1.2), one can attribute the change of conductance to the higher density of non-occupied states that are well above ϵ_F. As the system relaxes, the electrons arranged below Fermi level, and conductance electrons have less neighboring free sites to hop to. In addition (or alternatively), the Coulomb gap that was established around ϵ_F (Ch. 1.4) reduces the DOS of the equilibrated system. Changing V_g results in a change in the Fermi level, which effectively erases the Coulomb gap, thus increasing G.

---

[4] Perhaps a better quantity to measure is the electrical capacitance, which is directly related to the internal energy of the electrons [88]. Yet, due to the high resistance and capacitance of the disordered samples, it is not practical with the current configuration, and is therefore not included in the scope of this work.

[5] For a more detailed and quantitative description of this theory see Section 9.3 and Figure 9.7 below.

Chapter 7

Experimental Techniques and Characteristic Results of Conductance Dynamics

A measurement of the conductance of macroscopical samples in the range of several kohm to several Mohms might not seem like a true challenge. However, significant thermal noise and mesoscopic fluctuations might be an issue while measuring highly disordered discontinuous films. In addition, in order to maintain the true nature of the glass and not affect it with the external electric field, the applied V_{SD} must be maintained within the linear response regime, hence possibly causing the signal-to-noise ratio to be significantly low.

Furthermore, as we will show in the next chapters, our results indicate that the maximal temperature, T_{max}, is a critical parameter in glassy systems. We therefore had to use a unique fabrication method, the 'quench condensation' technique, to evaporate our samples on cold substrates and measure them in-situ. For this reason, using a cryogenic probe with temperature control is not enough, and we had to also consider ultra-high vacuum (UHV) conditions for the evaporation.

7.1 Experimental setup and instrumentation

Field effect geometry

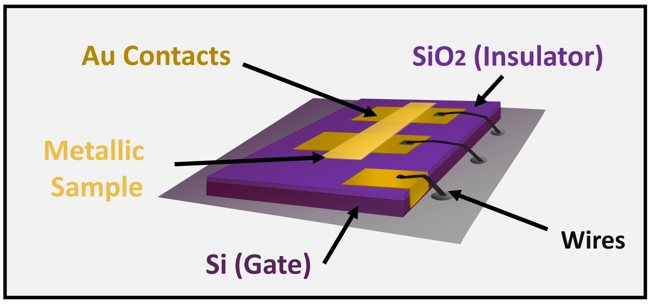

Figure 7.1: Sketch of the sample and substrate configuration. The sample is evaporated on the doped SiO_2 layer between two pre-prepared Au contacts. The bottom gate Si layer is connected from below to a voltage source, applying a high electric field on the sample.

As mentioned above, a common excitation method of EG samples is changing a gate voltage. In our samples, gate voltage was applied using pre-prepared conductive silicon substrates with a 100/500nm highly doped silicon-oxide (SiO_2) insulating layer on top. The sample was placed on the insulating layer, and a voltage source was connected to the bottom part (see Fig. 7.1).

This configuration, which is similar to the metal-insulator-semiconductor-field effect transistor (MOSFET), enables the application of high electric fields on the sample due to this thin insulating layer. The doped SiO_2 has a dielectric strength of 9.5 MV/cm [89], that is, the maximal gate voltage which could be applied to the 100/500nm layer is ±95/450V, respectively. The width of the memory dip depends on the temperature and resistivity, yet in most cases, applying up to ±20V in the 100nm case and ±100V in the 500nm case was enough to observe the whole dip and the surrounding conductance 'background'.

Cryogenic design and temperature control

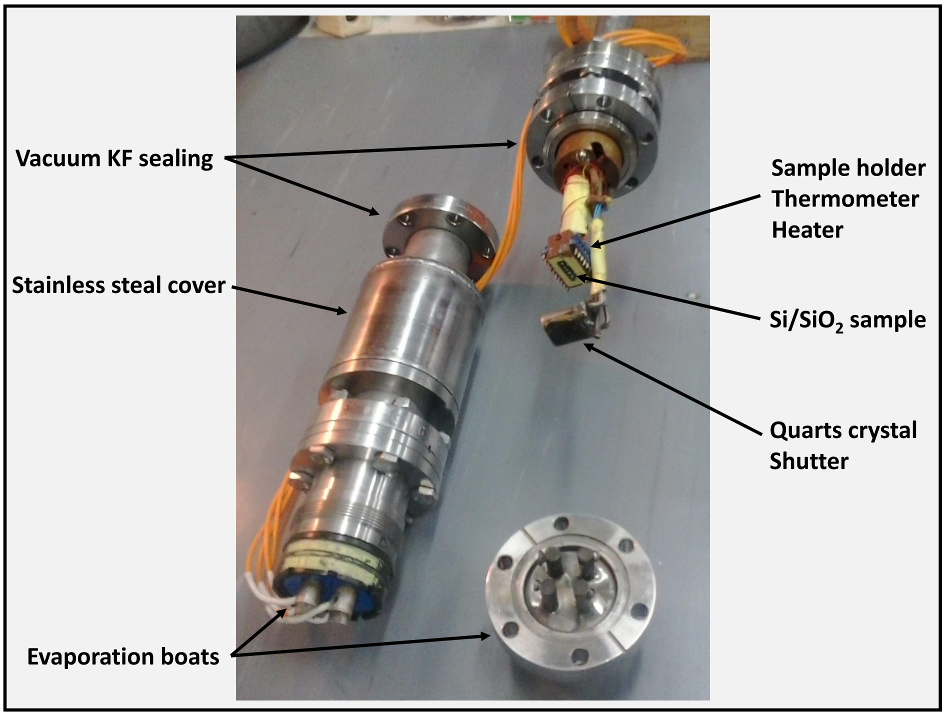

Figure 7.2: Photograph of cryogenic probe. Temperature control allows the measurement of temperature of a range between liquid He (4.11K) and room temperature (300K).

The samples were measured in a variety of temperatures, between 4.11 and 300K, by a designated probe (Fig. 7.2) that consisted of a stainless still vacuum-sealed body, an oxygen-free copper sample-holder, silicon diode or platinum thermometers (LakeShore DT-470/PT-100), and a heater resistor (50Ω, 0.5W). In addition, for the quench-condensation process (see next chapter), an evaporation boat was implemented at the bottom of the probe, connected by two external wires to a high-power electric source. A quartz crystal was placed near the sample in order to measure the evaporation rate.

The sealed probe was pumped out and immersed into liquid helium or liquid nitrogen dewar (Fig. 7.3). The temperature was controlled by a LakeShore 330

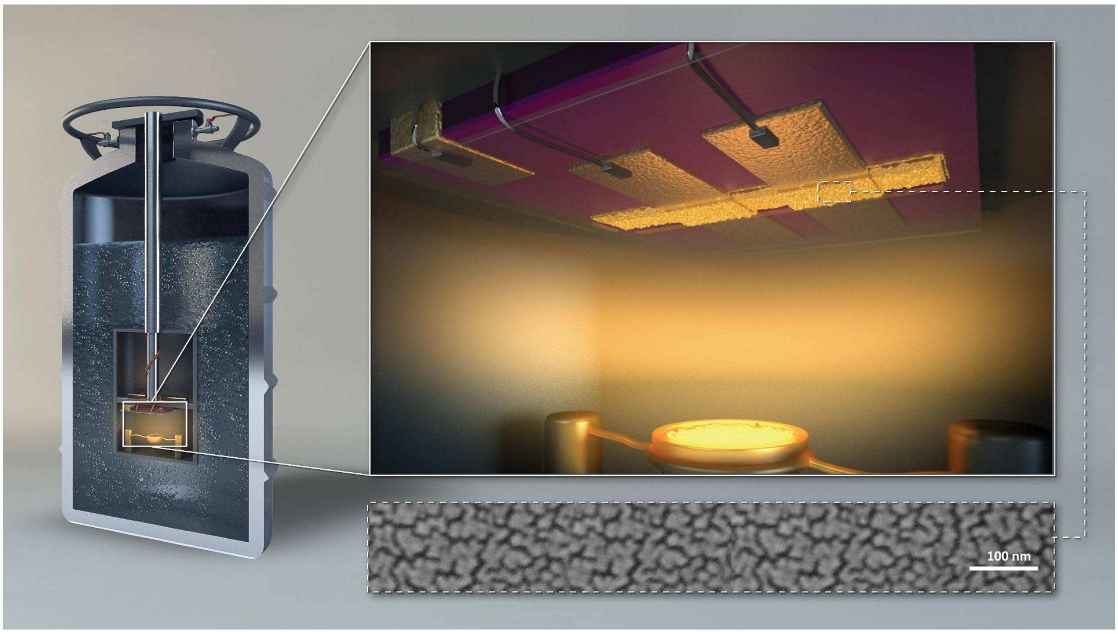

Figure 7.3: A Si/SiO substrate with pre-prepared Au contacts is placed on a sample holder (in gray), situated on a high vacuum measuring probe, which is immersed in to a liquid He bath. Thin films are evaporated through a shadow mask (transparent layer in the sketch) and condensed on the SiO substrate (pink) at cryogenic temperatures. A voltage source is connected to the Si layer (purple), for the application of gate voltage (far left electrode). Source-drain voltage across the sample is applied for conductivity measurement. **Bottom:** A scanning electron microscope image section of a typical quench-condensed Au sample taken at $T =$ 300K, illustrating the discontinuous nature of the film. The quenched disorder in the geometry, combined with the long-ranged Coulomb interactions, leads to frustration, which is at the heart of this system's glassiness.

Temperature Controller, at a range between 4.11K (liquid helium) or 78K (liquid nitrogen) up to room temperature, 300K, with a resolution of ±0.005K.

The probe is pumped prior to cooling by a rotatory oil pump to 10^{-3} torr, and then by a cryogenic pump to 10^{-6} torr. This level of vacuum defines a mean-free-path of the evaporated molecules of several meters [90], which allows direct flow of the metal atoms through the 10cm path from the evaporation boat to the substrate.

To seal the probe at these low temperatures, we have used CF vacuum connectors with copper gaskets between them.

Quench-condensation technique

The major part of the studied samples were prepared by quench-condensation (QC), i.e. evaporation of a metal film on a substrate that is already held at cryogenic temperatures and ultrahigh vacuum [50, 91, 92].

After the probe reaches the required temperature , an electric current is induced in the evaporation boat, heating it to the evaporation point of the metal. The metal vapor aggregates between the pre-deposited gold pads on the SiO_2 substrate through a shadow mask (see Fig. 7.3). Conductance is measured continuously throughout the entire sample growth and measurement protocol, and allows the fabrication of samples with resistances from a few KOhms up to several GOhms, and at temperatures between $8 - 300$K[1]. This technique enables exploring the dependence of conductance properties on the working temperature, T, on the temperature the sample was fabricated at, T_{fab}, and the highest temperature the system was exposed to, T_{max} (which was eventually found to be an important parameter in conductivity dynamics) - without exposing the samples to higher temperatures or to the ambient atmosphere.

Other samples were made by conventional fabrication methods at room temperature using a thermal and e-beam evaporator, and were exposed to the atmosphere prior to cooling and measurement. This method, in contrast to QC, enables precise control of the deposition rate (r) and chamber pressure (P) which are found to have great influence on film morphology.

The resultant films in both methods are discontinuous films of about 5nm thickness, composed of clusters of grains organized in a strenuous geometric arrangement, as shown in the bottom part of Fig. 7.3 (see also Fig. 8.5 below). Due

---

[1] Naturally, the heat produced by the hot metal vapor and radiation during the QC increase the base temperature from 4.11K to about 8K.

to the strong disorder of the films, the electronic states are localized and transport is governed by hopping conductivity, following Efros-Shklovskii-type VRH temperature dependence (Eq. 1.16), $G \propto \exp(-T_0/T)^{0.5}$, as depicted in Fig. 7.4.

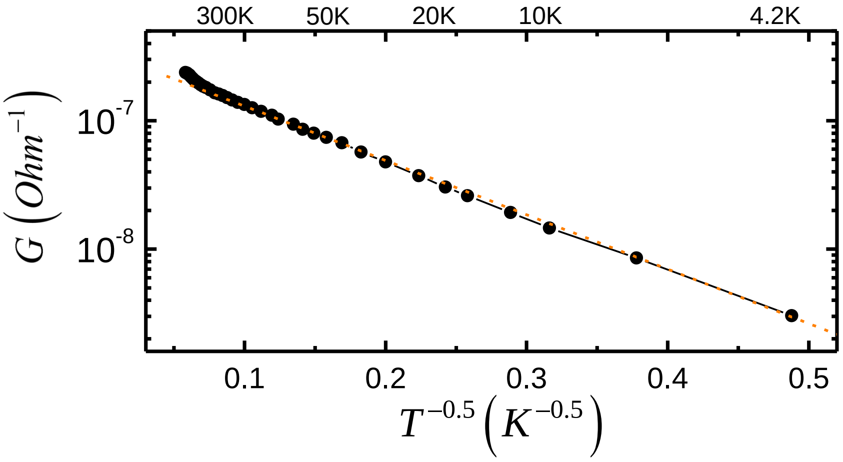

Figure 7.4: Conductance versus temperature of a discontinuous Au film (black circles) and a fit to Efros-Shklovskii variable range hopping conductivity with $T_0 = 95K$ (orange dashed line).

Right after the fabrication (in the films made by QC) or cooling (in the other films), conductance of the quench-condensed sample was allowed to equilibrate for 10 hours, after which the measurement protocol was applied.

Due to the repetitive form of glass with changing V_g, a sequence of several measurements could be applied on every sample, at various temperatures. However, since the logarithmic rate could be very slow at low temperatures, the protocol included a period of heating to T_{fab} (or T_{max}) between consecutive measurements.

Electronic setup

Conductance was measured by the two-probe method using either an ac or dc current without apparent difference between the two. The vast majority of the measurements was executed using an EG&G lock-in amplifier applying ac voltage with an amplitude of 0.1/0.5V and frequencies of up to 17Hz. The lock-in was connected to the probe by BNC connectors and 75Ohm impedance coaxial cables. A Keithley 2400 Source-Meter was connected to the silicon layer of the substrate, applying dc gate voltage.

All three instruments (lock-in, voltage source and temperature controller) were connected via GPIB cables to a National Instruments GPIB-to-USB converter (NI GPIB-USB-HS), and were controlled simultaneously by an automated LabView-programmed interface.

The grounds of all of the electrical measurement devices, including their cabinet, were connected directly to a wet ground outside the lab. This reduced the overall noise to less than 0.1% of the measured conductance at 300K, and less than 0.01% at lower temperatures. As noted before, the glassy effect amplitude is around 1%, hence we faced significant noise at the higher temperatures.

7.2 Determination of the relaxation rate

Although the logarithmic slope of glassy relaxation does not bear a characteristic timescale, several methods have been proposed to define the rate of glass dynamics. In this work, we used two of these methods.

The logarithmic slope S

The natural parameter used to characterize the sluggishness of the system is the logarithmic slope, S -

$$\Delta G \equiv G_0 - G(t) = S \cdot \log(t) \tag{7.1}$$

However, the memory dip amplitude significantly changes with T, presumably due to thermal screening, hence comparing different temperatures can not be done

directly. Based on the assumption that the relaxation process is a result of many simultaneous small re-configurations of electrons in the metal, where each such process contributes to the conductance decay an average amount denoted as δG, and assuming that the thermal screening alters δG - we suggest that this temperature dependence of S can be eliminated with a simple normalization by ΔG_0 (the change of conductance at $t = 1$sec after switching from V_{g1} to V_{g2}).
Namely -

$$s \equiv \frac{S}{\Delta G_0}, \tag{7.2}$$

since the overall change of conductance is also directly related to this δG.

Indeed, to normalize the new formation of a dip with δG_0 of a dip that was formed at another T, or to compare the amplitude of two memory dips induced at different temperatures (see next chapter), we have to also assume that δG_0 does not depend on their origin temperatures, and the only thing that changes between the two is the normalized slope s. In other words, while measuring at a particular temperature T, we assume that the only thing that characterizes the history of the two memory dips is their amplitude, while the relaxation rate is related only to T. This assumption underlies all EG experimental results in the last two decades. Nevertheless, recent results of EG dynamics in AlO systems, observed by Delahaye and Grenet, imply that this is not always the case, as in some cases, the two dips have identical amplitudes but very different dynamic rates [93]. Thus, the current understanding of EG dynamics is questioned, and further research must be carried out to determine if this is a general behavior. This, however, is not in the scope of the current work.

In order to make the measurements repeatable and the normalization by ΔG_0 true, we used a strict protocol: Heating the sample to the maximal temperature for $t_{eq} = 5000$sec at V_{g1}, cooling it to the required T, waiting 1000sec for stabilization, switching to V_{g2} and determining the slope for another 5000sec.

An example of several normalized slope measurements is presented in Fig. 7.5, showing s values between 11.4% and 3.25% per order of magnitude in time.

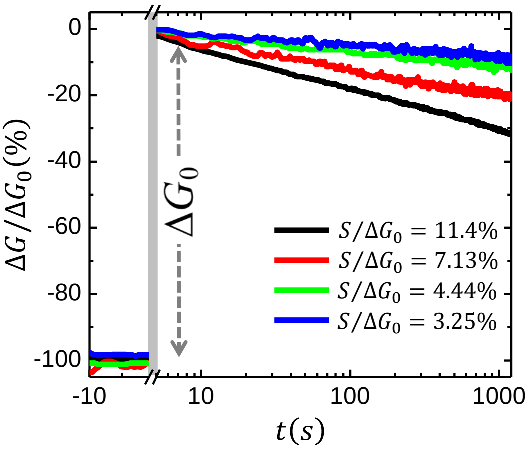

Figure 7.5: Normalized conductance as a function of time after a change in V_g of 4 different samples, showing relatively fast decay (black) and relatively slow relaxations (blue).

The two-dip experiment

In some cases, it has been the custom to address a more intuitive measure of the relaxation, i.e. a characteristic time for the relaxation process. Unlike exponential or power law slopes, there is no well-defined value for the logarithmic process (which originates in the uniform distribution of potential barriers), and another method has to be used.

Here, we adopt a version of the 'two dip experiment' (TDE) suggested by Ovadyahu et al. [77, 94]. In this protocol, the sample is allowed to equilibrate for a long time t_{eq} under a gate voltage V_{g1}, leading to the build-up of a memory dip centered around V_{g1}. The gate voltage is then abruptly changed to V_{g2}, leading to an increase of conductance by an amount defined as ΔG_0 (see Fig. 7.6). Then, fast $G(V_g)$ scans are performed at selected time intervals, showing the amplitude growth of the new memory dip around V_{g2} over time. The characteristic relaxation time, τ, is defined as the time in which the amplitudes of the new dip $\Delta G(t)$ equal $\Delta G_0/2$.

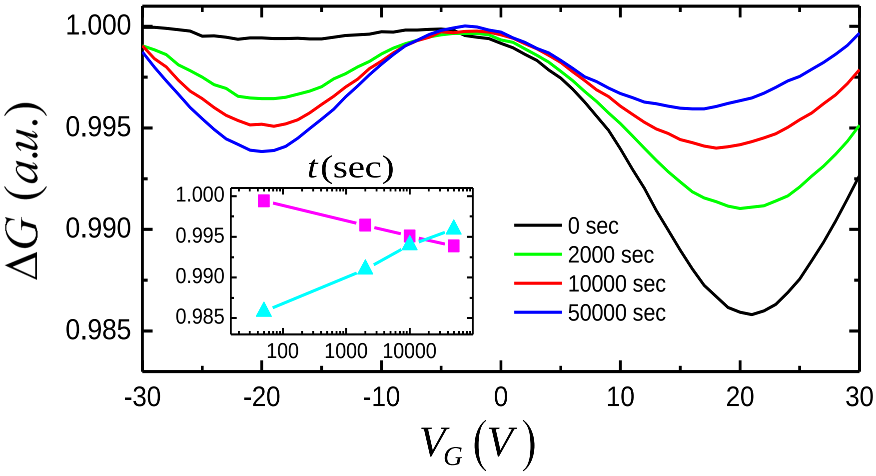

Figure 7.6: Conductance as a function of gate voltage at selected times after switching V_g from $V_{g1} = 20$V to $V_{g2} = -20$V. The black curve shows the initial memory dip at V_{g1}, with a new dip growing around V_{g2}. The scan time here is 30 seconds. In the inset, the amplitude of the dips is plotted versus time, showing the logarithmic decay. The characteristic time τ is the time at which the amplitudes cross each other, about 15000 seconds.

This definition of τ is only a **relative** measurement of the timescale, and does not bear any immanent physical value, since logarithmic relaxation does not stop even after few millions of seconds (weeks).More specifically, ΔG_0 is set by the time period at which it was allowed to equilibrate at V_{g1}, t_{eq}, by the same logarithmic relation. Therefore, comparing the new dip to the amplitude of the old one does not give any information on the more physical parameter, S.

Another drawback of TDE is the time needed to scan the whole range of gate voltages. Due to the capacitance between the sample and the gate, the minimal scanning time, t_{scan}, is about 10 seconds. During this period, a part of the new dip at V_{g2} is erased.

The above two effects were shown to set a constant τ, which is determined only by the experimental procedure [6, 95]. If we assume the system relaxes for t_{eq} seconds at V_{g1}, a dip is formed with an amplitude of -

$$\Delta G_0 = S \cdot \log\left(t_{\text{eq}}\right). \tag{7.3}$$

Starting the measurement at $t = 0$, a new dip beings to establish at V_{g2} with the same rate. While scanning the gate voltage at time t, the amplitude of the observed new dip with time is equal to -

$$\Delta G(t) = S \cdot \log\left(t\right) - S \cdot \log\left(t_{\text{scan}}\right) = S \cdot \log\left(\frac{t}{t_{\text{scan}}}\right). \tag{7.4}$$

The new dip will satisfy the TDE condition after τ seconds, i.e. -

$$S \cdot \log\left(\frac{\tau}{t_{\text{scan}}}\right) = \frac{S \cdot \log\left(t_{\text{eq}}\right)}{2}, \tag{7.5}$$

leading to the following constant value of τ, which is in fact independent of S:

$$\tau_{\text{const}} = \sqrt{t_{\text{eq}} \cdot t_{\text{scan}}}. \tag{7.6}$$

Nevertheless, this trivial result is true only if the first and second dips were formed under the same physical conditions. Since S is temperature-dependent, TDE can provide useful information if the first dip is built at a higher temperature T_2 and the second dip at T_1. The characteristic time τ in this case reflects the ratio between the timescales at the different temperatures, and consequently holds information on the relative dependence of the slope on temperature $S(T_1)/S(T_2)$. The results from a variety of temperatures provide information on the relation between glassy dynamics and temperature $S(T)$. This relation at different temperatures is the main goal of the next two chapters[2].

In our measurement protocol, the samples were heated for a period of $t_{\text{eq}} = 10$ hours to $T_{\max}$ in V_{g1}, and were then cooled down to the measurement temperature T. Subsequent to a short stabilization period, the gate voltage was swiftly scanned and then fixed on V_{g2}. This first scan indicated the amplitude of the dip, which formed at $T_{\max}$ at the measurement temperature ΔG_0. Other fast V_g scans were performed at chosen times, t_{probe}, introducing the development of the new dip. The amplitude of this new dip, $\Delta G(t)$, was compared to ΔG_0, and the time at which $\Delta G(t)$ was equal to $\Delta G_0/2$ was defined as τ (see inset of Fig. 7.6).

7.3 Extrapolation of τ

As the temperature is lowered, glass dynamics slow down considerably (see Eq. 8.1 in the next chapter), and it becomes impractical to wait for the new dip to realize the condition of $\Delta G(t) = \Delta G_0/2$. Therefore, we determined the value of τ by an extrapolation based on the logarithmic growth of the peak amplitude with time.

Considering the glassy logarithmic slope (Eq. 6.5), one may presume that the new dip's amplitude at t_{probe} would be equal to $S \cdot \log(t_{\text{probe}})$. However, as was discussed earlier, during the scan time, a fraction of this amplitude is erased, and the resulting amplitude follows -

$$\Delta G(t_{\text{probe}}) = S \log(t_{\text{probe}}) - S \log(t_{\text{scan}}). \tag{7.7}$$

---

[2] The TDE and the direct observation of conductance evolution in the previous section with normalization via ΔG_0 (Fig. 7.6) are very similar, and are both based on the assumption that the dynamics of a dip at T_1 do not depend on T_2, as mentioned above.

Hence, extracting S from this relation is possible by:

$$S = \frac{\Delta G(t_{\text{probe}})}{\log(t_{\text{probe}}/t_{\text{scan}})}. \tag{7.8}$$

On the other hand, the initial amplitude of the 'old' dip, ΔG_0, is also not the true one, as it was also erased by $S\log(t_{\text{scan}})$, i.e. -

$$\Delta G_0^{\text{eff}} = \Delta G_0 + S\log(t_{\text{scan}}). \tag{7.9}$$

τ is the time at which $\Delta G(t)$ equals $\Delta G_0^{\text{eff}}/2$, hence:

$$S\log(\tau) = \frac{\Delta G_0^{\text{eff}}}{2} = \frac{\Delta G_0}{2} + S\log(t_{\text{scan}}), \tag{7.10}$$

and by using the above expression for S, we have -

$$\frac{\Delta G_0}{2} = S\log\left(\frac{\tau}{t_{\text{scan}}}\right) = \Delta G(t_{\text{probe}}) \cdot \frac{\log\left(\tau/t_{\text{scan}}\right)}{\log(t_{\text{probe}}/t_{\text{scan}})}. \tag{7.11}$$

Therefore, the characteristic relaxation time may be calculated using the following expression:

$$\tau = t_{scan}\exp\left[\log\left(\frac{t_{probe}}{t_{\text{scan}}}\right) \cdot \frac{2\Delta G(t_{probe})}{\Delta G_0}\right]. \tag{7.12}$$

This is the process that was employed to determine τ in Fig. 9.4, 9.5, 9.6 and 9.8, where τ was averaged in several V_g scans at different t_{probe}.

Chapter 8

The Effect of Maximal Temperature on EG Dynamics

In this chapter, we present a study of the conductance relaxation of electron glass Au, Ni and Ag samples that were fabricated at low temperatures. The results suggest that under the right conditions, glass can also possess a different type of memory. Remarkably, the dynamics have been found to be dependent not only on the ambient measurement temperature, but also on the maximum temperature to which the system has been exposed. Hence, the system 'remembers' its highest temperature.

As we discuss below, this effect may be qualitatively understood in terms of energy barriers and local minima in a configuration space, and may therefore be a general property of the glass state.

This study was recently published in Physical Review Letters, in collaboration with T. Havdala, J. Delahaye, T. Grenet and A. Amir [49].

Introduction

As we have mentioned earlier, a glassy system is often characterized by a typical glass temperature T_G, below which its dynamics slow down dramatically. The sluggishness is attributed to multiple local minima separated by energy barriers in the configuration space. At high temperatures, the system can explore the entire configuration space and is thus ergodic. As the temperature is lowered below T_G, the system becomes trapped in a subsystem of metastable states and is no longer ergodic.

In EG, however, glass temperature was never discovered. Prior to the current study, electronic glassy effects were measured only between 2K to 30K, but no slow-down of the dynamics was observed. For this reason, T_G was suggested to be $T = 0$, similar to quantum phase transitions [77].

This study explores a situation where glass never had the chance to 'visit' the entire configuration space: What is the temperature dependence of the dynamics if the system is prepared in a glassy state and is 'born' non-ergodic?

We investigate the dynamics of electron glass systems fabricated using the quench-condensation technique, which enables the preparation of glassy systems at cryogenically low temperatures. Studying the temperature dependence of conductance relaxation as a consequence of gate voltage excitation under these conditions reveals a striking effect: The dynamics are found to be dependent not only on the working temperature, but they are also strongly affected by the maximal temperature at which the sample was allowed to equilibrate.

8.1 Results

In the following section, we present results of the conductance dynamic in thin metal films with a variety of resistances and at temperature ranges between 4 and 300K. The experimental procedure followed both the TDE protocol and the direct slope measurement. First, to examine the effect of $T_{\max}$ on the dynamics, we tested the same system before and after heating to a new $T_{\max}$.

In Fig. 8.1**a**, we present the memory dip amplitude as a function of time for a discontinuous Au film that was prepared at $T = 140$K (black squares). A clear logarithmic slow relaxation of conductance was observed, consistent with Eq. 6.5. Heating the sample to 170K for ~1600sec and cooling it back down had a relatively small effect on resistance (~20%), indicating that there is no great change in the microstructure; however, it was found that the dynamics slowed down dramatically. The slope of the logarithmic curve was found to be decreased by a factor of 3 as a result of the heating-cooling cycle (blue circles). Repeating this process had no further effect on the dynamics (green triangles), demonstrating that it is the first heating to $T = 170K$ that has the remarkable influence on the relaxation.

A related finding is shown in Fig. 8.2, depicting conductance relaxation of a series of samples that were heated to various maximal temperatures $T_{\max}$ for relatively long periods, and cooled back to T=130K, such that the resistance $R_{130\mathrm{K}} \sim 100M\Omega$ for all samples. One can see that the slope of these curves s increases monotonously with $T_{\max}$ and can be approximately described by:

$$s \propto \frac{T}{T_{\max}}, \tag{8.1}$$

as is illustrated in the inset.

Apparently, the system remembers that it was exposed to temperature $T_{\max}$. The higher this temperature, the slower the dynamics are at $T < T_{\max}$. Evidently, the highest temperature experienced by the sample is encrypted in the dynamics of the system.

This behavior was observed in samples spanning a large range of fabrication temperatures. The dependence of s on the measurement temperature T, for three

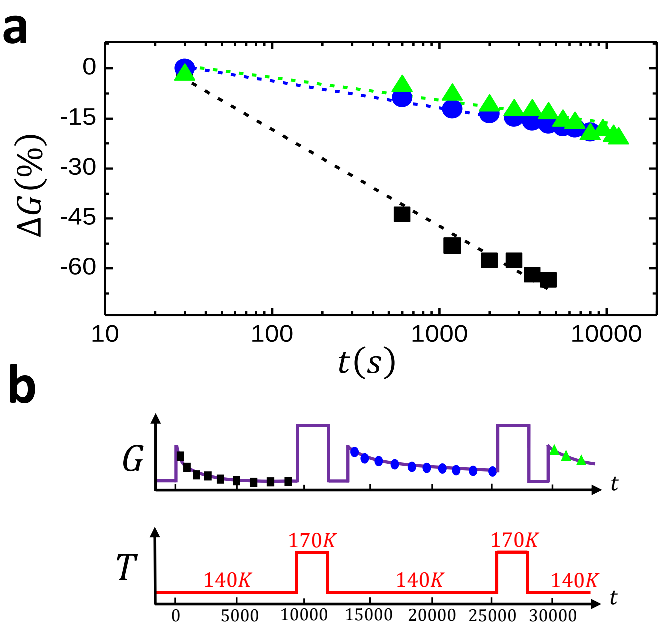

Figure 8.1: **a**: $\Delta G = [G(t) - G_0] / \Delta G_0$ as a function of time for a discontinuous Au film that was excited out of equilibrium at 140K. The black squares indicate the initial curve in which $T = T_{\max} = 140$K ($R = 2M\Omega$). The blue circles depict conductance versus time measured after the sample was heated to 170K and cooled back to 140K, thus defining $T_{\max} = 170$K ($R = 2.4M\Omega$). The green triangles show the results after a second heating-cooling cycle. The experimental protocol is illustrated in panel **b**.

discontinuous Au films prepared at different temperatures and accordingly having different $T_{\max}$ - can be seen in Fig. 8.3. Once again, the dependence of the dynamics on both T and $T_{\max}$ is evident. For all three samples, $s \approx 7$ at $T = T_{\max}$, and it decreases considerably as T is lowered. The slope was found to be a function of $T/T_{\max}$, and it roughly follows Eq. 8.1.

Similar $s(T)$ curves to those shown in Fig. 8.3 were obtained for over 20 Au samples, with resistances ranging between a few kohms to several hundred Mohms, and sizes ranging from 20×50 μm to 7×7mm. Circa half of them were fabricated at room temperature and exposed to air prior to measurement (3 such samples are presented in the appendix below), while the rest had various lower $T_{\max}$. We observed similar results in 4 quench-condensed Ni films and 2 Al films. Similar to

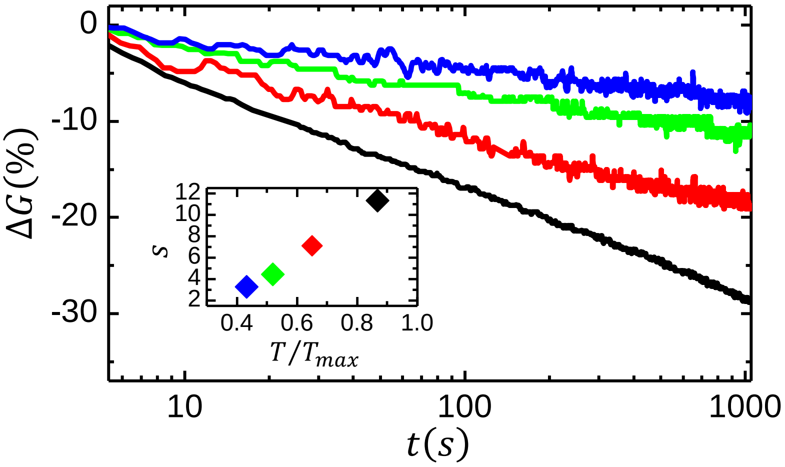

Figure 8.2: Conductance relaxation over time, measured at $T = 130\text{K}$ for four discontinuous Au films having T_{max} of 150K (bottom black line), 200K (red line), 250K (green line) and 300K (top blue line). For all samples, resistance at $T = 130\text{K}$ was ~$100M\Omega$. **Inset:** The slope of the $G(t)$ curves ($s = S/\Delta G_0$) as a function of T/T_{max} for the four samples, demonstrating the dependence of Eq. 8.1.

other EGs [6, 7], we observed no dependence of s on the cooling rate within the experimental abilities, in contrast to other types of glasses.

It is important to note that a film grown on a cryo-cooled substrate is amorphous, while samples fabricated or heated to room temperature may indeed be crystalline [96]. However, we did not observe any difference in the results obtained on different samples that were prepared at different temperatures. This is consistent with the conjecture that conductance is governed by hopping between islands in the discontinuous sample, and not by the atomic order in the islands.

8.2 Discussion

The fact that the dynamics depend strongly on T is naturally understood in terms of energy scales of the potential landscape versus thermal energy (see Eq. 6.1). But how can one understand the dependence on T_{max}? We suggest an explanation that

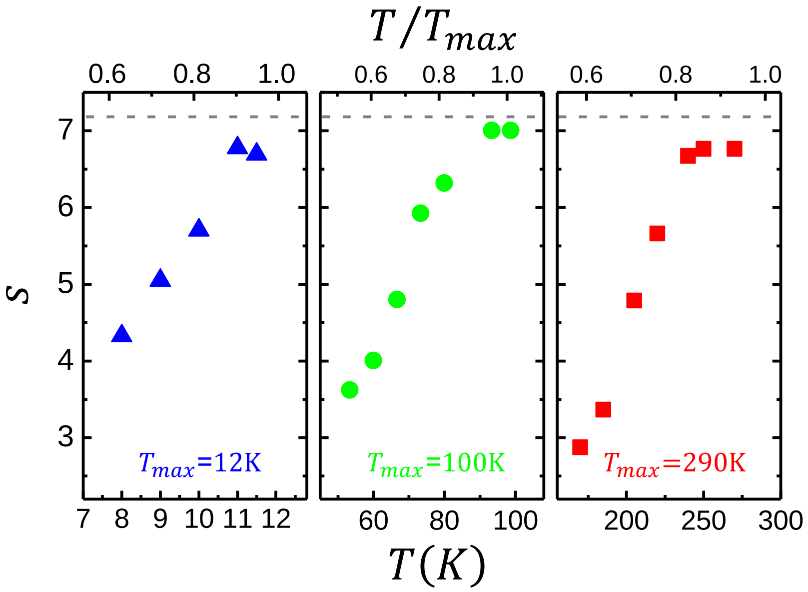

Figure 8.3: The conductance relaxation slope, s, as a function of temperature T and of $T/T_{\max}$, for three discontinuous Au films with a $T_{\max}$ of 12, 100 and 290K, from left to right, respectively. All samples were allowed to equilibrate at $T_{\max}$ for several hours and were then cooled down to T just before measurement. The dashed line marks the experimental limit in a large s which is set by the measurement protocol (Eq. 7.6).

may be generic to glassy systems prepared at temperatures in which the system is already glassy.

A general property of glass is that the presence of interactions may cause the system to be trapped in metastable states in the configuration space. The energy barriers between these states have a wide distribution, which leads to a slow relaxation process toward equilibrium over many orders of magnitude. Heating the glass to a higher temperature exposes the system to an even wider distribution of barriers, and consequently causes the relaxation process to become slower after the sample is cooled back down to a lower temperature.

Considering the exact assumption of Eq. 6.4 for conductance dynamics, i.e. thermally activated simultaneous processes with uniform distribution, leads to the following relation -

$$\Delta G(t) \propto \sum_{\lambda} e^{-\lambda t} = \int_{\lambda_{\min}}^{\lambda_{\max}} e^{-\lambda t} P(\lambda) d\lambda \approx C \left[-\gamma_E - \log(\lambda_{\min} t)\right], \tag{8.2}$$

where, as was mentioned earlier, $\lambda_{\min}$ and $\lambda_{\max}$ are the minimal and maximal rates in the system, and γ_E is the Euler-Macheronni constant. As in Eq. 6.3, C is proportional to the density of the energy barrier.

As the system relaxes toward lower energy values, each relaxation lowers the conductance by an amount δ_G, namely

$$G(t) = G_0 - \delta_G C \cdot \log(t), \tag{8.3}$$

where δ_G may also depend on the temperature. In order to eliminate this non-universal dependence, it is sensible to normalize the slope by ΔG_0, since:

$$\Delta G_0 = \int_{\lambda_{\min}}^{\lambda_{\max}} \delta_G P(\lambda) d\lambda = C \delta_G \log\left(\frac{\lambda_{\max}}{\lambda_{\min}}\right) \approx C \delta_G U/T. \tag{8.4}$$

Thus, we find that the normalized conductance relaxation $\Delta G(t) = (G(t) - G_0)/\Delta G_0$ scales logarithmically, with a slope proportional to T/U.

Again, we note that this analysis is based on several assumptions: (A) a uniform distribution of energy barriers, (B) each microscopical process equally contributes to the overall conductance change, δG, and (C) δG depends only on the ambient temperature and not on the thermal history of the sample. As far as we can tell, these assumptions are fully supported by the experimental results.

The experimental results indicate that for our systems, which were prepared at a low temperature (below T_G), and therefore never had the chance to explore large parts of the configuration space, the relevant energy scale of the barriers is

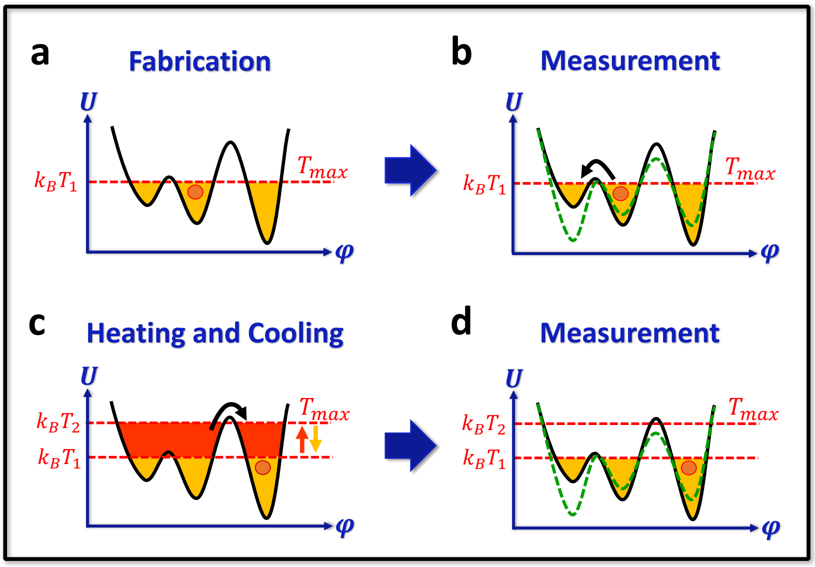

Figure 8.4: Sketch of a section of the potential landscape in phase space. The black solid lines describe the landscape in its initial state. Applying a gate voltage changes this potential line (green dashed lines) and ignites a relaxation process. For all steps, the system tends to minimize its free energy, i.e. to thermally equilibrate to a configuration with the lowest possible potential. At the first stage (**a** and **b**), accessible energy is bounded by the barriers of the order of fabrication temperature T_1. Heating to a new maximal temperature T_2 results in the system exploring deeper potential wells, and is hence characterized by slower relaxation processes after recooling to T_1, as is discussed in the main text (**c** and **d**).

$U \propto T_{\rm max}$; hence, the distribution of relaxation depends on $T_{\rm max}$. Since thermal activation also dominates relaxation processes at a lower temperature T, we obtain a logarithmic relaxation with the slope: $s_{\rm new} = W \cdot \frac{T}{T_{\rm max}}$, as is indeed depicted in Fig. 8.1, 8.2, 8.3 and 8.5, and is expressed in Eq. 8.1. The factor W depends on the waiting time at $T = T_{\rm max}$, $t_{\rm eq}$, which was kept constant throughout the measurements.

An intuitive way to understand this result is to consider a simple potential landscape in the phase space, illustrated in Fig. 8.4, undergoing the following sequence of events:

a. The system is prepared at temperature T_1. Here the electrons are limited to exploring potential wells in the configuration space that are separated by barriers,

U, where $U \propto k_B T_1$.

b. The system is excited by a gate voltage change at $t = 0$, thus modifying the underlying electronic potential landscape. The relaxation is dominated by barriers whose magnitude is set by $k_B T_1$.

c. The system is heated to $T_{\max} = T_2 > T_1$. This enables electrons to enter deeper wells separated by higher barriers proportional to $k_B T_{\max}$. Upon a sequential cool down, the system is frozen in regions of phase space with larger potential wells

d. After excitation of the system, relaxation is now dominated by barriers whose magnitude is set by $k_B T_{\max}$, and the dynamics slow down considerably.

8.3 Intrinsic or extrinsic?

As we presented above, and in following with many previous studies, conductance dynamics in electron glasses are argued as driven by 'intrinsic' effects, menaining, processes that are governed by conduction electrons [82, 84, 87]. Yet, one may wonder whether the above temperature dependence is related to 'extrinsic' processes ,since heating the sample may affect the microstructure of the films. The experimental findings, however, show that morphology change does not affect the temperature dependence of the dynamics.

Fig. 8.5 shows 3 discontinuous Au films having the same $T_{\max}$ but very different geometries due to different preparation conditions.

The three samples were fabricated at $T = 300$K (thus defining $T_{\max} = 300K$ for all three) under different evaporation conditions, using a standard evaporator (i.e. not the QC technique). The lower panels of the figure depict scanning electron microscope (SEM) images of the three samples, clearly showing that the microscopic geometry is significantly different. Specifically, the grain average size and inter-grain spacing vary from sample to sample.

The upper panels show the logarithmic slope s of the conduction relaxation, following an abrupt excitation as a function of temperature. It is seen that $s(T)$ is similar for the three films. This result demonstrates that glassy properties, and the temperature dependence of the relaxation rate in particular, are relatively insensitive to film microstructure or geometry details. We therefore conclude that the dependence of $s(T)$ on $T_{\max}$ presented in the main text is not related to 'extrinsic' morphology variations, but rather originates from 'intrinsic' electronic processes.

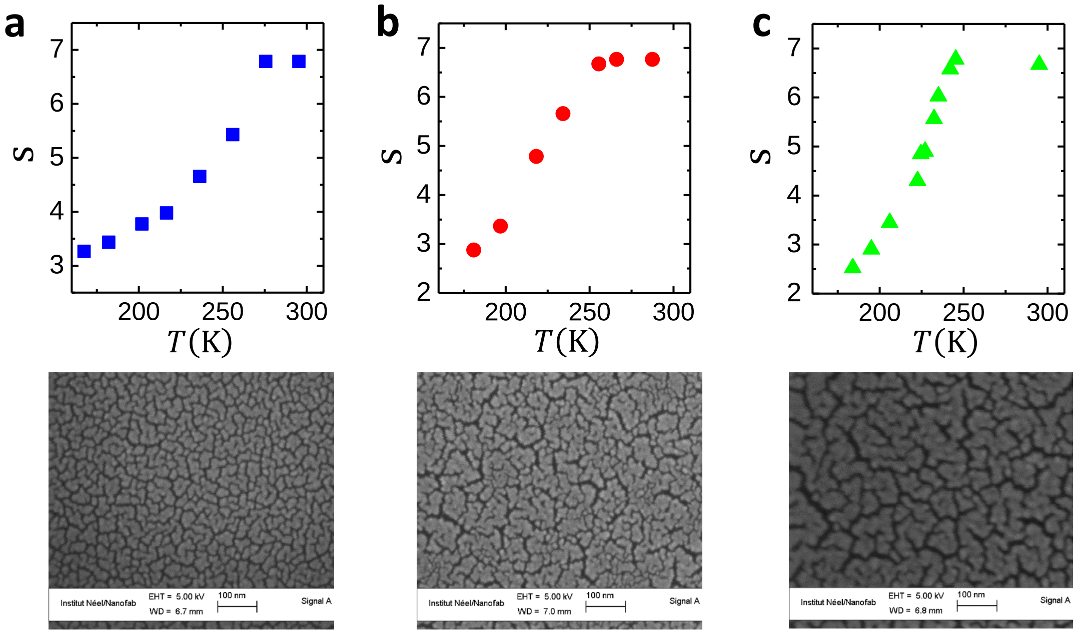

Figure 8.5: Upper frames: The slope of the conductance after an abrupt change in gate voltage, s, as a function of temperature for three Au films with $T_{\max} = 300\mathrm{K}$. The samples were evaporated under different partial pressures in the evaporation chamber (p) and evaporation rates (r), as follows: **a:** $p = 2 \cdot 10^{-7} mb$, $r = 0.4 nm/s$; **b:** $p = 5 \cdot 10^{-7} mb$, $r = 0.1 nm/s$. **c:** $p = 2 \cdot 10^{-6} mb$, $r = 0.05 nm/s$; **Lower frames:** The corresponding SEM micrographs of the samples.

8.4 Conclusions

Naturally, temperature is a crucial quantity in determining the dynamics of a glass. In recent years, a number of nontrivial effects of temperature have been reported, such as rejuvenation memory [97, 98], temperature chaos [54, 99], cooling rate memory effects [64, 65], and possible cooling-induced sample maturing. The dependence of glassy properties on the highest temperature $T_{\rm max}$ presented in this study is a novel, intriguing temperature effect, which demonstrates that the dynamics of a glass can reveal the glass's highest temperature. This is made possible by use of the quench-condensation technique which enables the preparation of samples at temperatures in which the system is already glassy. This unique memory may be a general feature of glasses prepared at $T < T_G$, in which the sample could only explore a limited fraction of the configuration space. In a sense, $T_{\rm max}$ takes the role of an effective T_G in controlling the relaxation processes of the glass. It would be interesting to explore additional glasses to discover the regime of applicability of this novel phenomenon.

Chapter 9

Crossover from Classic to Quantum Glassy Dynamics

As was shown in the previous chapter, in discontinuous metallic films, the characteristic relaxation time slows down dramatically with decreasing temperature. Here, we show that this process is limited to relatively high temperatures, above ~$0.5T_{\mathrm{max}}$. Below this point, the dynamics become temperature-independent. We discuss these results and attribute them to a crossover from thermally activated to quantum tunneling dominated relaxation processes. We present a model that suggests that the temperature range of the experiments (which is proportional to T_{max}), as well as the sample microstructure, determine the relevant statistics and scales of the energy barriers governing the electronic properties of the system.

This part of the work is a direct continuation of the results from the previous chapter, and is currently in preparation for publication in a peer-reviewed journal.

9.1 Introduction

In contrast to temperature dependence in other glassy systems and in the results presented in Chapter 8, in previous results in high carrier concentration indium oxide [100] and in granular aluminum films [81], τ was found to be independent of T, and in low carrier concentration indium oxide, it was reported to even *decrease* with a decreasing T (see Fig. 6.7**b** and Fig. 9.1) [100]. These results were taken as an indication of the importance of quantum effects, in which the barriers are overcome by quantum-mechanical tunneling rather than thermal activation. One can expect tunneling to dominate the relaxation of any glass at sufficiently low temperatures. Apparently, in indium oxide and granular aluminum, tunneling is the dominant mechanism for electronic relaxation up to the highest studied experimental temperature (~30K).

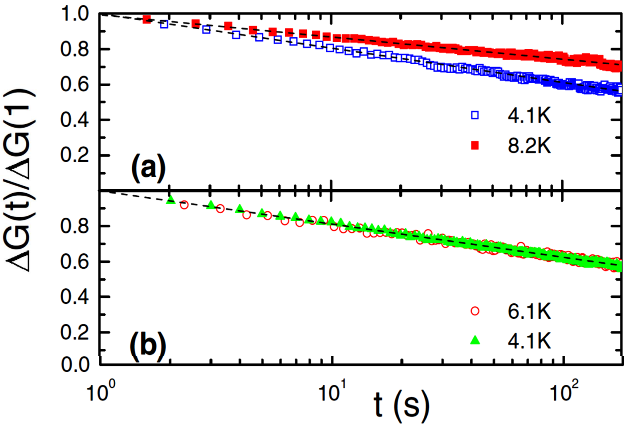

Figure 9.1: Conductance relaxation after V_g change at different temperatures - in low carrier concentration In_2O_{3-x} (**a**), and high carrier concentration In_2O_{3-x} (**b**) (see text) (Z. Ovadyahu, 2007 [100]).

In contrast, recent experiments on NbSi [83] (Fig. 9.2) and discontinuous metal films [49, 50] (see previous chapter) performed up to $T = 300$K, showing a clear temperature dependence of the dynamics, which slow down as the temperature decreases, though the effect of T was different for the two systems. Specifically, as demonstrated in the previous chapter, in discontinuous Au films, the characteristic relaxation slope was found to follow $s \propto \exp\{T_{\max}/T\}$, where $T_{\max}$ is the highest temperature experienced by the sample (Eq. 8.1).

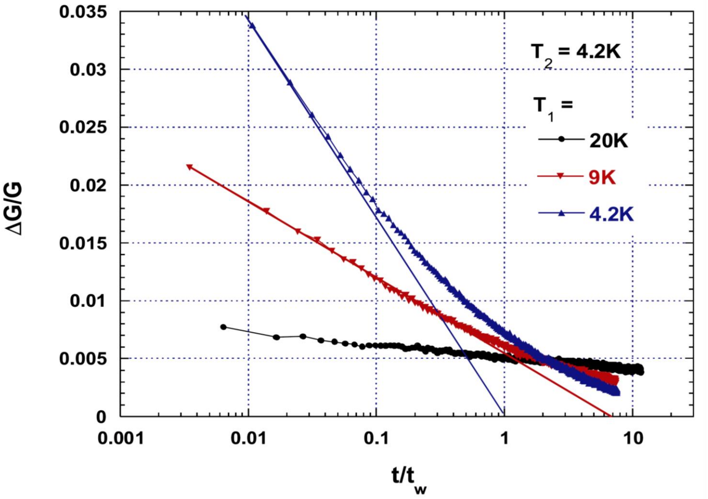

Figure 9.2: Conductance relaxation after V_g change to V_{g2} at $4.2K$, after a period of 20000 seconds with V_{g1} at 20K (black), 9K (red) and 4.2K (blue). At higher temperature the memory dip amplitude is higher, indicating temperature-dependent glass dynamics (J. Delahaye et al., 2014[83]).

In this chapter, we present comprehensive results on the temperature dependence of the dynamics of discontinuous Au films in a wide temperature range below room temperature (300K). Our main finding is that the dynamics follow Eq. 8.1 only for a limited temperature range below 300K, and at a low enough temperature, the dynamics become temperature-independent. These results are interpreted as a crossover from classic to quantum glassy behavior, where the crossover temperature depends on the film microstructure and on the sample fabrication temperature, T_{fab}, which plays the role of $T_{\max}$ if the sample is not heated beyond this temperature. This explanation is also in agreement with earlier results on In_2O_{3-x} and granular Al, as they were made at room temperature or above, and were cooled to the quantum regime prior to measurement.

Experimental methodology

Similar to the samples presented in Chapter 8, part of the films in this study were made utilizing the quench condensation-technique, and the other part via conventional room temperature evaporation. However, in contrast to the previous chapter and due to convenience reasons, in this study we used the two-dip experiment (TDE) to extract the characteristic time τ, as was defined in the last section of Chapter 7.2. The relation between the two measurements protocols is as follows (see Eq. 7.11):

$$s = \frac{S}{\Delta G_0} = \frac{1}{2\log\left(\frac{\tau}{t_{\text{scan}}}\right)}, \tag{9.1}$$

where t_{scan} is about 10 seconds.

The samples here were made at T_{fab}, which is effectively the maximal temperature they were exposed to (i.e. $T_{\text{max}} = T_{\text{fab}}$), and were then allowed to equilibrate for 10 hours at T_{fab} before each measurement.

9.2 Results

Fig. 9.3 depicts the time-dependent evolution of a new memory dip at 6 different temperatures for a discontinuous Au with $T_{\text{fab}} = 290K$. It can be seen that cooling from $T = 240K$ to $T = 125K$ results in a significant slowing down of the dynamics. Additionally, τ increases from $10^4 s$ at $210K$ to $10^8 s$ at $125K$, clearly demonstrating the temperature dependence of EG dynamics. Interestingly, further cooling to $T = 80K$ has very minor influence on τ. The full dependence of τ on T depicted in Fig. 9.4 exhibits the following features: **(i)** a narrow plateau around

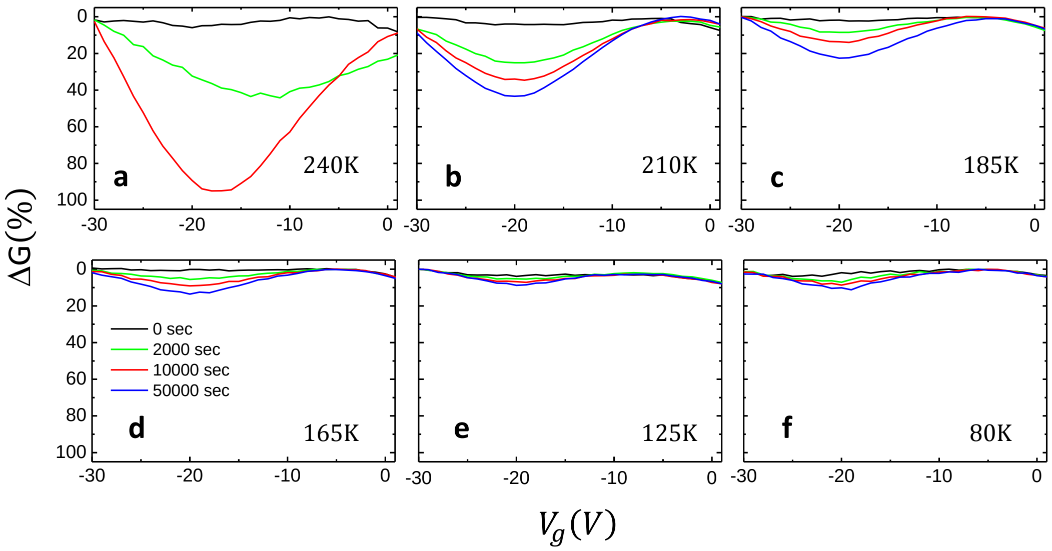

Figure 9.3: Normalized conductance change as a function of gate voltage for different times after a gate voltage change from $+20V$ to $-20V$. This thin Au layer was heated to room temperature for 10 hours, and cooled to various temperatures prior to measurement. ΔG_0 was found in measurements **a-f** to be $0.59\%, 1.42\%, 1.61\%, 1.58\%, 1.6\%$ and 1.35% of G_0, respectively. It is noteworthy that ΔG_0 was found to be approximately temperature independent below 165K. At the higher temperatures, the new dip reached 50% of ΔG_0 after $\tau \sim 2500$sec, while extrapolation of memory dip at lower temperatures led to τ which is higher than 10^{10}sec, showing the slow down of the glassy dynamics.

$T_{\max}$ for which $\tau \sim 1200s$, **(ii)** a sharp increase with decreasing temperature, and **(iii)** temperature independence at low T.

Feature **(i)** results from the measurement procedure and it is the trivial time for the TDE, protocol where the first and second dips are formed at the same temperature with a waiting time of 10 hours and a scan time of about 10sec. At temperatures that are very close to T_{fab}, the finite scan time limits the minimal τ to this value, since very fast processes cannot be measured.

Feature **(ii)** represents the exponential slowing down of the dynamics with T typical of classic glasses, as was shown in the previous chapter (Eq. 6.1).

Feature **(iii)**, the low temperature saturation of τ with T, may be interpreted

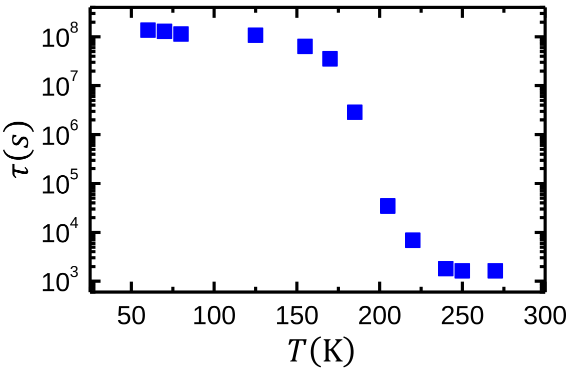

Figure 9.4: The characteristic relaxation time of the Au sample presented in Fig. 9.3, as a function of temperature. The dynamics show the exponential slow down at the higher T, and a saturation below a certain crossover temperature, T_{co}.

as a crossover from a thermally activated to tunneling dominated regime of the relaxation processes as we discuss below. Similar results were observed in over 10 Au samples.

For the sample of Fig. 9.3 and 9.4, the crossover temperature, T_{co}, from activated to saturated behavior of τ, is $\sim 150K$. One may wonder what determines this value? A clue to this question may be found in Fig. 9.5 which shows τ versus T for 3 different Au films grown at 300K under different evaporation conditions. As discussed above, the SEM pictures show that the microstructure of the discontinuous Au is strongly affected by the deposition rate (r) and the partial pressure (P) in the deposition chamber. As the vacuum and deposition rate are reduced, and the typical cluster size as well as the width of the gaps between clusters grow, the temperature-dependent dynamics are also changed. The thermally activated region of the dynamics grows with the cluster/gap size, leading to an increase in the saturation value of τ. Eventually, for the largest cluster-sized sample, the low temperature τ becomes too large to be measured, and the crossover to the saturation of the $\tau(T)$ curve becomes experimentally inaccessible.

An additional parameter that influences the temperature dependence of the

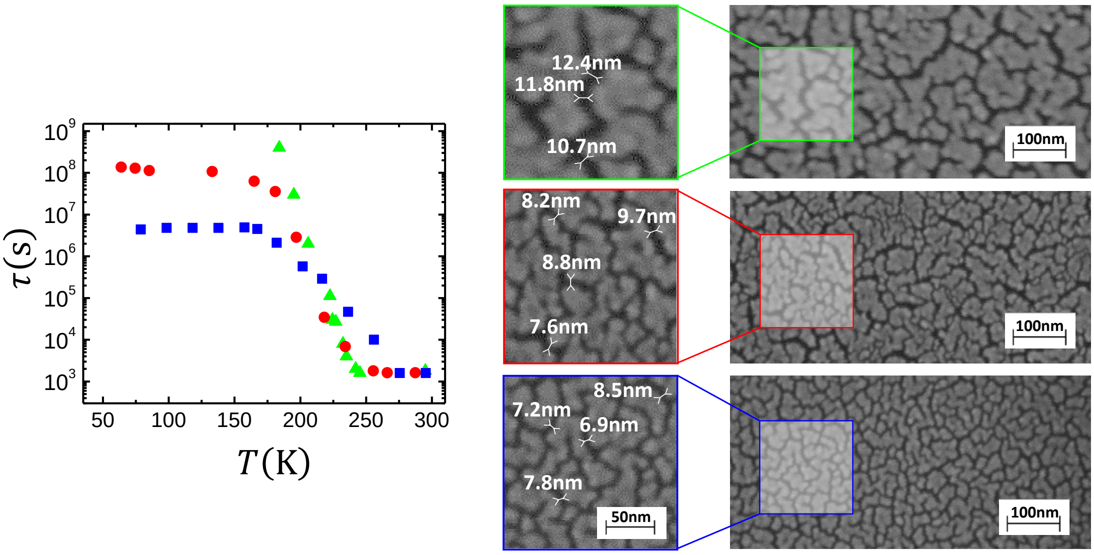

Figure 9.5: Temperature dependence of τ (**left panel**) and the corresponding SEM micrographs (**right**) for three discontinuous films prepared at room temperature under different chamber pressures, P, and deposition rates, r. THe green triangles and top micrograph are for $P = 2 \cdot 10^{-6} mb$, $r = 0.05 \frac{nm}{s}$. The red circles and middle micrograph are for $P = 5 \cdot 10^{-7} mb$, $r = 0.1 \frac{nm}{s}$. Blue circles and bottom micrograph are for $P = 2 \cdot 10^{-7} mb$, $r = 0.4 \frac{nm}{s}$. The typical barrier widths W are extracted from an image analysis of the three micrographs and were found to be: $W \sim 11.18$, 9.25, and $7.98 nm$, respectively.

relaxation time is the fabrication temperature, T_{fab} (or equivalently, T_{max}). Fig. 9.6 presents $\tau(T)$ curves for 3 samples fabricated using the QC method at different T_{fab}. Though the qualitative curve is similar for the three films, the saturation value of τ grows with T_{fab}. In addition, the crossover temperature T_{co} is also found to grow monotonously with the fabrication temperature, and roughly follows $T_{\text{co}} \sim T_{\text{fab}}/2$.

9.3 Discussion

The observed temperature dependence is naturally interpreted as a crossover from a glass that is dominated by thermal activation processes to a glass that is domi-

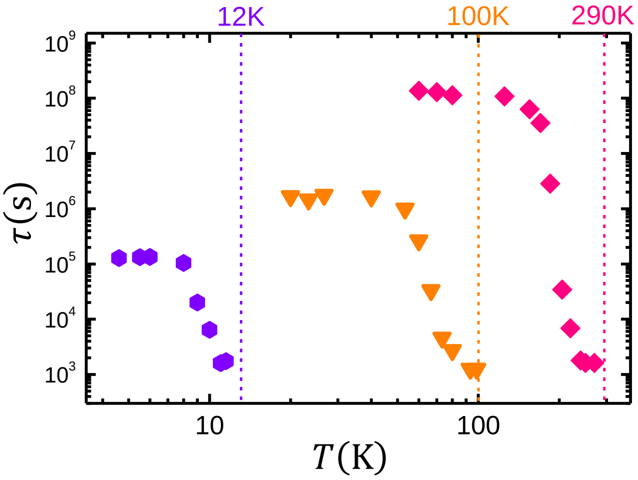

Figure 9.6: Characteristic relaxation time τ as a function of temperature for three discontinuous *Au* films having T_{fab} of 12K (purple hexagons), 100K (orange triangles) and 290K (pink diamonds), fabricated using the quench-condensation technique. All samples show a crossover from an exponential with T (classic) regime and an independent (quantum) regime, while the crossover temperature T_{co} is proportional to $T_{\text{fab/max}}$, as predicted by Eq. 9.5 (see text).

nated by tunneling processes. As the temperature is lowered and the relevant energy barriers in the phase space become increasingly larger, it becomes more likely for the many-body interacting electronic system to tunnel between metastable states rather than to be activated by a phonon above them. One may ask why this crossover is uniquely observed only in discontinuous metal films - why has it not been observed in other EGs? In the following subsections, we suggest a model to explain the findings and the conditions for observing the classic-to-quantum glass crossover.

Model

The correlation between the dynamics and granular geometry illustrated in Fig. 9.5 leads us to suggest that the properties of the glassy temperature dependence are governed by charging energies in the metallic islands and by the width of the gaps between them. The microscope images show that the system consists of a large number of islands with varying sizes, separated by relatively thick (several nm) barriers. The tunneling matrix element between neighboring grains is exponential in the gap width, W, leading to a broad distribution of hopping rates between grains, which are proportional to $exp\left(-W/\xi\right)$, where ξ is a localization length. Due to the exponentially different hopping rates, it is plausible that the relevant paths for conduction through the system consist of a complex network that may be described via the framework of percolation theory [13, 101, 102]. Conductivity through the main percolation paths is affected by adjacent charged islands. Changing V_g changes the potential landscape of the glass, which in turn drives electrons into or out of these nearby islands. Relaxation processes may involve simultaneous tunneling of many electrons in this complex network, making the treatment of such a model extremely complicated. Here, with the welcome help of A. Amir[1], we present a more quantitative analysis of a particular and relatively simple process: Single tunneling between two grains through an intermediate, smaller grain (see Fig. 9.7), which undergoes a crossover from thermal activation to elastic (quantum) co-tunneling as a function of T. This process possesses several properties consistent with the experimental data, namely:

1. At high temperatures, the rate of the process is governed by thermal activation, with an activation energy proportional to the fabrication temperature.

2. At low temperatures, the rate saturates to a temperature-independent value, which is related to the microstructure geometry.

3. The crossover temperature between the two regimes, T_{co}, is proportional to the fabrication temperature.

---

[1] The following calculations are based on an extension of Eq. 6.4 and on Ref. [6], a the case where relaxation rates and probabilities depend also on the distribution of gaps between metallic islands

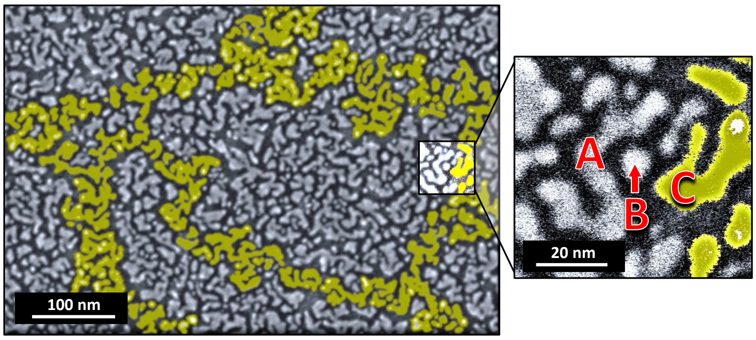

Figure 9.7: Illustration of the process of relaxation via a small intermediate quantum dot: The image shows an scanning electron microscope picture of one of the gold films after thresholding the image. The colored grains (schematically) show the percolating backbone, which supports most of the electronic conduction. At high temperatures, a charge may be trapped on the large quantum dot A, affecting the conductance in grain C. In order to diffuse out of dot A, it is favorable for this charge to pass through dot B. This can occur either through thermal activation or through quantum tunneling, depending on the temperature.

Crossover temperature

Consider a system that was fabricated at T_{fab} and allowed to equilibrate. All islands with charging energy E_C comparable to (or smaller than) T_{fab} can be occupied (**B** in Fig. 9.7) and affect the conductivity in the grains, which are part of the percolation backbone (**C**). Following a temperature decrease, electrons can be trapped on islands separated from the percolating backbone (**A**) by these small islands with charging energy $E_C \sim$ RT. At $T \ll E_c$, this charge is Coulomb-blocked and is forbidden from re-entering the intermediate quantum dot **B**.

The relaxation process in which the trapped electrons will be 'freed' can occur in two ways: Electrons may receive enough energy from thermal phonons to enter into **B**, and from there tunnel to **C**; alternatively, at arbitrarily low temperatures, the electrons may co-tunnel through dot **B**. The latter process can occur either via elastic or inelastic processes.

It was found [103], up to coefficients of order unity, that for $T \ll E_c$, the conductances corresponding to these processes are:

$$\sigma_{activation} \sim \frac{G_L G_R}{G_L + G_R}\frac{E_c}{T}e^{-E_c/T}, \tag{9.2}$$

$$\sigma_{inelastic} \sim \frac{G_L G_R T^2}{e^2/hE_c^2}, \tag{9.3}$$

$$\sigma_{elastic} \sim \frac{G_L G_R \delta E}{e^2/hE_c}, \tag{9.4}$$

where R_Q is the quantum resistance, $G_{L/R}$ are the conductances between the dot and the left/right lead, respectively, and δE is the level spacing.

The characteristic level spacing corresponds to a metallic quantum dot with the typical size of $100nm$, and $G_{L,R}$ can be estimated within a WKB approximation, considering a typical gap spacing of $5nm$ and inter-gap potential of several eV (the work function of the metal). For these parameters, elastic tunneling or thermal activation always dominate over the contribution of inelastic tunneling, which can therefore be neglected.

One should note that while the rate of the thermal process is proportional to $\frac{|M_{12}|^2|M_{23}|^2}{|M_{12}|^2+|M_{23}|^2}$, where M_{ij} is the relevant tunneling matrix element, co-tunneling is of higher order in the matrix elements, proportional to $|M_{12}|^2|M_{23}|^2$. Due to the thick barriers between grains, the rates for co-tunneling can be smaller by several orders of magnitude. Despite this, at sufficiently low temperatures, the exponential suppression of the thermally activated processes will lead to co-tunneling being the dominant process.

Hence, we expect a crossover from a thermally activated regime (Eq. 9.2) to a temperature-independent regime (Eq. 9.4). The crossover temperature can be readily found by equating the two equations, leading to:

$$T_{\mathrm{co}} \sim E_c / \log\left(\frac{E_c^2}{T_{\mathrm{co}}\delta E} \cdot \frac{e^2/h}{2G}\right). \tag{9.5}$$

Since the relevant charging energies are of the order of the fabrication temperature T_{fab}, this model predicts a crossover between the two regimes at a temperature that is in the scale of T_{fab}, which is measurable in our discontinuous metallic films..

Moreover, we can conclude that T_{co} should be proportional to T_{fab} (up to logarithmic corrections). This relation is indeed observed in 3 samples grown at different temperatures, presented in Fig. 9.6.

Quantum regime

Experimentally, the relaxations appear to be approximately logarithmic, both in the case where they are temperature-dependent (classical, thermally activated) and in the temperature-independent (quantum tunneling) regime. This implies that the exponential dependence of the rates on the separation (gap) between the grains has to be significant: In the quantum regime (see Eq. 9.4) the charging energies only enter polynomially, while in order to have logarithmic relaxations, one needs to have an *exponential* dependence on the parameter, which can only be accounted for by the exponential dependence of the prefactor G on the oxide barrier thickness.

For this reason, we can *neglect* the polynomial dependence on E_c in the quantum tunneling regime. We assume that $G \propto e^{-x/\xi}$ (with x as the gap thickness and ξ as the lengthscale associated with the exponential decay of the wavefunction in the gap, which is related to the work function of the materials involved)), and that the distribution of x is uniform in the interval $[0, W]$, i.e. W is the maximal gap for the particular geometry considered. Since the rates are proportional to the conductance, we have $\lambda \sim G^2$, leading to:

$$p(\lambda) = p(x)|\frac{dx}{d\lambda}| = \frac{\xi}{2W}\frac{1}{\lambda}. \tag{9.6}$$

Hence, the relaxation process is involved in simultaneous individual tunneling of many electrons with different rates, with the above probability. The $1/\lambda$ distribution was shown to result in the logarithmic relaxation of glass [6] -

$$\Delta G(t) \propto \sum_{\lambda} e^{-\lambda t} = \int e^{-\lambda t} P(\lambda) d\lambda = \frac{\xi}{2W} \cdot log(t). \tag{9.7}$$

As noted in Eq. 9.1, τ depends exponentially on the inverse of the logarithmic pre-factor [49]. Thus, in the tunneling regime, we obtain the characteristic time as -

$$\tau \propto exp\left(\frac{2W}{\xi}\right). \tag{9.8}$$

Classical regime

In the thermally activated regime, the calculation is slightly more evolved. In this case, we have (neglecting the polynomial corrections):

$$\lambda \sim e^{-E_c/T - x/\xi}. \tag{9.9}$$

Since both E_c and x are random variables, we have to take their *joint* distribution into account when evaluating $p(\lambda)$. We shall assume that these two variables are uncorrelated, which is plausible since the local gap between grains should not depend on the particular size or morphology of that grain. As before, the distribution of x is assumed to be uniform in the interval $[0, W]$, while that of E_c is assumed to be uniform in the interval $[0, U_{\max}]$. We shall later argue that $U_{\max} \sim T_{\text{fab}}$, since the fabrication temperature "selects" which charging energies can be relevant; namely, only those with $E_c < T_{\text{fab}}$ could trap charges in them at the temperature T_{fab} [49].

Consider now the distribution of the variable $m \equiv E_c/T + x/\xi$. We have:

$$p(m) = \int_0^{U_{\max}} \int_0^W p(x, E_c)\delta(m - E_c/T - x/\xi)dxdE_c. \tag{9.10}$$

Hence:

$$p(m) = \frac{1}{WU_{mac}} \int_0^{U_{\max}} \int_0^W \delta(m - E_c/T - x/\xi)dxdE_c. \tag{9.11}$$

Performing the integration over x we find that:

$$p(m) = \frac{1}{WU_{\max}} \int_0^{U_{\max}} \xi\theta(m - E_c/T)\theta(E_c/T - m + W/\xi)dE_c. \tag{9.12}$$

Considering possible values of m in the interval $m < max(W/\xi, U_{\max}/T)$, we find:

$$p(m) = \frac{\xi}{WU_{\max}} \int_0^{mT} dE_c = \frac{T\xi}{2WU_{\max}} m. \tag{9.13}$$

Now it is straightforward to find the distribution of relaxation rates using $\lambda = e^{-m}$:

$$p(\lambda) = p(m)|\frac{dm}{d\lambda}| = \frac{T\xi}{2WU_{\max}} |\log(\lambda)|/\lambda. \tag{9.14}$$

Thus, up to logarithmic corrections the distribution is proportional to $\frac{1}{\lambda}$, which

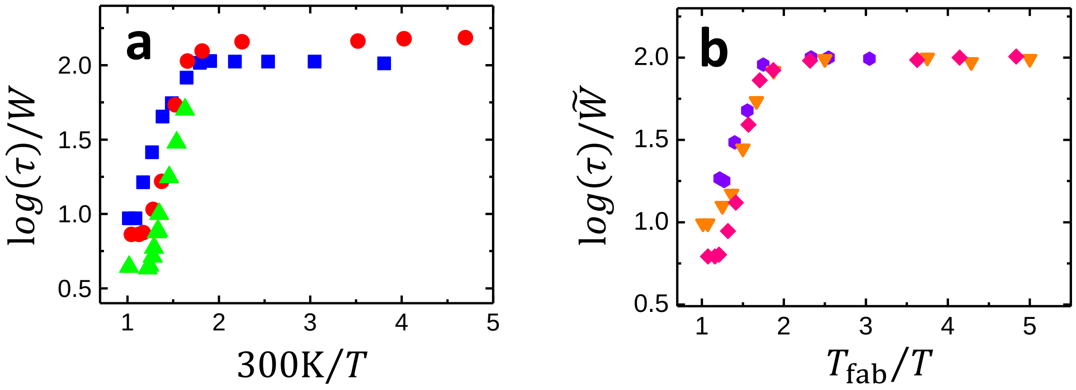

Figure 9.8: Panel a: A fit of the results of Fig. 9.5 with Eq. 9.8 and Eq. 9.15, for the values of W extracted from the SEM micrographs (see caption of Fig. 9.5). In these samples, 300K is approximately the fabrication temperature. **Panel b:** A similar fit of Fig. 9.6. The quench-condensation technique does not allow reliable SEM scans, however, normalizing $log(\tau)$ by an estimated barrier width $\widetilde{W}$ shows a reasonable fit for both regimes.

again would lead to logarithmic relaxation (as long as U_{max} or W are large enough compared to the temperature, such that the distribution of effective barriers m is smooth enough on the scale of the temperature). Hence, τ depends also on the width W in the classical regime -

$$\tau \propto exp\left(\frac{2WT_{\text{fab}}}{T\xi}\right). \tag{9.15}$$

The theoretical result of both regimes (Eq. 9.8 and Eq. 9.15) and the crossover temperature (Eq. 9.5) are presented in Fig. 9.8, illustrating that they are reasonably fitting with the experiments.

Though this model considers only a simple single-electron process, it may describe the basic building block for the dynamics in real electron glass that is governed by simultaneous many electron tunneling processes. Indeed, the model is able to capture many of the experimental results.

The above interpretation of the results is based on the assumption that τ

is a good representative of glassy dynamics. This assumption is correct only if the memory dips can be fully described by their amplitude, and therefore, the comparison of the new memory dip with the one built at $T = T_{\max}$ is true. As noted above, a recent finding in granular AlO systems [93] indicates that this is not always the case. Moreover, the claim that $T_{\max}$ sets the energy scale of both the classical and the quantum regime is based on the above protocol, where the 'old' dip was created at $T_{\max}$. Therefore, in principle, this T_{old} temperature can be a more substantial value. Consequently, applying the TDE protocol relative to a memory dip formed at $T_{\text{old}} < T_{\max}$ might lead to different results. In our system, however, the drastic slow down of the dynamics below $T_{\max}$ and the relatively wide memory dips in $G\left(V_g\right)$ scans, make this experiment inaccessible.

9.4 Conclusions

In this study, we presented an experimental study of temperature dependent-dynamics of discontinuous metal films. The relaxation time increases rapidly with temperature, until, at a low enough temperature, it saturates. These results were interpreted as a crossover from thermal activation above energy barriers in the framework of the configuration space, to tunneling through them. Glassy effects are seen at temperatures as high as $300K$ and the crossover temperature can be as large as ~$150K$. Hence, the quantum regime extends to unusually high temperatures.

Summary

This Ph.D dissertation discusses the nature of electronic transport in amorphous metals, which, despite its broad relevance in condensed matter physics and the fact that it was the main subject of countless papers and works, still includes many open questions.

In the first part of this work, I dealt with this issue with an exact calculation of the quantum electronic conductance in 1D inhomogeneous wires, using the NEGF method. I showed that in a wide range of disorder levels, temperatures and system sizes, a significant part of the electronic states does not contribute to conductance, due to the lack of overlap with surrounding electronic modes in the leads. I thereafter discussed the effect of Fermi distribution smearing in these systems, within a range where T is comparable with the mean level spacing in the system. In this range, increasing T results in more conductive quantum levels, as electronic populations in the leads are widened around Fermi energy. This effect, along with the highly skewed log-normal distribution of conductance values in disordered systems, leads to a significant increase of the overall current.

The second part of the work discussed another non-trivial and not fully understood phenomenon - electron glass, where strong disorder coupled with Coulomb interactions results in glass-like dynamics. I presented experimental findings on thin Au, Ag and Ni films, which show three novel characteristics of electron glasses: (**A**) There is a clear temperature dependence of the rate of the logarithmic glass

relaxation. (**B**) The relaxation rate is inversely related to the maximal temperature the amorphous metal was exposed to. (**C**) In some cases, EG films exhibit a crossover from thermally activated glass at relatively high temperatures, to quantum-mechanics dominated dynamics at low T. These results were discussed in the framework of the configuration space, and proved to be effectively varied at the different temperatures.

Despite being common in everyday nature, and in particular, in physics research and engineering applications, after more than a 100 years of research, the nature of electrons in amorphous materials shows many non-trivial phenomena and is yet to be completely comprehended.

The puzzle of quantum interference within the metal, the effect of strong Coulomb interactions together with disorder, and the role of temperature and phonons, are all awaiting an improved and more unified theory. More specifically, many systems that are believed to be metallic with a perfect internal order, such as graphene nanotubes, metallic quantum dots, and even semiconductor devices and solar cells - in actual fact, all possess some level of disorder. This, in turn, might bring about quantum effects of localization and interference, in addition to the effect of temperature, connection to leads and Coulomb interactions. Therefore, in many metallic systems, researchers report an inexplicably slow time dependence and mysterious deviations from the VRH relation at low temperatures. These effects may be related to the electron glass phenomenon, the hidden modes and the phonon-less temperature dependence, which are all discussed and characterized in this work.

As is commonly stated, the behavior of macroscopical condensed systems is more complicated and unexpected than the sum of many microscopical separated processes. The lack of a simple, coherent theory for electronic behavior in disordered solid state physics makes it an exciting research field, with many discoveries waiting to be revealed.

However, employing a traditional study procedure, that is, hypothesis, prediction and experiment, is much harder in this field, due to the absence of a trustworthy theoretical framework. Hence, many of the state-of-the-art findings in this field were discovered accidentally. We tried to take an intermediate course, and looked for new effects in places where previous studies showed interesting but unexplained manifestations.

Today, electron glass is still under great debate: How do electrons generate such long relaxation processes? What is the exact role of Coulomb interactions? Does the electron glass possess a true glass-transition temperature? How does the rearrangement of electrons affect conductivity? Despite the comprehensive experimental data on conductance fluctuations in disordered systems, these major questions remain unanswered, and theories can not always address all the experimental results.

In this work, I discussed only some of these intriguing effects; many more aspects need to be explored in-depth, and future experiments must be carried out in an attempt to formulate a complete theory on the temperature dependence of disordered quantum systems. Nevertheless, despite its incompleteness, and perhaps for this very reason, I believe that this study can pave the way for an additional fascinating findings in this field.

Bibliography

[1] Allen M. Goldman and Nina Markovic *"Superconductor-insulator transitions in the two-dimensional limit"*, Phys. Today 51, 39 (1998)

[2] Daniel Sherman, Boris Gorshunov, Shachaf Poran, Nandini Trivedi, Eli Farber, Martin Dressel, Aviad Frydman, *"Effect of Coulomb interactions on the disorder-driven superconductor-insulator transition"*, Phys. Rev. B 89, 035149 (2014)).

[3] Valerii M. Vinokur, Tatyana I. Baturina, Mikhail V. Fistul, Aleksey Yu. Mironov, Mikhail R. Baklanov and Christoph Strunk, *"Superinsulator and quantum synchronization"*, Nature 452, 613 (2008).

[4] Tatyana I. Baturina, Valerii M. Vinokur, *"Superinsulator–superconductor duality in two dimensions"*, Ann. Phys. 331, 236 (2013).

[5] N. Auerbach, V. Zelevinsky, *"Super-radiant dynamics, doorways and resonances in nuclei and other open mesoscopic systems"*, Rep. Prog. Phys. 74, 106301 (2011).

[6] A. Amir, y. Oreg and .J Imry, *"Electron Glass Dynamics"*. Annu. Rev. Condens. Matter Phys., 2, 235 (2011).

[7] For more detailed review on electron-glass see: M. Pollak, M. Ortuño, A. Frydman *"The Electron Glass"*. Cambridge. (2013)

[8] P. W. Anderson *"Absence of diffusion in certain random lattices"*. Physical Review, 109(5), 1492–1505. (1958).

[9] C.A. Miller and D. Delande, *"Disorder and interference: localization phenomena"* arXiv:1005.0915 (2010).

[10] N. F. Mott *"Electrons in disordered structures"*. Advances in Physics, 16, 49–144. (1967).

[11] N.F. Mott, *"Conduction in non-crystalline materials"* Phil. Mag. **19**, 835 (1969)

[12] A. Miller and E. Abrahams *"Impurity conduction at low concentrations"*. Physical Review, 120(3), 745–755 (1960).

[13] V. Ambegaokar, B. I. Halperin and J. S. Langer, *"Hopping Conductivity in Disordered Systems"*. Phys. Rev. B, 4, 2612–2620 (1971).

[14] A. L. Efros and B. I. Shklovskii *"Coulomb gap and low temperature conductivity of disordered systems"*. J. Phys. C: Solid State Phys. 8, L49 (1975).

[15] J. Zhang et al. *"Absence of diffusion in certain random lattices"*. Phys. Rev. B, 48(4), 2312–2319. (1993).

[16] E. Abrahams, P. W. Anderson, D. C. Licciardello, and T. V. Ramakrishnan, *"Scaling Theory of Localization: Absence of Quantum Diffusion in Two Dimensions"*, Phys. Rev. Lett. 42, 673 (1979).

[17] J. M. Valles Jr., N. Trivedi and V. Dobrosavljevic *"Conductor Insulator Quantum Phase Transitions"*, Oxford University Press, 2012.

[18] A. Eilmes, R. A. Römer and M. Schreiber *"The two-dimensional Anderson model of localization with random hopping—* Eur. Phys. J. B, 1, 29 (1998)

[19] R.A. Römer and M. Schreiber, *"No enhancement of the localization length for two interacting particles in a random potential"*, Phys. Rev. Lett. **78**, 515 (1997).

[20] Henk van Houten and Carlo Beenakker, *"Quantum Point Contacts"*, Physics Today 49, 22 (1996)

[21] B. J. van Wees, H. van Houten, C. W. J. Beenakker, J. G. Williamson, L. P. Kouwenhoven, D. van der Marel, and C. T. Foxon. *"Quantized Conductance of Point Contacts in a Two-Dimensional Electron Gas"*, Phys. Rev. Lett. 60, 848–850 (1988).

[22] R. Kubo *"Statistical-mechanical theory of irreversible Processes"*, J. Phys. Soc. Jpn. 12, 570 (1957).

[23] S. Datta. *"Electronic Transport in Mesoscopic Systems"*. Cambridge University Press. (1995)

[24] R. Usmani *"Inversion of Jacobi's tridiagonal matrix"* Comput. Math. Appl., 27, pp. 59–66 (1994).

[25] C.M. da Fonseca, *"On the eigenvalues of some tridiagonal matrices"*, J. Comput. Appl. Math. 200, 283 (2007).

[26] A. Eisenbach, Y. Bliokh, V. Freilkher, M. Kaveh, R. Berkovits. *"Transmission resonances anomaly in 1D disordered quantum systems"* Phys. Rev. B 94, 014207 (2016)

[27] Y. P. Bliokh, V. Freilkher, Z. Shi, A. Genack and F. Nori, *"Hidden Modes in Open Disordered Media: Analytical, Numerical, and Experimental Results"* New J. Phys. **17**, 113009 (2015).

[28] E.S.C. Ching, P.T. Leung, A. Maassen van den Brink, W.M. Suen, S.S. Tong, and K. Young, *"Quasinormal-mode expansion for waves in open systems"* Rev. Mod. Phys., **70**, 1545 (1998).

[29] P. T. Leung, S. Y. Liu, and K. Young, *" Completeness and orthogonality of quasinormal modes in leaky optical cavities"* Phys. Rev. A **49,** 3057 (1994).

[30] N. Hatano and G. Ordonez, *"Time-reversal symmetric resolution of unity without background integrals in open quantum systems"* J. Math. Phys., 55, 122106 (2014).

[31] J. Wang, Z. Shi, M. Davy, and A. Z. Genack, *"Wave propagation and localization via quasi-normal modes and transmission eigenchannels"* Int. J. Mod. Phys. Conf. Ser., **11**, 1 (2012).

[32] J. Wang and A.Z. Genack, *"Transport through modes in random media"* Nature **471**, 345 (2011).

[33] R. Pnini and B. Shapiro, *"Intensity fluctuations in closed and open systems"* Phys. Rev. E **54**, R1032 (1996).

[34] R. A. Webb, A. Hartstein, J. J. Wainer, and A. B. Fowler, *"Origin of the Peaked Structure in the Conductance of One-Dimensional Silicon Accumulation Layers"*, Phys. Rev. Lett., **54**, 1577 (1985).

[35] D. A. Wharam, T. J. Thornton, R. Newbury, M. Pepper, H. Ahmed, J. E. F. Frost, D. G. Hasko, D. C. Peacockt, D. A. Ritchie and G. A. C. Jones, *"One-dimensional transport and the quantisation of the ballistic resistance"*, J. Phys. C: Solid State Phys., **21**, L209 (1988).

[36] U. Meirav, M. A. Kastner, and S. J. Wind, *"Single-electron charging and periodic conductance resonances in GaAs nanostructures"*, Phys. Rev. Lett., **65**, 771 (1990).

[37] L.P. Kouwenhoven, F.W.J. Hekking, B.J. van Wees, C.J.P.M. Harmans, C.E. Timmering, and C.T. Foxon *"Transport through a finite one-dimensional crystal"*, Phys. Rev. Lett. **65**, 361 (1990)

[38] F. M. de Aguiar and D. A. Wharam, *"Transport through one-dimensional channels"*, Phys. Rev. B. **43**, 9984(R) (1991).

[39] B. Stojetz, Ch. Hagen, Ch. Hendlmeier, E. Ljubović, L. Forró and Ch. Strunk, *"Ensemble averaging of conductance fluctuations in multiwall carbon nanotubes"*, New J. Phys. **6**, 27 (2004).

[40] S. Roche, J. Jiang, F. Triozon, and R. Saito, *"Conductance and coherence lengths in disordered carbon nanotubes: Role of lattice defects and phonon vibrations"*, Phys. Rev. B **72**, 113410 (2005).

[41] Y. Alhassid, *"The statistical theory of quantum dots"*, Rev. Mod. Phys. **72**, 895 (2000).

[42] N. Moiseev, *"Non-Hermitian Quantum Mechanics"*, Cambridge Univ. Press (2011).

[43] C. W. J. Beenakker *"Random-matrix theory of quantum transport"*. Rev. Mod. Phys. 69, 731 (1997)

[44] Y. Imry and R. Landauer, *"Conductance viewed as transmission"*, Rev. Mod. Phys. **71**, S306 (1999).

[45] A. Edelman and E. Kostlan, *"How many zeros of a random polynomial are real?"*, Bull. Amer. Math. Soc. **32**, 14 (1995).

[46] I.S. Gradshteyn and I. M. Ryzhik *"Table of Integrals, Series, and Products"*, 7th ed., New York: Academic, pp. 1–2 (2007).

[47] A. B. Fowler, A. Hartstein, and R. A. Webb, Phys. *"Conductance in Restricted-Dimensionality Accumulation Layers"* Rev. Lett. 48, 196 (1982).

[48] B. Sandow, K. Gloos, R. Rentzsch, A. N. Ionov, and W. Schirmacher, *"Electronic correlation effects and the Coulomb gap at finite temperature"*, Phys. Rev. Lett., 86(9), 1845–1848 (2001).

[49] A. Eisenbach, T. Havdala, J. Delahaye, T. Grenet, A. Amir, and A. Frydman, *“Glassy Dynamics in Disordered Electronic Systems Reveal Striking Thermal Memory Effects”* Phys. Rev. Lett., 117, 116601 (2016).

[50] T. Havdala, A. Eisenbach and A. Frydman *"Ultra-slow relaxation in discontinuous-film–based electron glasses"*. Europhys. Lett. 98, 67006 (2012)

[51] R. Edgeworth, B. J. Dalton and T. Parnell *"The pitch drop experiment"* Eur. J. Phys., 5, 4 (1984).

[52] P. G. Debenedetti and F. H. Stillinger *Supercooled liquids and the glass transition* Nature 410, 259 (2001).

[53] Z. P. Lu and C. T. Liu, *"Glass formation criterion for various glass-forming systems"*, Phys. Rev. Lett. 91, 115505 (2003).

[54] M. Mezard, G. Parisi and M.A. Virasoro, *"Spin glass theory and beyond"*, Singapore, World Scientific (1987).

[55] G.G. Kenning, G.F. Rodriguez, and R. Orbach, *"End of Aging in a Complex System"* Phys. Rev. Lett. **97**, 057201 (2006).

[56] Raymond E. Wetton and Harry G. Moneypenny, *"Fundamental Properties of Densified Polymeric Glasses"*, Br. Polym. J. 7, 51 (1975).

[57] A. Gurevich and H. Kupferm, *"Time scales of the flux creep in superconductors"*, Phys. Rev. B **48**, 6477 (1993).

[58] B. E. Vugmeister and M. D. Glinchuk *"Dipole glass and ferroelectricity in random-site electric dipole systems"*. Rev. Mod. Phys. 62, 993–1026 (1990)

[59] A. Amir, S. Borini, Y. Oreg, and Y. Imry, *"Huge (but Finite) Time Scales in Slow Relaxations: Beyond Simple Aging"*, Phys. Rev. Lett. **107**, 186407 (2011).

[60] K. Matan, R. B. Williams, T. A. Witten, and S. R. Nagel *"Crumpling a Thin Sheet"*. Phys. Rev. Lett., 88, 076101 (2002).

[61] B. Rinn, P. Maass, and J.P. Bouchaud, *"Hopping in the glass configuration space: Subaging and generalized scaling laws"* Phys. Rev. B **64**, 104417 (2001).

[62] E. D. Zanotoo *"Do cathedral glasses flow?"* Am. J. Phys., 66, 392 (1998).

[63] A. Amir, Y. Oreg and Y. Imry, *"Slow Relaxations and Aging in the Electron Glass"*, Phys. Rev. Lett. **103**, 126403 (2009).

[64] K. Jonason, E. Vincent, J. Hammann, J. P. Bouchaud, and P. Nordblad, Phys. Rev. Lett. **81**, 3243 (1998).

[65] T. Jonsson, K. Jonason, P. Jönsson, and P. Nordblad, Phys. Rev. B **59**, 8770 (1999).

[66] J. H. Davies, P. A. Lee, and T. M. Rice *"Electron glass"*. Phys. Rev. Lett. 49, 758 (1982)

[67] M. Grunewald, B. Pohlman, L. Schweitzer, and D. Wurtz, *"Mean field approach to the electron glass"*, J. Phys. C ,**15**, L1153 (1982).

[68] M. Pollak and M. Ortuno, *"Coulomb interactions in Anderson localized disordered systems"*, Sol. Energy Mater. **8**, 81 (1982).

[69] M. Pollak, *"Non-ergodic behaviour of Anderson insulators with and without Coulomb interactions"*, Philos. Mag. B **50,** 265 (1984).

[70] G. Vignale, *"Quantum electron glass"*, Phys. Rev. B, **36**, 8192 (1987).

[71] C. J. Adkins, J. D. Benjamin, J. M. D. Thomas, J. W. Gardner and A. J. McGeown, *"Potential disorder in granular metal systems: the field effect in discontinuous metal films"*. J. Phys. C 17, 4633 (1984)

[72] M. Ben-Chorin, D. Kowal, and Z. Ovadyahu, *"Anomalous field effect in gated Anderson insulators"*, Phys. Rev. B **44**, 3420 (1991).

[73] M. Ben-Chorin, Z. Ovadyahu and M. Pollak, *"Nonequilibrium transport and slow relaxation in hopping conductivity"*. Phys. Rev. B, 48, 15025. (1993)

[74] A. Vaknin, Z. Ovadyahu and M. Pollak, *"Evidence for Interactions in Nonergodic Electronic Transport"*. Phys. Rev. Lett., 81, 669. (1998).

[75] A. Vaknin, Z. Ovadyahu and M. Pollak, *"Aging Effects in an Anderson Insulator"*. Phys. Rev. Lett., 84, 3402 (2000).

[76] A. Vaknin, Z. Ovadyahu, and M. Pollak, *"Nonequilibrium field effect and memory in the electron glass"*, Phys. Rev. B **65**, 134208 (2002).

[77] Z. Ovadyahu, *"Temperature- and field-dependence of Dynamics in the Electron-Glass"*, Phys. Rev. B 73, 214208. (2006)

[78] G. Martinez-Arizala, D.E. Grupp, C. Christiansen, A.M. Mack, N. Markovic, Y. Seguchi, and A.M. Goldman, *"Anomalous Field Effect in Ultrathin Films of Metals near the Superconductor-Insulator Transition"*, Phys. Rev. Lett. **78**, 1130 (1997).

[79] G. Martinez-Arizala, C. Christiansen, D. E. Grupp, N. Markovic, A. M. Mack and A. M. Goldman, *"Coulomb-glass-like behavior of ultrathin films of metals"*. Phys. Rev. B. 57, R670 (1998)

[80] T. Grenet, *"Symmetrical field effect and slow electron relaxation in granular aluminium"*, Eur. Phys. J. B **32**, 275 (2003).

[81] T. Grenet, J. Delahaye, M. Sabra and F. Gay *"Anomalous electric-field effect and glassy behaviour in granular aluminium thin films: electron glass?"*. Eur. Phys. J. B 56, 183 (2007)

[82] Z. Ovadyahu *"Intrinsic electron glassiness in strongly localized Be films"*. Phys. Rev. B, 82, 195404, (2010)

[83] J. Delahaye, T. Grenet, C.A. Marrache-Kikuchi, A.A. Drillien, and L. Berge, *"Observation of thermally activated glassiness and memory dip in a-NbSi insulating thin films"*, Europhys. Lett., **106**, 67006 (2014).

[84] Z. Ovadyahu, *"Intrinsic electron-glass effects in strongly localized* Tl_2O_{3-x} *films"*, Phys. Rev. B, **88**, 085106 (2013).

[85] Z. Ovadyahu, *"Coexistence of electron-glass phase and persistent photoconductivity in GeSbTe compounds"*, Phys. Rev. B **91**, 094204 (2015).

[86] N. Kurzweil and A. Frydman, *"Inverse slow relaxation in granular hopping systems"*. Phys. Rev. B **75**, 020202(R) (2007).

[87] Z. Ovadyahu, *"Slow conductance relaxations: Distinguishing the electron glass from extrinsic mechanisms"*, Phys. Rev. B. **78**, 195120 (2008).

[88] V. Orlyanchik and Z. Ovadyahu, *"Stress Aging in the Electron Glass"*. Phys. Rev. Lett., 92, 066801. (2004).

[89] N. Klein and H. Gafni, *"The maximum dielectric strength of thin silicon oxide films"* IEEE Trans. Electron Devices, 13, 281 (1966).

[90] S.G Jennings, *"The mean free path in air"*, J. Aerosol Sci. 19, 159 (1988).

[91] A. Frydman and R.C. Dynes, *"Magnetoresistance of granular ferromagnets—observation of a magnetic proximity effect?"*, Sol. State Comm. 110, 485 (1999).

[92] A. Frydman, T.L. Kirk and R.C. Dynes, *"Superparamagnetism in discontinuous Ni films"*, Solid State Commun. 114, 481 (2000).

[93] T. Grenet and J. Delahaye, Private communications.

[94] Z. Ovadyahu and M. Pollak, *Disorder and magnetic field dependence of slow electronic relaxation"* Phys. Rev. Lett. 79, 459 (1997).

[95] T. Grenet and J. Delahaye, *"Determination of characteristic relaxation times and their significance in glassy Anderson insulators"*, Phys. Rev. B **85**, 235114 (2012).

[96] K. L. Ekinci and J. M. Valles, Jr., *"Thickness dependence of the morphology of ultrathin quench condensed gold films"*, Phys. Rev. B, **58**, 7347 (1998).

[97] F. Lefloch, J. Hammann, M. Ocio and E. Vincent, Europhys. Lett. **18**, 647 (1992).

[98] V. Dupuis, E. Vincent, J.-P. Bouchaud, J. Hammann, A Ito, and H. A. Katori, Phys. Rev. B **64**, 174204 (2001).

[99] A. J. Bray and M. A. Moore, *"Chaotic Nature of the Spin-Glass Phase"*, Phys. Rev. Lett. **58**, 57 (1987).

[100] Z. Ovadyahu, *"Relaxation Dynamics in Quantum Electron Glasses"*, Phys. Rev. Lett. 99, 226603 (2007).

[101] M. Pollak, *"A percolation treatment of dc hopping conduction"*, Journal of Non-Crystalline Solids 11, 24 (1972).

[102] B. I. Shklovskii, *"Hopping Conductivity of Semiconductors in Strong Magnetic Fields"*, JETP 34, 1084 (1972).

[103] M. Pustilnik and L.I. Glazman, *"Nanophysics: Coherence and Transport"* edited by H. Bouchiat, Y. Gefen, S. Gueron, G. Montambaux, and J. Dalibard (Elsevier, New York 2005) Chap. 7, pp. 427.

דינמיקה תלוית טמפרטורה במתכות לא מסודרות

חיבור לשם קבלת התואר "דוקטור לפילוסופיה"

מאת:

אריאל איזנבך

המחלקה לפיזיקה

הוגש לסנט של אוניברסיטת בר אילן
רמת גן תמוז תשע"ז

עבודה זו נעשתה בהדרכתם של
פרופ׳ ריצ׳רד ברקוביץ׳
ופרופ׳ אביעד פרידמן
מן המחלקה לפיזיקה של אוניברסיטת בר-אילן

תוכן עניינים

תקציר

״בכל כאוס יש קוסמוס, בכל אי סדר יש סדר נסתר.״ (קרל יונג)

א. מבוא

עבודת המחקר המוצגת בחיבור זה עוסקת בתכונות המוליכות של מתכות לא מסודרות, ובתלות שלהן בטמפרטורה, בהתבסס על מחקר ניסיוני, נומרי ואנליטי. בדומה למערכות אחרות בפיסיקה של המצב המוצק, התנהגות האלקטרונים בסריג לא מסודר עדיין איננה מובנת במלואה. בשל המורכבות של מערכות אלה פעמים רבות ניתוח תיאורטי או סטטיסטי לא מצליח להביא בחשבון את כל התהליכים הפיסיקליים והראיות הנסיוניות, ולכן גם לא מצליח לנבא תוצאות עתידיות.

הדינמיקה של אלקטרונים במתכות לא מסודרות שונה באופן מהותי מהדינמיקה במערכות מסודרות, דוגמת מתכות או מוליכים למחצה. כבר בשנות החמישים של המאה ה-20, בעבודה שזיכתה אותו בפרס נובל, הראה פיליפ אנדרסון (P.W. Anderson) כי כאשר הסריג המתכתי אינו מסודר האלקטרונים הופכים להיות ממוקמים במרחב, והמוליכות החשמלית מתבצעת על ידי דילוג בין מצבים ממוקמים אלו. בחינה של הדינמיקה על ידי מדידת המוליכות כתוצאה מתנאים שונים יכולה לספק מידע רב על הטבע של האלקטרונים והאטומים במערכת, כמו רמת אי הסדר; חשיבות אינטרקציות בין האלקטרונים; השפעת הטמפרטורה ועוד.

בדיסרטציה זו אני מציג מחקר שבוצע על מערכות בעלות מגוון ממדים ורמות אי סדר, הן על ידי שיטות חישוביות והן על ידי ניסוי במעבדה. בחלק הראשון של העבודה (Part I) מוצג מבוא קצר למוליכות של אלקטרונים במערכות לא מסודרות, החל בהצגה של מבודדי אנדרסון ותופעת הלוקליזציה, דרך הפיתוח של תיאוריית המוליכות של נוויל מוט (N.F. Mott), ״דילוג לטווחים משתנים״ (VRH) והקשר לפונונים, ועד להשפעה של אינטרקציות בין אלקטרונים על המוליכות.

בחלק השני (Part II) אני מציג את החלק החישובי של המחקר, שבוצע תחת הדרכתו של פרופ' ריצ'רד ברקוביץ, ובו חישבנו את פונקציית ההעברה ואת המוליכות של מערכות חד ממדיות לא מסודרות על ידי "פונקציית גרין מחוץ לשווי משקל" (NEGF). שימוש בפונקציית גרין מאפשר לכלול את ההשפעה של המגעים המוליכים על האלקטרונים, ולקחת בחשבון בקירוב גם את השפעתם של פונונים ושל אינטרקציות בין האלקטרונים. הפרק הראשון בחלק זה מציג את עקרונות שיטת החישוב ואת ההנחות עליהן היא מתבססת, כמו גם את התיאור המתמטי של הבעיה הפיסיקלית על ידי "המילטוניאן אנדרסון". שני הפרקים האחרונים של החלק השני פורשים את התוצאות עיקריות של המחקר החישובי החושפות תופעות מפתיעות של המוליכות במערכת חד ממדית בנוכחות אי סדר.

החלק השלישי של הדיסרטציה דן במחקר ניסיוני בנושא "זכוכית אלקטרונים" (Electron Glass), אותו ביצעתי בהדרכתו ובמעבדתו של פרופ' אביעד פרידמן. בדומה למערכות זכוכיתיות אחרות בטבע, גם זכוכית אלקטרונים מראה דעיכה ארוכה לשווי משקל אנרגטי ותופעת זיכרון. בתחילת חלק זה אני מציג את התוצאות הקודמות בתחום, את המערכת הניסיונית שבה השתמשתי ואת שיטות המדידה. בהמשך אני סוקר שתי תופעות חדשות אותן גילינו במעבדה במדידות מוליכות של שכבות דקות של מתכת, המראות תלות חזקה של הדינמיקה הזכוכיתית בטמפרטורה המדידה ובטמפרטורה שבה הדגם נוצר.

ב. הקדמה תיאורטית

כפי שהראה אנדרסון, ובניגוד לפונקציית בלוך בסריג המסודר, במתכות לא מסודרות האלקטרונים ממוקמים במרחב, ופונקציית הגל שלהם דועכת אקספוננציאלית

$$\left|\psi_i\left(\vec{r}\right)\right| \propto \exp\left(-\frac{\left|\vec{r}-\vec{r}_i\right|}{\xi}\right)$$

כאשר $\vec{r}_i$ הוא מיקום פונקציית הגל ה-i בסריג ו-ξ הוא מרחק הלוקליזציה (איור 1.1). מערכות אלה נקראות "מבודדי אנדרסון" (Anderson Insulators).

במקרה של מערכות שבהן מרחק הלוקליזציה קטן מגודלו של הדגם כולו, המוליכות אינה יכולה להתבצע על ידי מעבר פשוט של אלקטרונים במתכת, הנגרם בשל הפרישה במרחב של פונקציית הגל. במערכת כזו המוליכות מתרחשת על ידי תופעת הדילוג הקוונטי (Quantum Hopping) – אלקטרון הנמצא במצב i נעלם ומופיע מיד במצב j, בשל חפיפה קטנה של פונקציית הגל של

שני המצבים i ו-j (איור **1.2**). כדי להתגבר על הפרשי האנרגיה בין המצבים דרושים פונונים אשר תורמים\מקבלים את האנרגיה החסרה\העודפת.

בשל התנהגות זו של פונקציות הגל הממוקמות, וכתוצאה מהתפלגות האכלוס של הפונונים באנרגיה, הסיכוי לתהליך דילוג כזה הוא דועך בצורה מעריכית עם המרחק בין האתרים הממוקמים ועם הפרשי האנרגיות העצמיות ביניהם. הנחה של צפיפות מצבים אחידה במרחב ובאנרגיה, והנחה כי בשל הדעיכה המעריכית עיקר התרומה למוליכות נובע מהדילוגים המסתברים ביותר, מובילה לתלות של מרחקי הדילוג האופייניים עבור טמפרטורות שונות, ולכן גם בתלות של המוליכות בטמפרטורה:

$$G = G_0 \exp\left[-\left(\frac{T_0}{T}\right)^{1/d+1}\right]$$

כאשר G הוא המוליכות, d הוא הממדיות של המערכת, T היא הטמפרטורה, ו-T_0 הוא קבוע התלוי במרחק הלוקליזציה וצפיפות המצבים במערכת. ניתוח זה נקרא "דילוג למרחקים משתנים" (Variable Range Hopping, VRH), והוא המודל המקובל למוליכות במערכות לא מסודרות.

אחת התוצאות של המודל היא שבמערכות בעלות ממד גדול מאחד $(d > 1)$ עיקר הזרם האלקטרוני יזרום דרך רשת פרקולציה דלילה של אתרים ממוקמים. ניתן לתאר זאת על ידי רשת של נגדים בין האתרים, אשר התנגדותם קשורה ישירות לאחד חלקי סיכוי הדילוג בין האתרים הסמוכים. בשל ההתפלגות האקספוננציאלית של הנגדים, הזרם "יבחר" את הדרך בה ההתנגדות הכוללת היא הנמוכה ביותר, וכמעט לא יעבור דרך שאר האתרים (איור **1.3**).

תופעה זו יוצרת עוד סקלת אורך למערכת, מרחק הפרקולציה, שהוא המרחק האופייני בין ערוצי רשת הפרקולציה, או לחילופין בין "נגדים" שהתנגדותם היא בסדר גודל של התנגדות המערכת. מרחק הפרקולציה תלוי בעיקר ברמת אי הסדר במערכת, ובדרך כלל הוא גדול בכמה סדרי גודל מאורך הלוקליזציה, ויכול להגיע עד לגדלים של עשרות ומאות מיקרונים. בשל התנהגות זו, שהיא בעלת תכונות של תופעות קוונטיות מיקרוסקופיות אבל בעלות סקלת אורך של מספר מקרוסקופי של חלקיקים, מתוארות מערכות אלה כמערכות 'מזוסקופיות' ('meso'=ביניים). תופעה זו יוצרת שינויים חדים במוליכות הכללית של המערכת כתוצאה משינוי תנאי הסביבה, או בין דגמים זהים לכאורה. שינויים אלה, היכולים להיגרם כתוצאה משינוי המתח החשמלי, הטמפרטורה או שדה חשמלי ניצב (מתח שער), יוצרים אפקט הדומה לרעש תרמי אבל הוא נובע ישירות מהתכונות הקוונטית של המתכת, ונקרא 'פלקטואציות מזוסקופיות' (Mesoscopic Fluctuations).

תופעה חשובה נוספת במבודדי אנדרסון היא פער האנרגיה הקולומבי, שהוא תוצאה ישירה של אינטרקציית הדחייה בין אלקטרונים סמוכים. דחייה זו יוצרת עדיפות להמצאות מצבים מלאים

ליד מצבים ריקים, דבר הסותר את הנטייה של האלקטרונים להסתדר כולם מתחת לאנרגיית פרמי בטמפרטורה נמוכה. בשל כך, המצבים הקרובים לאנרגיית פרמי נדחים לאנרגיות גבוהות או נמוכות יותר, ונוצר פער אנרגיה "רך" שמשמעותו התמעטות של מספר המצבים סביב אנרגיית פרמי (אך לא התאפסות מוחלטת שלהם). תופעה זו, והעובדה כי עיקר הזרם במערכת נגרם על ידי אלקטרונים סביב אנרגיית פרמי, מובילה למוליכות קטנה יותר בטמפרטורות נמוכות, ולתלות הבאה של המוליכות בטמפרטורה:

$$G = G_0 \exp\left[-\left(\frac{T_0}{T}\right)^{1/2}\right].$$

ג. תקציר המחקר החישובי

ג. 1. המודל ושיטת החישוב

על מנת לחשב את המוליכות במערכות קוונטיות לא מסודרות אנו נדרשים ראשית לתאר את המערכת בצורה תיאורטית. אחד הכלים המקובלים לשם כך הוא קירוב האלקטרון הקשור (tight binding), המניח כי פונקציית הגל של האלקטרון מרוכזת כולה סביב מרכז האטום. תחת הנחה זו ניתן לכתוב את ההמילטוניאן החד-חלקיקי בצורת מטריצה כאשר כל עמודה מתארת אטום בסריג המתכתי. האיברים על האלכסון בהמילטוניאן הם ערכי אנרגיית הקשר של האלקטרון לאטום, ε_i, והאיברים שאינם על האלכסון מציינים את התרומה לאנרגיה של דילוג האלקטרונים בין האטומים, t_{ij}.

במקרה החד ממדי, ובהנחה כי האלקטרונים קשורים היטב ולכן יכולים לדלג רק לאטומים השכנים הקרובים ביותר, ההמילטונאן הוא מהצורה הבאה:

$$\hat{H} = \begin{pmatrix} \varepsilon_1 & -t_{12} & 0 & 0 \\ -t_{21} & \varepsilon_2 & -t_{23} & 0 \\ 0 & -t_{32} & \ddots & \vdots \\ 0 & 0 & \cdots & \varepsilon_N \end{pmatrix}.$$

במערכת לא מסודרת, אנרגיית הקשר על האלכסון של המטריצה או ערכי הדילוג (או שניהם) אינם אחידים, ולקוחים מתוך פונקציית צפיפות הסתברות, הקובעת את רמת אי הסדר. ניתן

להראות כי שתי האפשרויות הן זהות בעיקרן, ולכן בשל שיקולי נוחות בחרנו את אנרגיות הדילוג t_{ij} להיות אחידות ושוות 1. קביעה זו קובעת גם את סקלת האנרגיה של ההמילטוניאן. את ε_i לקחנו בצורה אקראית מתוך התפלגות אחידה בטווח $\left[-\mathrm{W}/2,\mathrm{W}/2\right]$, כאשר W קובע את רמת אי הסדר וקשור למרחק הלוקליזציה על ידי היחס הבא:

$$\xi \approx \frac{105t^2}{\mathrm{W}^2}.$$

פונקציית גרין למערכות מחוץ לשווי משקל (Non Equilibrium Green's Function) היא שיטה המרחיבה את הטכניקה של פונקציות גרין על מנת לפתור משוואות דיפרנציאליות, דוגמת משוואת שרדינגר, כאשר המשוואות אינן הרמיטיות. פונקציית גרין, שהיא תגובת השדה המתואר על ידי המשוואה לעירור נקודתי, מתארת במערכת קוונטית את אמפליטודת סיכוי ההתקדמות של החלקיק בזמן ובמקום. משום כך, חישוב סיכוי ההעברה דרך המערכת הקוונטית קשור ישירות לפונקציית גרין בריבוע. הכללת גורמים חיצוניים, דוגמת חיבור המערכת למגעים או הכללת אינטרקציות, נעשית על ידי הוספת גורם מדומה לאנרגיה של המשוואה, האנרגיה העצמונית (Self-Energy). בדרך זו, מלבד ההנחות שבמודל האלקטרון הקשור, ניתן לתאר במדויק מערכות קוונטיות עם תנאי שפה וממדים מגוונים. בשל אילוצי זמן חישוב, המערכות אותן אנחנו בחנו הן מערכות חד ממדיות, אך עם רמות אי סדר ותנאי שפה שונים.

ג. 2. מצבי תהודה נסתרים במערכת קוונטית לא מסודרת

בדומה למהוד אופטי, למערכת קוונטית ישנן מצבי תהודה בפונקציית ההעברה האלקטרונית, שקשורים באופן ישיר למצבים העצמיים של ההמילטוניאן. במערכת קוונטית סגורה, המנותקת מהעולם החיצוני, המצבים העצמיים באנרגיה הם ממשיים ומצבי התהודה נמצאים בדיוק באותם ערכי האנרגיה. אולם, כאשר מחברים את המערכת למגעים, הערכים העצמיים של ההמילטוניאן הופכים להיות גדלים מרוכבים, כאשר החלק הממשי שלהם קשור לאנרגיה של המצבים הקוואזי-עצמיים של המערכת (למערכת לא הרמיטית לא ניתן להגדיר במדויק ערכים עצמיים), והחלק המדומה קשור לזמן החיים של האלקטרון במצב זה. באופן דומה, גם פונקציית ההעברה משתנה ומצבי התהודה מתרחבים, עד שבמצב של מערכת פתוחה לחלוטין הם נעלמים לגמרי ופונקציית ההעברה של האלקטרונים שווה 1 לכל ערך באנרגיה.

על כל פנים, במערכת בעלת אי סדר מצבי התהודה מופיעים גם במערכת פתוחה לחלוטין, מכיוון שבאופן אפקטיבי המצבים הממוקמים מנותקים באופן חלקי מהמגעים.

במחקר חישבנו באופן נומרי מגוון רחב של מערכות לא מסודרות, עם רמות אי סדר שונות וחוזקי צימוד שונים בין המערכת למגעים. חישובים אלו הראו תוצאה מפתיעה –חלק גדול ממצבי התהודה בפונקציית ההעברה נעלמים לגמרי כאשר החיבור למגעים חזק מספיק. ניתוח של מספר המצבים הנסתרים במערכות חד מימדיות מראה כי עבור טווח גדול של רמות אי סדר נותרים בדיוק $\sqrt{2/5}\cdot N$ מתוך N המצבים העצמיים במערכת (ראה איורים **5.2** ו**5.5**).

בחינת פונקציות הגל של המצבים הנעלמים מראה כי הגורם להיעלמות זו היא התאחדות של מצבים קוונטיים בתוך המערכת עם המגעים. פונקציית הגל של האלקטרון מתרכזת כולה סביב קצה הדגם ובתוך המגעים עצמם, ולכן כלל לא תורמת להולכה החשמלית (איור **5.4**). בהתאם לכך, כאשר רמות אי הסדר גבוהות מספיק ומצבים אלקטרוניים רבים ממוקמים בצורה כזו שאין להם כלל אינטרקציה עם קצות הדגם ועם המגעים (כאשר $\xi < N$), מספר מצבי התהודה גדל והולך, ומגיע קרוב ל-N ברמות אי סדר גבוהות מאוד (איורים **5.5-5.6**).

תופעה זו והתוצאות החישוביות המופיעות בפרק פורסמו לאחרונה בכתב העת Physical Review B, ראה הפנייה [26].

ג.3. התלות בטמפרטורה של המוליכות בהעדר פונונים

תוצאה נוספת המוצגת בעבודה היא תלות מפתיעה של המוליכות בטמפרטורה, גם בהעדר פונונים. תוצאה זו מפתיעה משום שהתיאוריה המקובלת לתלות בטמפרטורה, VRH, מבוססת על דילוג בין אתרים ממוקמים על ידי פונונים. לפי התוצאות החישוביות המוצגות בעבודה, המוליכות גדלה עם הטמפרטורה לאורך טווח של כמה סדרי גודל בטמפרטורה, גם במקרה בו הפונונים לא נלקחו בחשבון בחישוב הקוונטי (איור **6.7**).

חישוב הזרם האלסטי (ללא פיזור), שהוא תוצאה של הפריסה החלקית של פונקציות הגל, מראה כי במערכת שבה מרחק הלוקליזציה אינו קטן בהרבה מאורך המערכת החד-ממדית ערכי המוליכות אינם קטנים מאוד. ניתוח של פונקציית ההעברה במצב כזה, מגלה כי התפלגות הסיכוי למעבר אלקטרונים הוא פונקציה לוג-נורמלית (איור **6.3**). התפלגות לוג-נורמלית נובעת ישירות מתוך מכפלה של הרבה ערכים אקראיים, והיא מאופיינת באזור רחב של ערכים הקרובים לאפס, וזנב צר של ערכים גבוהים אקספוננציאלית. אכן, בשל תופעת התהודה של ההעברה במערכת הקוונטית, עבור רוב ערכי האנרגיה סיכוי המעבר הוא קטן מאוד, ורק קרוב מאוד למצב התהודה מתקבל סיכוי שהוא קרוב יותר ל-1 (איור **6.2**).

בהעדר טמפרטורה, חישוב המוליכות מתבצע על ידי אינטגרציה על פונקציית ההעברה על פני כל ערכי האנרגיה שבהם קיים אלקטרון במוליך בצד אחד, ואין אלקטרון במוליך שבצד השני. הפרש זה הוא בדיוק המתח המופעל על המערכת. אולם, כאשר הטמפרטורה סופית התפלגות האכלוס של האלקטרונים במגעים אינו מוגבל לאנרגיות מסוימות, והוא מתואר על ידי פונקציית פרמי

דיראק. ככל שהטמפרטורה גדלה, פונקציית פרמי דיראק מתרחבת ולכן האינטגרציה פרושה על פני טווח אנרגיות גדול יותר (איור **6.1**).

חישוב זהיר מגלה כי צירוף של שתי עובדות אלה יוצר גידול משמעותי של המוליכות כאשר הטמפרטורה גדלה, מכיוון וההסתברות שמצב תהודה בעל העברה גבוהה ייכלל בגבולות האינטגרציה גדל גם הוא. במערכת ללא מצבי תהודה, או בעל התפלגות ערכי העברה שאינה מוטה, פתרון האינטגרל היה זהה עבור כל טמפרטורה. במקרה הלא מסודר, בשל העובדה כי הפונקציה הלוג-נורמלית היא בעלת הטיה גבוהה (skewness), מתקבלת תלות חזקה בטמפטורה (איור **6.8**). תוצאה חישובית זו יכולה להסביר את הסטיות הניסיוניות מתיאוריית הדילוג עליה בטמפרטורות נמוכות.

תקציר המחקר הניסיוני

ד. 1. מבוא לזכוכית אלקטרונים

בדומה למערכות זכוכיתיות אחרות, זכוכית אלקטרונים מתאפיינת בהעדר שווי משקל, בדעיכה ארוכה של האנרגיה הפנימית במערכת, ובתופעות זיכרון. תופעות זכוכיתיות מתרחשות במערכות בעלות אי סדר גבוה ואינטרקציות חזקות, דוגמת האינטרקציה בין אטומי הסיליקון והחמצן בזכוכית המוכרת לנו מחיי היום יום.

כאשר ישנו אי סדר פנימי בחומר, דוגמת מערכת לא מסודרת של ספינים במתכתות מסוימות (זכוכית-ספין), או בקירור מהיר של זכוכית שאינו מאפשר לאטומים להסתדר, לא מופיע ארגון פנימי כמו בחומר המוצק, ובמקום לעבור מעבר פאזה מנוזל למוצק המערכת "נתקעת" במצב ביניים, בשווי משקל מדומה (איור **7.1**). בטמפרטורה סופית תהליך ההסתדרות של הזכוכית מתרחש בכל זאת אך בקצב איטי מאוד על ידי מעבר בין מצבי שווי משקל מדומה מעל מחסומי אנרגיה. התלות של הקצב בטמפרטורה נקבע על פי חוק אהרניוס

$$\lambda = \gamma_0 \exp\left(-\frac{U}{k_B T}\right)$$

כאשר U הוא גובה מחסום האנרגיה, k_B הוא קבוע בולצמן ו-γ_0 הוא קבוע שנקבע על ידי תכונות המערכת.

כדי להציג טוב יותר מערכות מסוג זה, ניתן לתאר אותן על ידי מרחב הקונפיגרציות שלהן. בהצגה זו כל סידור של האטומים/ספינים/אלקטרונים מציין נקודה במרחב רב ממדי. פריסת האנרגיה של הקונפיגורציות השונות במרחב יוצרת פונקציה המתארת את פוטנציאל האנרגיה של המערכת (איור 7.3). לאחר קירור מהיר של הזכוכית המערכת נמצאת באחד מערכי המינימום המקומיים של מצבי פוטנציאל אלה, ובתהליך הדעיכה היא עוברת דרך נקודת מקסימום אל ערך נמוך יותר באנרגיה (איור 7.4).

זכוכית אלקטרונים היא תופעה חדשה יחסית בתחום זה, והיא נוצרת במתכות בעלות אי סדר פנימי גבוה וצפיפות נושאי מטען גבוהה, שגורם לאינטרקציות חזקות בין האלקטרונים. במצב כזה המוליכות הנמדדת מראה קשר ישיר לאנרגיה הפנימית של האלקטרונים, ואחרי קירור מהיר או שינוי של השדה החשמלי על הדגם (על ידי מתח ישיר או מתח שער) ישנה דעיכה איטית של המוליכות.

ניתן להראות כי כאשר התפלגות מחסומי האנרגיה במערכת היא רחבה מאוד ומתפלגת בצורה אחידה, הדעיכה הכללית של המוליכות, שהיא תוצאה של חיבור אינספור תהליכים מקרוסקופיים, תהיה לוגריתמית בזמן. ואכן, במדידות שנעשו ב-20 השנים האחרונות מערכות מתכתיות רבות מראות דעיכה עם תלות לוגריתמית על פני הרבה סדרי גודל בזמן (איור **7.7**):

$$G = G_0 - S\log(t)$$

כאשר G_0 היא המוליכות במצב המעורר, t הוא הזמן ו- S הוא קצב הדעיכה.

בנוסף, ובשונה מתהליכים כימיים ופיסיקליים אחרים, תהליך העירור של האלקטרונים הוא בעיקרו זהה לתהליך הדעיכה, ומתרחש גם הוא באופן איטי. בשל כך, נוצרת תופעה הידועה כ"זכרון" של המערכת את מצב שווי המשקל המדומה, ולכן של ההיסטוריה החשמלית והתרמית של הדגמים. בזכוכית אלקטרונים ניתן לצפות בתופעה זו ביתר בירור, בשל העובדה שלא נדרש לשנות את הטמפרטורה על מנת לעורר את המערכת, וניתן לעשות זאת על ידי שדה חשמלי ניצב, בקונפיגורציה דומה לזו של שערים לוגיים במוליכים למחצה (MOSFET). כאשר המערכת נמצאת זמן רב במתח שער מסוים המוליכות בו דועכת. שינוי של מתח השער משנה את מספר האלקטרונים במערכת ולכן מוציא אותה משווי משקל באופן מיידי, ונצפית עלייה מהירה במוליכות, שאחריה דעיכה מחודשת לקראת שווי משקל חדש. במצב כזה, ובשל תהליך הזכרון, סריקה מהירה של מתח השער יוצרת צורת שקע סביב הערך הקודם של המתח (איור **7.9**). צורה זו נקראת 'שקע זכרון' (Memory Dip).

באופן מפתיע, עד לאחרונה קצב הדעיכה בזכוכית אלקטרונים לא הראה ירידה עם ירידת הטמפרטורה, כפי שמתחייב מחוק אהרניוס ובניגוד לכל המערכות הזכוכיתיות האחרות (איור **10.1**). בשל כך נטען כי התהליכים השולטים בהסתדרות האלקטרונים במתכת אינם תהליכיים

תרמיים שנגרמים על ידי פונונים, אלא תהליכים קוונטיים, בהם האלקטרונים עוברים ממצב למצב על ידי תופעת המינהור.

ד. 2. דינמיקה תלוית טמפרטורה וזכרון הטמפרטורה המקסימלית

אנו חקרנו את המוליכות בשכבות דקות של זהב, ניקל וכסף, שנודפו בשיטת "עיבוי קר" – נידוף תרמי על מצע של סיליקון אוקסיד שקורר לטמפרטורות נמוכות (איורים 8.1-8.3). באמצעות שיטה זו יכולנו לשלוט בטמפרטורה המקסימלית אליה נחשפו הדגמים, ולחמם אותם לאחר מכן לטמפרטורה גבוהה יותר.

בניגוד לתוצאות הקודמות במערכות של זכוכית אלקטרונים, דינמיקת הדעיכה לשווי משקל הראתה האטה דרמטית בטמפרטורות נמוכות מזו שבה המערכת נוצרה. יתר על כן, חימום לטמפרטורה מקסימלית חדשה הראה קצב דומה לזה שהיה בטמפרטורת הנידוף, אך קירור חזרה לטמפרטורת הנידוף יצר האטה משמעותית. על כן, שתי מדידות זהות שנעשו בטמפרטורת הנידוף, אחת לפני החימום ואחת אחריו, הראו קצבי דעיכה שונים מאוד זה מזה (איור **9.1**).

באופן יותר מפורט, סדרה של מדידות בטמפרטורות שונות עד לטמפרטורת החדר הראו תלות ליניארית של קצב הדעיכה עם הטמפרטורה, ותלות לינארית הפוכה לטמפרטורה המקסימלית בה הדגם היה (איור **9.4**):

$$S \propto \frac{T}{T_{\max}}$$

שתי תוצאות מפתיעות אלה – האטה כתוצאה מקירור, ושינוי של סקלת הטמפרטורה עם הטמפרטורה המקסימלית, הובילו אותנו למסקנה כי (א) בטווח מסוים של טמפרטורות זכוכית אלקטרונים כן נשלטת על ידי אקטיבציה תרמית של פונונים. (ב) כאשר היא מיוצרת בטמפרטורה שנמוכה מטמפרטורת הזכוכית שלהן, סקלת האנרגיה בזכוכיות אלקטרונים נקבעת על ידי הטמפרטורה המקסימלית שבה היא הייתה.

על ידי ההצגה של מרחב הקונפיגורציות ניתן להסביר את התצפיות הללו בצורה הבאה: כאשר הזכוכית מעולם לא הייתה בטמפרטורה גבוהה מספיק לא היה באפשרות האלקטרונים לסקור את כל מרחב הקונפיגורציות, ולכן הם נתקעים במצבים של שווי משקל מדומה שעומקם פורפורציונלי ל $T_{\max}$. בשל כך התפלגות הקצבים של התהליכים נקבע גם הוא על ידי $T_{\max}$ וקצב הדעיכה משתנה. כאשר הזכוכית נחשפת לטמפרטורה גבוהה יותר, האלקטרונים מוצאים את דרכם לבורות פוטנציאל עמוקים יותר, מה שמאט את קצב הדעיכה (איור **9.5**).

תוצאות פרק זה פורסמו לאחרונה בכתב העת Physical Review Letters, ראה הפנייה [50].

ד. 3. מעבר מדינמיקה קלאסית לדינמיקה קוונטית בטמפרטורות נמוכות

קירור נוסף של הדגמים עד קרוב לטמפרטורה של הליום נוזלי (4.2 מעלות קלווין), גילה תופעה מפתיעה נוספת: ההאטה בדינמיקה נעצרת מתחת לטמפרטורה ששווה בערך ל $T_{\max}/2$, והופכת להיות קבועה. לדוגמא, במקרים בהם הדגם יוצר בטמפרטורת החדר טמפרטורת המעבר הייתה סביב 150 מעלות קלווין (איורים **10.4-10.6**)

כפי שנטען בעבר, חוסר תלות בטמפרטורה יכול להצביע על אפקט של זכוכית קוונטית, אך במערכת שלנו נראה כי ישנם שני תחומים – תחום תרמי-קלאסי, ותחום קוונטי, ומעבר בינהם.

כדי להבין את המעבר הזה, ומדוע הוא לא נצפה במחקרים בחומרים אחרים, סרקנו תמונות SEM של הדגמים. מהסריקות נראה שהמבנה הגאומטרי של הדגמים אינו רק בעל אי סדר גבוה, אלא הוא גם אינו רציף. המתכת המנודפת מעדיפה להסתדר במבנה פרקטלי של גרגירים מתכתיים עם רווחים בינהם. סדר הגודל של הגרגירים הוא עד 100 ננומטר, ושל המרווחים עד כ-50 ננומטר (איור **10.5**).

ביחד עם פרופ' אריאל אמיר (הרווארד) פיתחנו תיאוריה המבוססת על הגאומטריה המיוחדת הזו ועל התפלגות הגדלים של הגרגירים. לאלקטרון העובר בין שני חלקיקים גדולים דרך חלקיק שלישי, קטן יותר, ולכן גם בעל אנרגית טעינה גבוהה יותר, יש שתי אפשרויות עקרוניות לעשות זאת – 1. על ידי קליטת פונון, מעבר לחלקיק הקטן, ומעבר ממנו אל החלקיק השני (איור **10.7**). 2. על ידי מינהור קוונטי דרך החלקיק הקטן. ניתוח מפורט של המשוואות מראה כי אכן בתחום הגדלים והאנרגיות בהן אנו עוסקים ישנו מעבר בין עדיפות לתהליך התרמי בטמפרטורות גבוהות אל התהליך הקוונטי בטמפרטורות נמוכות.

הגודל הקבוע את נקודת המעבר הוא גודלו של החלקיק האמצעי הקטן והמרווחים בין הגרגירים. אכן, כאשר המערכת נוצרה בטמפרטורה נמוכה האלקטרונים לא יכולים לעבור דרך החלקיקים הקטנים יותר, ובשל ההתנהגות הפרקולטיבית של האלקטרונים אזורים שלמים נחסמים בפניהם. חימום של הדגם חושף חלקיקים חדשים לדינמיקה הזכוכיתית, ולכן גם משנה את נקודת המעבר בטמפרטורה.